I. Targeted ß-catenin Ubiquitination and Degradation Using Bifunctional Stapled Peptides II. Studies on Cell Penetration by Stapled Peptides

I. Targeted β-catenin Ubiquitination and Degradation Using Bifunctional Stapled Peptides

II. Studies on Cell Penetration by Stapled Peptides

A dissertation presented

by

Qian Chu

to

The Department of Chemistry and Chemical Biology

in partial fulfillment of the requirements

for the degree of

Doctor of Philosophy

In the subject of

Chemistry

Harvard University

Cambridge, Massachusetts

November 2013

Dissertation Advisor: Professor Gregory L. Verdine *Qian Chu*

I. Targeted β-catenin Ubiquitination and Degradation Using Bifunctional Stapled Peptides

II. Studies on Cell Penetration by Stapled Peptides

Abstract

Hydrocarbon-stapled α-helical peptides represent a relatively new class of synthetic peptidomimetics capable of inhibiting protein-protein interactions. It has been shown that hydrocarbon "staples" spanning one or two helical turns in a peptide increase α-helical content and protease resistance, enhance target binding affinity, and promote cell penetration. This technology has been applied to the development of cell-permeable ligands targeting several intracellular targets. This dissertation describes efforts to further the development of stapled peptide technology.

A bifunctional stapled peptide strategy was introduced to target a key regulator in the canonical Wnt signaling pathway, β-catenin, for ubiquitination and proteasomal degration. We designed and synthesized a panel of bifunctional stapled peptides and demonstrated that they can recruit the MDM2 protein, an ubiquitin E3 ligase, to β-catenin. An *in vitro* ubiquitination assay was developed to demonstrate specific β-catenin poly-ubiquitination mediated by bifunctional peptides. Furthermore, treatment of the human colorectal cancer line SW480 with bifunctional stapled peptides demonstrated dose-dependent knockdown in endogenous β-catenin levels. In addition, a reporter gene assay showed that the bifunctional stapled peptides can downregulate downstream gene

expression in the Wnt signaling pathway. Therefore, bifunctional stapled peptides may serve as potential pathway-specific drug candidates in the treatment of Wnt-addicted cancers, and are a unique research tool for probing the Wnt signaling pathway by targeted knockdown of β-catenin at the protein level.

We also studied the cell penetration property of stapled peptides, which is one of the most significant and poorly understood aspects of peptide stapling technology. We developed a high-throughput microscopy assay to quantitatively measure stapled peptide intracellular accumulation. Using this assay, we analyzed more than 200 discrete peptides with various sequences, stapling positions and types. We found that cell penetration is strongly related to stapling types and formal charge, i.e. stiched and cationic peptides. In addition, we used chemcal genetic screens to identify the specific pathway involved in stapled peptide internalization. These studies showed that stapled peptides penetrate cells through clathrin- and caveolin-independent endocytosis pathway that requires sulfated proteoglycans. These findings improve our understanding of stapled peptides as chemical probes and potential targeted therapeutics, and provide guidelines for the design of next-generation stapled peptides.

Table of Contents

Acknowledgements

The work described in this thesis would not have been possible without the generous help from many exceptional people. I am very grateful for their kindness.

First of all, I would like to thank my research advisor Professor Gregory L. Verdine for his guidance and continuous support during my graduate study. He is always encouraging, giving me confidence and offering invaluable advice in my research. As Isaac Newton once said: “If I have seen further, it is by standing on the shoulders on giants.” To me, Greg is such a giant. His ambition and enthusiasm in science always inspire me to pursue big questions in research, and will continue to guide me as I move on to my next challenge.

Secondly, I am also grateful for the invaluable support and advice from my committee members, Professors David Liu and Alan Saghatelian. They are always available when I need to discuss with them about my projects. More importantly, they have offered me numerous helpful suggestions and insights to my research.

I appreciate the Verdine lab members, past and present, to create a lovely, professional and friendly environment to conduct research. Lydia Carmosino and Besty Donovan, as lab administrators, are always willing to help me out on many topics, such as scheduling a meeting with professors, ordering reagents and discussing VISA status. Without their kind help, my graduate study would not have been as smooth as it is now. Dr. Shaunna Berkovitch was my mentor when I rotated in the lab. She gave me a comprehensive introduction to the research in the Verdine lab, which ultimately recruited

me to the lab. After I joined the lab, Shaunna not only taught me a lot to solve research problems, but also helped me to become familiar with American culture. I would also like to thank Dr. Johannes Yeh as he taught me many biology techniques that I used in the bifunctional stapled peptide project. Dr. Raymond Moellering and I collaborated on the project to study cell penetration of stapled peptides. With his help, I established the epifluorescence platform to quantitatively measure cellular access for fluorescence-labeled peptides. Dr. Jerry Hilinski is another important person in my graduate study, as he knows almost every aspect in the Verdine lab. Whenever I had any questions or problems, he was always the first person I will turn to for advice. No matter how tiny and silly my questions were, he was always willing to help me. In addition, I would give my special thanks to Shaunna, Jerry and Dr. Rou-Jia Sung and Dr. John McGee as they spent quite a lot of time on polishing my thesis. Many other Verdine lab colleagues also gave me numerous help in research and life throughout my graduate study, I definitely appreciate all their kindness and support.

Outside the Verdine lab, I am thankful to Dr. Lance Davidow in Professor Lee Rubin's laboratory, who taught me to use the confocal microscopy in their lab and offered me full access to their instruments. Professor Keith Foster at University of Reading, UK collaborated with us on the morpholino cellular delivery project discussed in Chapter III. His lab performed the *in vivo* assays to evaluate the conjugate efficacy. These collaborative experiences were especially valuable to me.

Finally, I would like to thank my family for their love and support throughout the years. I grew up in a big family, everyone helped to shape me into the person I am today. In

particular, my mom is always supportive, she has offered me great freedom to pursue my dreams, and allowed me to have my graduate study on the other end of the planet. My daughter, Emily, has brought me a lot of happiness, which cheered me up at those times when I experienced many failed experiments and lost my faith in the project. Lastly but most importantly, I owe all my success in the graduate study to my wife, Jiongjia, who has offered numerous support, encouragement and happiness in my life.

List of Abbreviations

2-DG	2-deoxyglucose
Antp	antennapedia peptide
APC	adenomatous polyposis coli
aPP	avian pancreatic polypeptide
AR	androgen receptor
ARM	armadillo
ATP	adenosine triphosphate
BCL-2	B-cell lymphoma 2
bct	β-catenin
Bisax	bifunctional stapled Axin peptide
CBD	β-catenin binding domain
cDNA	complementary DNA
CK1	casein kinase 1
CMV	cytomegalovirus
CPP	cell penetrating peptide
CTD	C-terminal domain
DAPI	4',6-diamidino-2-phenylindole
DCE	1,2-dichloroethane
Dex	dexamethasone
DIPEA	N,N-diisopropylethylamine
DMD	duchenne muscular dystrophy
DMEM	Dulbecco’s modified Eagle's medium

DMSO	dimethyl sulfoxide
DNA	deoxyribonucleic acid
DOS	diversity oriented synthesis
Dsh	dishevelled
DTT	dithiothreitol
E1	ubiquitin activating enzyme
E2	ubiquitin conjugating enzyme
E3	ubiquitin ligase
FACS	fluorescence-activated cell sorting
FBS	fetal bovine serum
FITC	fluorescein isothiocyanate
FKBP	FK506 binding protein
Fmoc	9-fluorenylmethyloxycarbonyl
FP	fluorescence polarization
FPLC	fast protein liquid chromatography
Fz	frizzled
GFP	green fluorescent protein
GR	glucocorticoid receptor
GSK3	glycogen synthase kinase 3
GST	glutathione S-transferase
HBS	hydrogen bond surrogate
HCTU	2-(6-Chloro-1-H-benzotriazole-1-yl)-1,1,3,3-tetramethylaminium hexafluorophosphate

HIV	human immunodeficiency virus
HPLC	high-performance liquid chromatography
IB	immunoblotting
IC_{50}	half maximal inhibitory concentration
IPTG	isopropyl β-D-1-thiogalactopyranoside
K_d	dissociation constant
LC/MS	liquid chromatography–mass spectrometry
LEF	lymphoid enhancer-binding factor
LRP	lipoprotein receptor-related proteins
LUV	large unilamellar phospholipid vesicle
MBP	maltose-binding protein
MDM2	murine double minute 2
Me	methyl
mTOR	mammalian target of rapamycin
MWCO	molecular weight cut off
NMP	N-methylpyrrolidone
NTA	nitrilotriacetic acid
NTD	N-terminal domain
OD	optical density
PAGE	polyacrylamide gel electrophoresis
PBS	phosphate buffered saline
PEG	polyethylene glycol
PMO	phosphorodiamidate morpholino oligomer

PMSF	phenylmethylsulfonyl fluoride
PROTACS	proteolysis targeting chimeric
PSA	polar surface area
PTD	protein transduction domain
RCM	ring-closing metathesis
RING	really interesting new gene
RNA	ribonucleic acid
RNAi	RNA interference
RT-PCR	reverse transcription polymerase chain reaction
SAHB	stapled α-helix of BCL-2 domain
SAHM	stapled α-helical MAML peptide
scGFP	supercharged GFP
SDS	sodium dodecyl sulfate
SMCC	succinimidyl-4-(N-maleimidomethyl)cyclohexane-1-carboxylate
StAx	stapled Axin-derived peptide
TBS	tris buffered saline
TCEP	tris(2-carboxyethyl)phosphine
TCF	T-cell factor
TEAA	triethylammonium acetate
TEM	transmission electron microscopy
TEV	tobacco etch virus
TFA	trifluoroacetic acid
TIS	triisopropylsilane

Tris	tris(hydroxymethyl)aminomethane
TRITC	tetramethylrhodamine isothiocyanate
Wnt	wingless and int-1
WT	wild-type
Ub	ubiquitin

Chapter I Introduction

Expanding the Druggable Genome

The human genome provides a great bulk of essential genetic information. It contains approximately 30,000 genes, most of which specify protein synthesis by cytoplasmic ribosomes. The proteins encoded by these genes collaborate extensively to form a complex interplay of signaling networks and thereby regulate a wealth of biological processes necessary for life[1-2]. Defects in critical signal transduction pathways often indicate the onset and progression of different types of diseases[3-5]. Extensive efforts have been made in the field of drug discovery to develop and apply therapeutic interventions to target disease-modifying proteins, resulting in two major classes of drugs, small molecule and protein therapeutics (also known as biologics)[6-9].

Small molecules are able to target, with high affinity and specificity, proteins which feature a deep, hydrophobic pocket on their surface[10-11]. Therefore, the common targets for small molecule therapeutics usually engage in protein-ligand interactions, such as receptor-ligand and enzyme-substrate/cofactor pairs[12-13]. The small molecule drugs compete against the native ligands in the already structured hollows. However, protein-protein interactions, as a broad class of interactions highlighted in signaling networks, are typically characterized by an extensive association between two relatively flat yet precisely complementary surfaces[14]. As a result, developing small molecules that modulate protein-protein interactions has proven difficult due to the lack of well-defined binding pocket at

protein surfaces[15]. Furthermore, targeting the complex signaling networks comprised of distinct protein-protein and protein-ligand interactions requires small molecules with great structural diversity, such as size, shape, functional groups and chirality[16-17]. Current synthetic strategies and designs, however, limit the accessibility of molecules with enough structural variation, resulting in delays in drug development. Therefore, only approximately 10% of proteins in the human genome can be accessed by small molecule therapeutics[18].

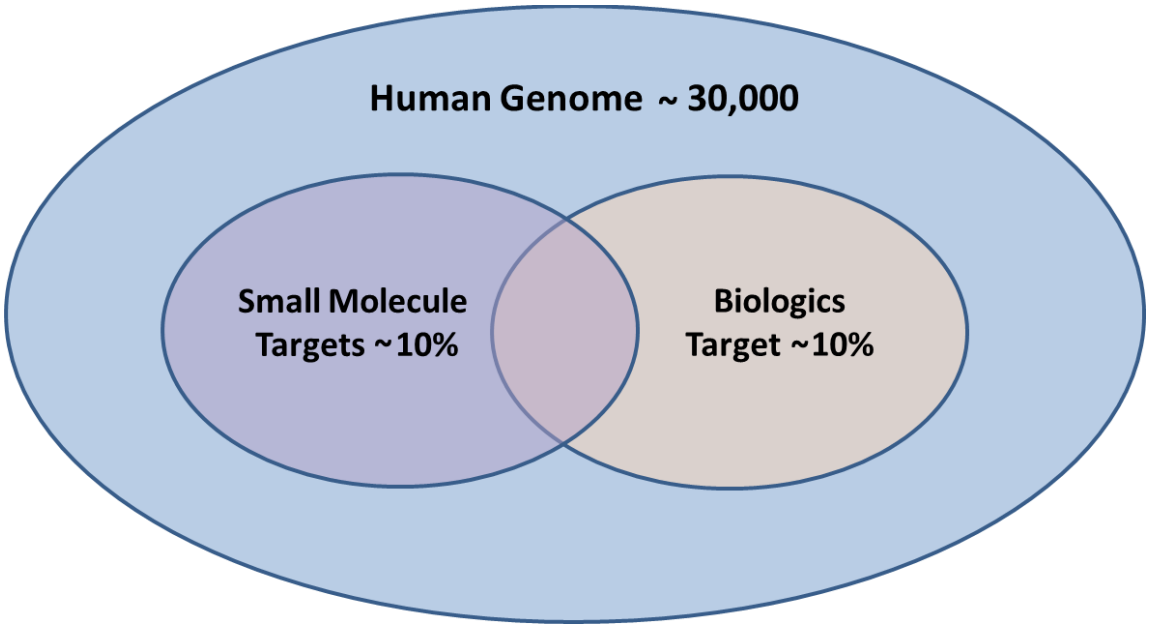

Figure 1.1 The druggable genome. The two major classes of drugs, small molecule and protein therapeutics, can each target approximately 10% of human proteins, indicating that more than 80% of the proteins are considered undruggable.

Protein therapeutics, on the other hand, are now well-established as a clinically and commercially important class of drugs. Compared with small molecules, proteins usually have rich three-dimensional structures as well as diverse surface variability, making them suitable to accommodate different protein partners and exerting their pharmacologic activities. In addition, the binding affinity and specificity of protein therapeutics to their

targets can be optimized by a variety of selection technologies such as phage, yeast or ribosome display. However, the major drawback of protein therapeutics involves an inability to translocate across the plasma membrane, limiting their effectiveness to cell surface or extracellular targets. Another shortcoming of protein therapeutics is that they undergo fast denaturation and proteolysis in the gut and are thus usually not orally bioavailable. To this end, protein therapeutics are able to access an estimated 10% of human proteins[18].

Each of these two classes of pharmacologic agents – small molecules and protein therapeutics – can access about 10% of protein targets in the human genome, indicating that at least 80% of human proteins are considered undruggable (Figure 1.1). Among these undruggable targets, there are incredibly important proteins, such as transcription factor "master regulators" and other key proteins that are root causes of a vast range of human diseases[19-20]. For example, c-myc transcription factor and the KRas GTPase play a pivotal role in many signaling cascades and are essential in numerous biological activities. Aberrant activation of these genes has proven to be involved in development of different types of cancers. However, they are considered undruggable targets since no molecule that directly targets either of these proteins has been reported. Therefore, access to such high value biological targets that are not amenable to current therapeutic intervention would expand treatment options and be a major boost for patients. Indeed, extensive studies have been performed to expand the druggable genome, and several promising results have been reported recently.

These efforts can be characterized into several different categories. First, modern technological advances have been employed to revisit the human genome and proteome in order to search for understudied and unannotated proteins that could be potential drug targets[21]. Defining the druggable genome is an exceptional sophisticated task, as several parameters could influence the count, including the coverage of DNA sequence databases, the algorithms used for sequence annotations, and the bioinformatics tools and biological information about protein function. Therefore, the outcome of counting the druggable genome largely depends on the resources and tools used in the studies, indicating there might be some underestimated proteins that could be targeted by traditional therapeutic strategies. Considering the rapid evolvement of related technology, it is possible to expand the druggable genome by identifying new sets of proteins accessible by therapeutic molecules[1-2].

The second approach is expanding the molecular diversity by new synthetic strategies[22-23]. Most current drug discovery efforts start with high-throughput screening of small molecule library to search for hits that can exert noticeable phenotype changes *in vitro* or *in vivo*. However, traditional screening libraries are composed of large numbers of structurally similar compounds. It is broadly accepted now that both library size and structural diversity are equally important. In response to this problem, Schreiber and coworkers at Harvard University pioneered a new synthetic strategy, "Diversity-Oriented Synthesis" (DOS), which utilizes "build – couple – pair" organic synthesis to make compounds covering as much chemical space as possible[24]. The DOS strategy usually takes limited steps of robust chemical reactions to convert simple starting materials to a library of compounds with a high degree of structural diversity, measured in terms of functional

groups, stereochemistry, and scaffold variability (Figure 1.2)[25]. Several promising results have been reported by screening DOS library compounds against a variety of targets, including traditionally undruggable proteins such as BCL-2 and Sonic Hedgehog[26-27].

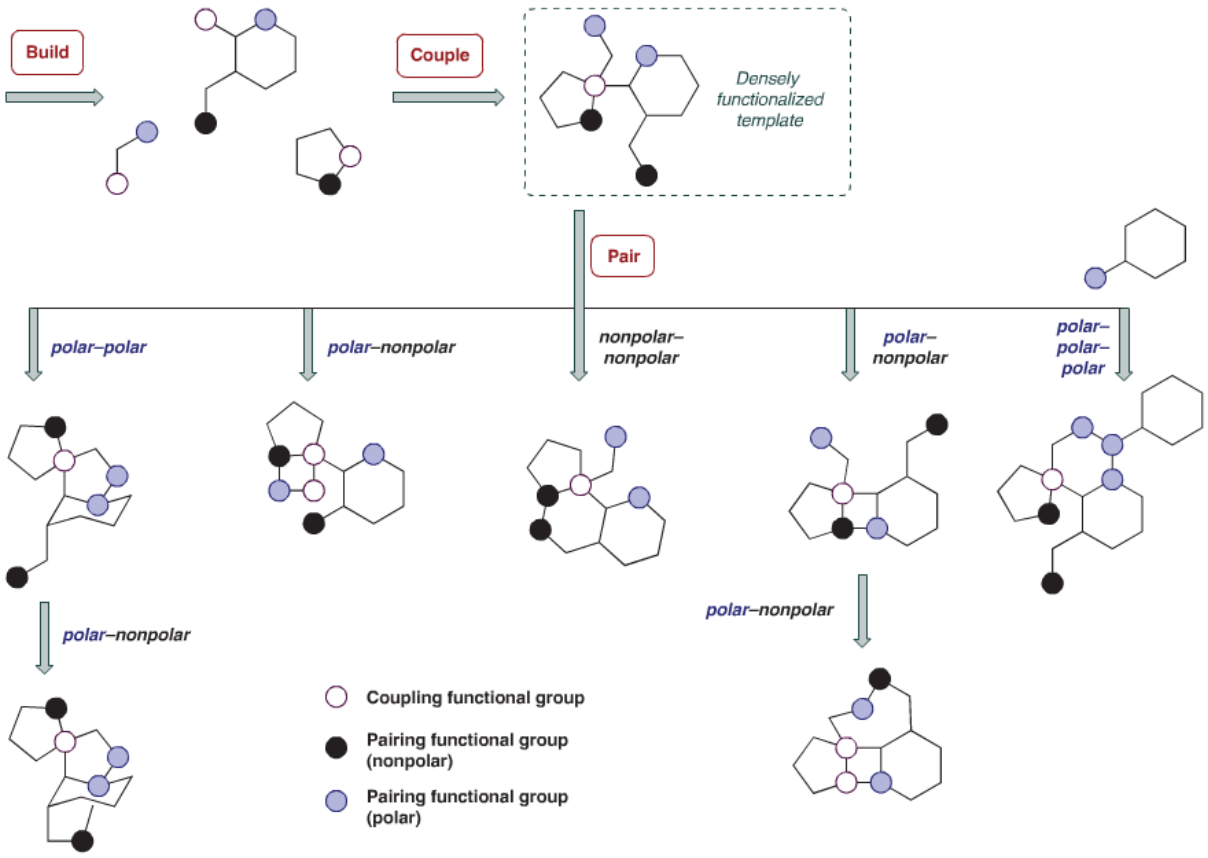

Figure 1.2 Diversity-oriented synthesis with a build-couple-pair strategy. Build: asymmetric synthesis of chiral building blocks. Couple: intermolecular coupling reactions with the building blocks synthesized in the "build" phase, which provides the basis for stereochemical diversity. Pair: intramolecular coupling reactions that join every possible combination of functional groups incorporated in the "build" phase (polar functional groups shown in blue, nonpolar in black). The skeletal diversity is generated in this "pair" phase. (This Figure is adapted from Reference 25)

A third category of efforts involves discovering new therapeutics by exploiting the druggable genome with innovative strategies. Traditional drug discovery either starts with screen-based identification of target protein binders and subsequent in vivo evaluation of activity or begins with *in vivo* phenotype screenings featuring no target bias followed by

the target identification for the lead compounds[28-30]. In order to improve the efficiency of these approaches, several new strategies have been invented. For example, fragment-based drug discovery has emerged in the past decade as a new approach to discover drug leads[31-34]. It starts with identifying small chemical fragments that bind only weakly to the target. These fragments are further expanded or linked to produce a lead with a higher affinity (Figure 1.3). The advantage of this strategy over conventional methods is the difference in the stringency of the initial screens. The starting binding affinity for a fragment-based screen is usually in the millimolar range, which is much easier to fulfill than micromolar-affinity hits in conventional screens.

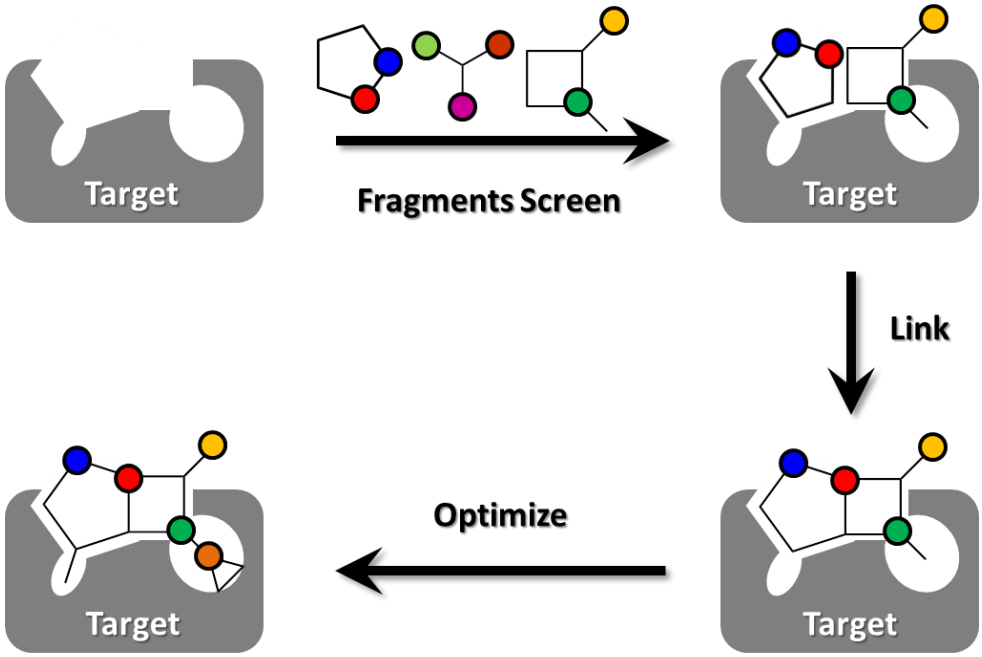

Figure 1.3 In fragment-based drug discovery, small molecule libraries with diverse chemical space (shown as different colored circles) are screened for initial low affinity binding fragments, which undergo rounds of optimization to yield high-affinity drug-like compounds for therapeutic application.

Another advantage of this strategy is the greater coverage of chemical diversity space in the screen, which often results in a wide collection of useful starting points for drug discovery.

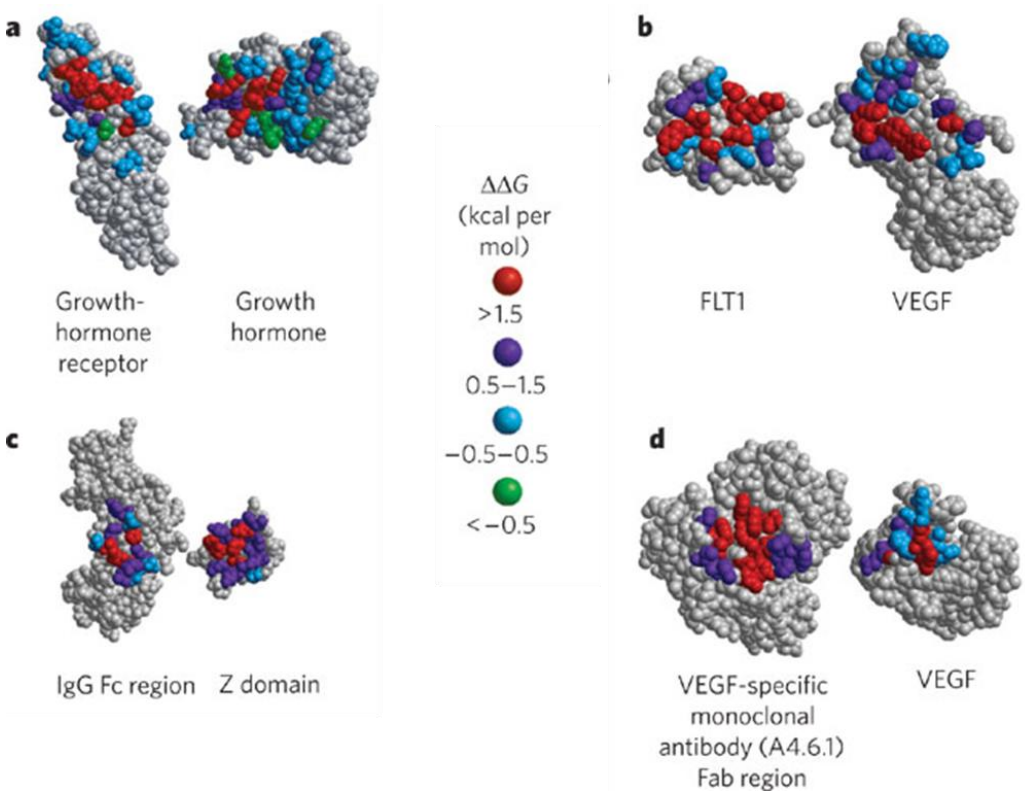

Figure 1.4 Alanine-scanning mutational analysis was carried out on the contact surface of four pairs of interacting proteins, a) growth hormone and growth hormone receptor, b) VEGF and FLT1, c) IgG Fc region and Z domain from *Staphylococcus aureus* protein A, d) VEGF and VEGF-specific monoclonal antibody. The resulting change in the free energy of binding compared with wild-type protein interactions (ΔΔG) is shown by different colored amino acids, from red (the most-disruptive changes) to green (those with the least effect). The protein hotspots are identified as a small number of residues (Red) which contribute most of the free energy regarding protein-protein interactions. (This figure is adapted from Reference 35)

A second example lies in the discovery of protein hotspots by assessing the binding energy generated by each residue present at a protein-protein interface. This demonstrates that although the interface itself might be largely featureless, a small subset of the residues involved contributes most of the free energy of binding. These so-called "hotspots" are usually found at the center of the contact interface, and occupy only a limited surface area (Figure 1.4). In this case, rather than targeting the entire flat and extended protein-protein interface, disrupting the contact between these critical binding residues may provide useful insights to discover therapeutics effective toward those undruggable targets[35-37].

As the two major classes of drugs cannot address all current therapeutic needs, however, current studies to expand drug discovery and improve drug efficacy focus on developing new chemical probes that can access the challenging targets in human genome[38-40]. In particular, novel peptide therapeutics are becoming increasingly popular and have exhibited in several cases profound pharmaceutical potential.

Peptide Therapeutics

The application of peptides in the clinic is not a new topic – certain naturally derived peptides have been successful drugs for many years. However, difficulties with delivery, stability, and synthesis are the major hurdles hampering the wide commercialization of peptides with therapeutic potential. With the advent of large biological and synthetic peptide libraries and high-throughput screening techniques, there has emerged a vast number of promising peptide candidates and a revived interest in the development of peptide therapeutics[41-44].

The differences between peptide therapeutics and protein therapeutics are ambiguous and still under debate. In this thesis, "peptide therapeutic" refers to peptides or peptidomimetics that contain no more than 50 amino acids and can be chemically synthesized. It is generally accepted that peptides can bind to protein targets with high affinity and specificity and can ideally overcome the drawbacks in small molecule and protein therapeutics. As peptides are generally larger than small molecules, they feature enough chemical diversity to render them suitable for specifically recognizing the usually undruggable protein-protein interface. Yet peptides are smaller than protein therapeutics,

which is likely to facilitate intracellular delivery as well as the avoidance of undesirable immune responses[45]. Another advantage of peptide therapeutics lies in the accessibility of multiple rounds of optimization by the utilization of molecular selection technology, such as phage and yeast cell surface display. For example, a phage display library can contain as many as 10^{11} distinct polypeptides, providing a much larger number of candidates than small molecule libraries. In addition, this selection process can be iterated multiple rounds until a peptide with the desired affinity and specificity is discovered. Furthermore, peptides are synthetically achievable so that a variety of non-natural amino acids with different chemically modified side chains can be incorporated into peptide sequences, further increasing the chemical diversity of peptide therapeutics and also preventing rapid degradation by rendering the peptide unrecognizable to proteases. Unfortunately, peptide therapeutics also have several notable shortcomings that restrain the transition from lead compounds to commercialized drugs[46-47]. For example, they generally have low stability in plasma, are sensitive to proteases and are removed quickly from circulation, resulting in low bioavailability and short *in vivo* half-lives. In addition, most peptides are generally not cell permeable, and exhibit high conformational flexibility which leads to a lack of selectivity involving interaction with different targets within a protein family.

Nevertheless, peptide therapeutics are making a huge impact in drug discovery and in the treatment of many human diseases. Table 1.1 illustrates the rapidly growing number of peptide drugs approved by the FDA over the past four years. It is worth noting not only the number of approved peptide drugs, but also their application toward a broad range of diseases, including those life-threatening ones which are largely incurable by conventional therapeutics, such as cancer, diabetes, and hepatitis C virus. Given the ongoing clinical trials

of many other peptide drug candidates, there will most certainly be more approvals in the next couple years.

Table 1.1 Peptide drugs approved by US FDA during the period 2009 – 2012.

Generic Name	Trade Name	Disease/Target	Properties	Year
Ecallantide	Kalbitor	Hereditary angioedema	Plasma kallikrein inhibitor	2009
Telavancin	Vibativ	Skin infection	Antibacterial agent	2009
Romidepsin	Istodax	Cutaneous T-cell lymphoma	HDAC inhibitor	2009
Liraglutide	Victoza	Type 2 diabetes	GLP-1 receptor agonist	2010
Boceprevir	Victrelis	Hepatitis C Virus genotype 1	NS3/4A protease inhibitor	2011
Telaprevir	Incivek	Hepatitis C Virus genotype 1	NS3/4A protease inhibitor	2011
Icatibant	Firazyr	Hereditary angioedema	Bradykinin B2 receptor antagonist	2011
Lucinactant	Surfaxin	Respiratory distress syndrome	Nonpyrogenic pulmonary surfactant	2012
Peginesatide	Omontys	Anemia related Chronic kidney disease	Erythropoietin analog	2012
Linaclotide	Linzess	Chronic idiopathic constipation and irritable bowel syndrome	Guanylate cyclase 2C agonist	2012
Pasireotide	Signifor	Cushing's disease	Somatostatin analog	2012
Teduglutide	Gattex	Short bowel syndrome	GLP-2 analog	2012

Current peptide drugs and those in clinical trials generally fall into three different categories: naturally structured peptides, macrocyclic peptides, and chemically stabilized peptides. In order to bind to targets with high affinity and specificity, peptide candidates generally need to be constrained into a folded structure. Otherwise, the structural flexibility will cause proteolytic lability and undesired off-target issues, especially for those targeting proteins with closely related homologs. Therefore, peptides with promising therapeutic applications are typically stabilized using one or more of a number of different

strategies. The first class is naturally structured peptides. Nature has already evolved a variety of polypeptides with constrained structures through electrostatic interactions, non-covalent hydrophobic interactions and covalent linkage like disulfide bonds. Learning from these naturally occurring strategies, peptide scaffolds are chosen in which certain residues make contacts to help the peptide fold in a desired scaffold while the other residues can be mutated to optimize binding affinity and specificity. For example, cystine-knot miniproteins, also known as knottins, are a family of proteins that share a common fold containing a conserved core of three tightly interwoven disulfide bonds. This structurally constrained scaffold confers extraordinary thermal and proteolytic stability, whereas a highly diverse loop region provides enough chemical variability for specific binding to protein targets. Correspondingly, knottins are being explored in a variety of therapeutic and diagnostic applications (Figure 1.5a)[48-50]. Another example is avian pancreatic polypeptide (aPP), which contains a solvent-exposed α-helix and a type II polyproline helix joined by a type I β-turn. Unlike knottins, which are stabilized by conserved disulfide bonds, the stability of aPP results primarily from hydrophobic interactions between the interior residues of the two helices. The exterior surfaces, on the other hand, are utilized for target recognition and can be engineered for improvement of binding affinity and specificity (Figure 1.5b). There have thus far been many successful cases using aPP as a probe to modulate protein-protein interactions, which might shed a light on the potential therapeutic and diagnostic applications[51-54].

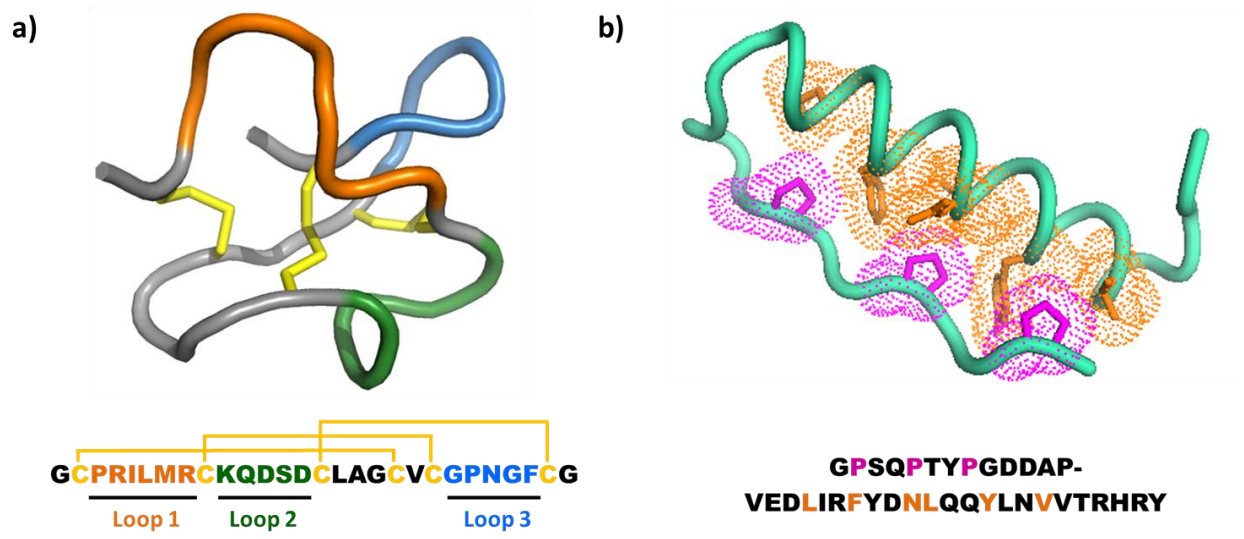

Figure 1.5 Crystal structures of naturally folded peptides. a) The molecular scaffold of one protein in the knottin family, the *E. elaterium* trypsin inhibitor-II (EETI-II, PDB 2ETI) with the sequence illustration at bottom. The three disulfide bonds in the cystine-knot core are highlighted in yellow and three distinct loops are colored in orange, green and blue, respectively. b) The crystal structure of avian pancreatic polypeptide (PDB 1PPT) with the sequence illustration at bottom. The interactions between proline residues in the polyproline helix (colored in magenta) and hydrophobic residues in the α-helix (colored in orange) constrain the peptide in a well-folded structure.

Macrocyclic peptides are another class of peptide therapeutics with defined structures. As bioactive natural peptides are often found to feature a ring conformation, it has been observed that cyclization of a linear peptide generally results in a cyclic peptide with considerably reduced flexibility compared to the parent peptide, which provides several advantages in terms of interaction with a molecular target[55-57]. First of all, the less flexible cyclized peptide is structurally pre-organized, which is entropically favorable upon interaction with its molecular target, resulting in a higher binding affinity. Another advantage of a cyclic peptide is an enhanced resistance to proteolytic degradation, especially by exoproteases, which leads to a longer *in vivo* half-life and better bioavailability. In this respect, many natural-product-like peptides feature macrocyclic motifs and have profound biological functions. For example, vancomycin and cyclosporine

are the most well-established cyclic peptides containing modified amino acids, and they have been applied in treatment of human diseases for many years (Figure 1.6)[58-59].

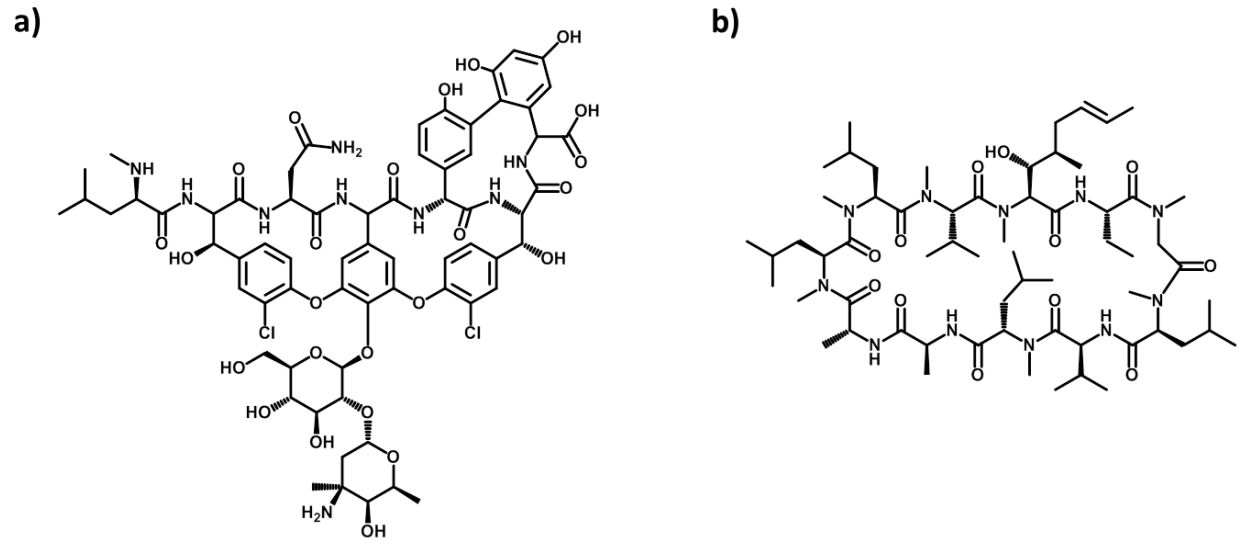

Figure 1.6 Structures of a) vancomycin and b) cyclosporine A. The pre-organized macrocylic backbones are entropically favorable upon binding to their molecular targets.

Lastly, chemical stabilization is an emerging strategy to fix polypeptides in a desired structure, and this method has demonstrated promising results in molecular targeting and therapeutic applications. A variety of chemical strategies have been employed to stabilize peptide secondary structures. Among them, stabilized α-helical peptides are becoming increasingly popular chemical biology probes in modulating protein-protein interactions. According to previous reports, 62% of the characterized protein complexes contain an α-helix at the protein-protein interface, highlighting the significance of the α-helical conformation in mediating protein-protein interactions[60]. Furthermore, these helical interfaces are generally involved in a broad range of biological functions throughout the entire cellular signaling network[61-63]. Therefore, studies have been performed to chemically stabilize a dominant negative peptide in its bioactive α-helical structure. The

stabilized α-helical peptides are expected to disrupt the targeted protein-protein interface and also exhibit increased resistance to proteases owing to structural rigidity as well as unnatural chemical moieties in some cases.

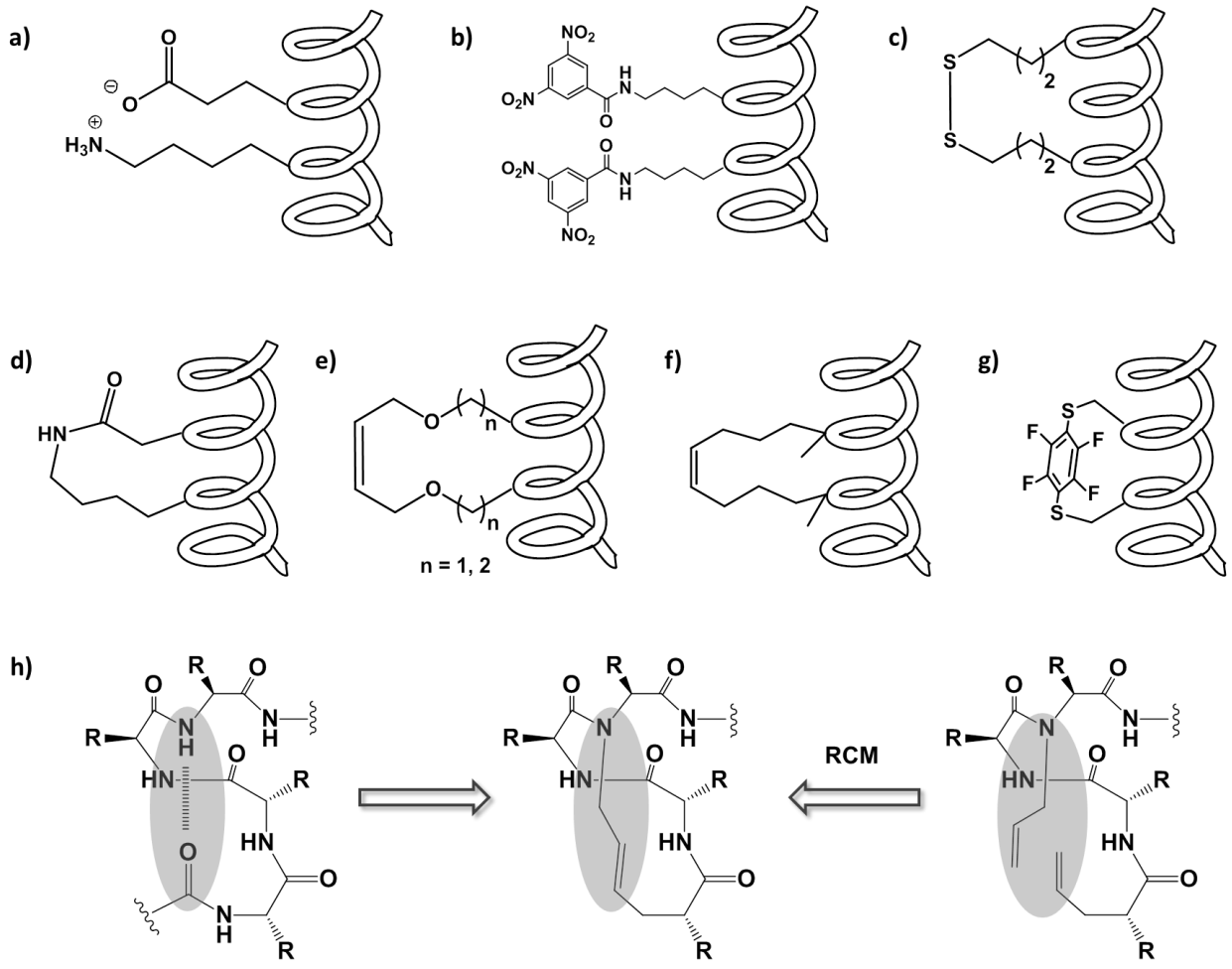

Figure 1.7 Strategies of stabilization of an α-helical peptide, a) salt bridges, b) hydrophobic interactions, c) disulfide bonds, d) lactam-based crosslinking, e) olefin metathesis via O-allyl serine or homoserine, f) α-methyl, α-alkenyl all-hydrocarbon crosslinking, g) perfluoroaryl-cysteine crosslinking, h) hydrogen bond surrogates.

There are three general categories of α-helical stabilization strategies as shown in Figure 1.7. The first category involves the introduction of non-covalent interactions, such as ion-pair salt bridge[64] and hydrophobic interactions[65], to reinforce the α-helical character. The second category involves covalent crosslinking of side chains, which can be achieved

by several different chemistry methods, including disulfide bond formation, lactam bridge formation, olefin metathesis of two alkenyl containing side chains and the recently invented perfluoroaryl-cysteine S_NAr reaction[66-71]. The common idea behind these different crosslinking strategies is to employ two reactive residues on the same face of the peptide helix, usually spanning one or two successive α-helical turns (i.e. i, i + 4 or i, i +7 positions), and promote α-helix nucleation by forming the side chain bridge. A third category of stabilization technique is the hydrogen bond surrogate (HBS) strategy which was developed by Arora and coworkers[72-75]. A classical α-helix is stabilized by the hydrogen bond between the oxygen atom of carbonyl group of a residue at the i position and the main chain amide –NH- at the i + 4 position. Inspired by this feature, one of the main chain hydrogen bonds is replaced by a covalent linkage to produce a highly stabilized, internally cross-linked α-helix. The advantage of this strategy is that the helix surface is not disturbed by the constraining element, allowing them to retain binding affinity to protein targets. All of these methods have shown the ability to chemically stabilize an α-helical peptide, and ongoing efforts are focusing on the optimization of their biological activities and applications in therapeutic and diagnostic uses.

All-Hydrocarbon Stapled α-Helical Peptides

As discussed above, an α-helical conformation can be chemically stabilized by many strategies. However, challenges are still present in terms of the production of stabilized α-helical peptides with properties that are essential to drug candidates, such as robust cell

penetration, proteolytic resistance, and the desired biological activity. Among these stabilized peptides, all-hydrocarbon stapled α-helical peptides ("stapled peptides") produced by ruthenium-mediated olefin metathesis of α-methyl, α-alkenyl di-substituted amino acids, are of particular interest owing to their exciting promise in therapeutic potential since several stapled peptides are currently in clinical trials[76-78].

Stapled peptide technology was developed by Verdine and coworkers at Harvard University in 2000. It employs a dominant negative strategy, in which a short α-helical peptide essential for target binding is chosen based on protein complex structures as a starting template. This small piece of peptide itself is not functional in general since it loses the bioactive conformation without the rest of protein as scaffolding. In order to restore the peptide to its bioactive α-helical conformation, two α-methyl, α-alkenyl disubstituted non-natural amino acids are incorporated into the peptide sequence followed by formation of an all-hydrocarbon "staple" through olefin metathesis (Figure 1.8a)[69]. The peptide stapling strategy uniquely combines two helix-stabilizing elements: α, α-disubstitution that exerts a local helical bias and a covalent macrocyclic bridge that further constrains the peptide into an α-helical conformation. Another advantage of the all-hydrocarbon crosslink over other stabilization methods is that it increases the hydrophobicity of the molecule, resulting in improved cell penetration. Overall, the reinforcement of α-helical character assures the peptide retains the desired secondary structure, which would also make it bind more tightly, resist proteolytic degradation, and exhibit cell permeability.

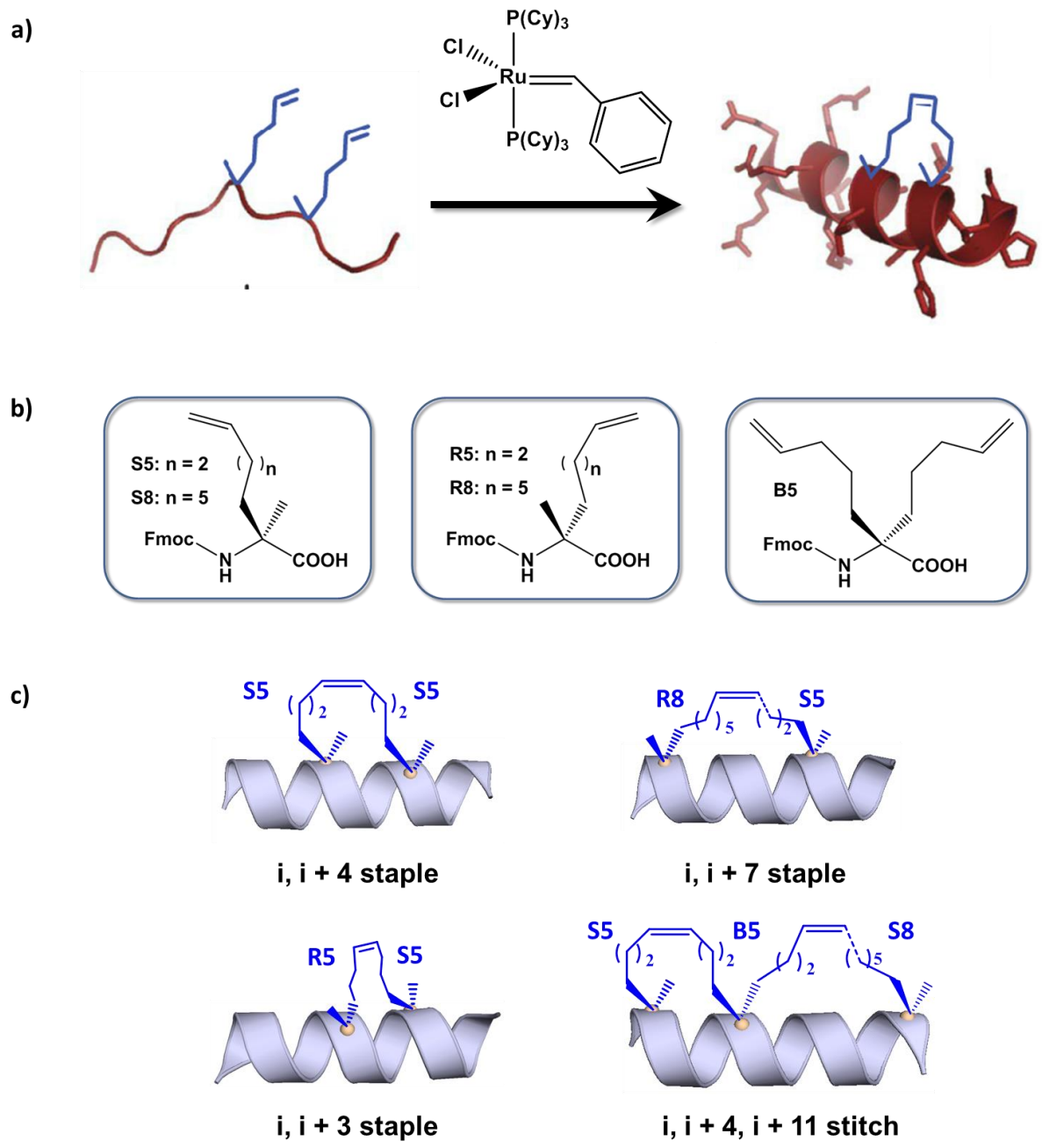

Figure 1.8 All-hydrocarbon stapled peptide technology. a) Schematic illustration of typical peptide stapling. Two alkenyl-bearing non-natural amino acids are incorporated at two positions in the peptide chain and then cross-linked by ruthenium-catalyzed ring-closing olefin metathesis. b) Different types of alkenyl-containing non-natural amino acids with distinct stereochemistry at the α-carbon and varied lengths of alkenyl side chains. c) Four types of stapled peptides with optimized combinations of non-natural amino acids (Figure 1.8a is adapted from Reference 87).

A panel of alkenyl-containing non-natural amino acids with varied stereochemistry at α-carbon and different lengths of alkenyl side chain have been investigated (Figure 1.8b).

The amino acids are named X_Y, where X refers to the stereochemistry (S or R) at the α-carbon and Y is the number of carbon atoms in the alkenyl side chain. In particular, an achiral amino acid B5 with two 5-atom-long alkenyl side chains at α-carbon is also prepared, which is used for tandem stapling. By incorporating these non-natural amino acids into peptide sequences, several types of stapled peptides have been optimized to feature the best α-helical character (Figure 1.8c)[79-82]. Generally, the optimization of the α-helical conformation depends on the nature of the non-natural amino acids (stereochemical configuration and length of alkenyl side chain) as well as their relative disposition in a peptide sequence. For example, two distinct stapling patterns (i, i + 3, and i, i + 4) can be used to obtain an all-hydrocarbon crosslink spanning approximately one α-helical turn. However, the optimized amino acid combination for i, i + 3 is R5 at i position and S5 at i + 3 position, whereas in the i, i + 4 case, placement of an S5 cross-linking amino acid at both the i and i + 4 positions results in the most stabilized peptides. To place an all-hydrocarbon tether over two successive α-helical turns, an R8 is placed at the i position and an S5 is placed at the i + 7 position. Recently, a new version of stapled peptide with tandem crosslinks, a so-called stitched peptide, was also successfully synthesized based on the idea that multiple staples in a single peptide will result in better α-helical stabilization. The stereochemistry of the non-natural amino acids are delicately aligned in stitched peptides, with S5 at the i position, B5 at the i + 4 position, and S8 at the i + 11 position. This arrangement perfectly satisfies the stereochemical requirements for two successive staples, and yields an 8-carbon staple over the i, i + 4 helical turn and an 11-carbon staple over the i + 4, i + 11 helical turns. It is important to point out that these optimized combinations of non-natural amino acids are not dependent on peptide sequences – the different stapling

patterns can be easily grafted to many peptide sequences and result in similar α-helical stabilization.

Stapled peptide targeting is based on a dominant negative strategy, in which the stapled peptides are derived from a binding partner of protein targets. The original design principle for a typical stapled peptide is to keep all the native peptide-protein contacts intact by positioning the all-hydrocarbon crosslink opposite the binding interface[78]. The design process usually starts with a high-resolution protein complex structure that perfectly illustrates the protein-protein interface of interest. Then one binding partner is stripped away until a short α-helical peptide essential for binding is identified. The residues in the peptide sequence that make contacts with the protein target are kept unchanged, whereas the corresponding amino acids on the opposite face are replaced by alkenyl-containing non-natural amino acids. Given that the hydrocarbon staple generally spans one or two α-helical turns, a panel of stapled peptides is designed with all possible staple positions sampled. The resulting stapled peptides with the best α-helical stabilization are then further investigated for biological activities. Interestingly, recent crystallography efforts on stapled-peptide and protein target complex structures indicate that the all-hydrocarbon staple can also contribute to binding, revealing an extra benefit of the stapled peptide strategy. Figure 1.9 shows the crystal structure of the MDM2 protein complexed with the stapled peptide SAH-p53-8 derived from the p53 protein[83]. In addition to retaining the native association of the three essential hydrophobic residues (F19, W23 and L26), the 11-carbon-atom staple of SAH-p53-8 also interacts extensively with MDM2. This observation further suggests new design principles for stapled peptide targeting at protein-protein interfaces. In place of the original strategy of avoiding interruption of

native interactions, peptides can be purposely designed with a staple right at the binding interface as the major driving force of the association. The biological outcome of this particular type of approach is under investigation.

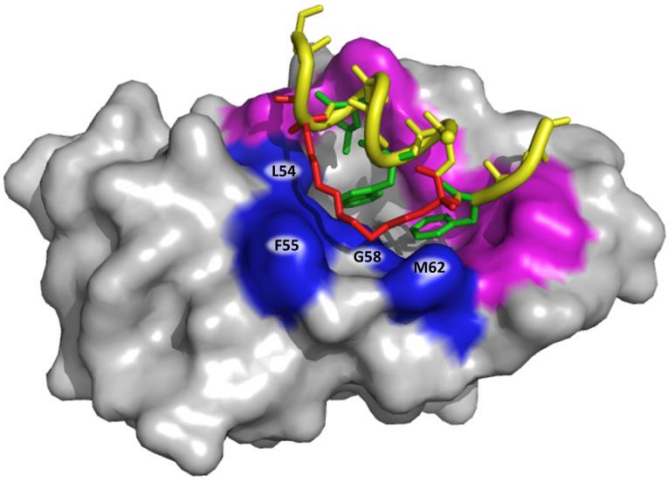

Figure 1.9 The crystal structure of stapled peptide SAH-p53-8 bound to MDM2 (PDB 3V3B) showing that the i, i + 7 staple successfully constrains the p53 derived peptide in α-helical conformation. The peptide retains all native interactions with MDM2 (shown in magenta) and the three key contacting residues in the peptide, F19, W23 and L26, are colored in green. Interestingly, the all-hydrocarbon brace itself (colored in red) also contributes to the binding, with its interacting residues colored in blue.

The stapling strategy can efficiently constrain a peptide in an α-helical conformation, but it does not guarantee any biological activity. The development of a stapled peptide possessing therapeutic potential is typically a multistep process involving iterative optimization of many critical properties, such as binding affinity, cell permeability, aqueous solubility, and *in vivo* activity. For example, in order to improve cell penetration, stapled peptides are designed with positive net charge[84-85]. One method is to avoid unnecessary negatively charged residues by the replacement of non-binding acidic amino acids, namely aspartic acid and glutamic acid, with asparagine and glutamine, respectively. Furthermore, an increase in net charge can also be accomplished by appending additional basic residues, especially arginine at the peptide terminus. Optimization of the binding affinity usually starts with screening different combinations of stapling patterns, hydrocarbon crosslink length, and stapling positions, while still keeping the peptide sequence similar to the

original one. If these attempts are unsuccessful, the stapled peptide can be further optimized by highly developed selection and screening techniques, such as phage and yeast cell surface display[85-86]. It is worth noting that these selection methods do not necessarily require a high-affinity binder as a starting point, making it possible to discover a stapled peptide *de novo*.

The promising features of stapled peptides suggest that they can act as a new class of inhibitors targeting intracellular protein-protein interfaces that have previously been intractable to inhibition by traditional small molecules or protein therapeutics. Indeed, many stapled peptides have been reported recently to show extraordinary biological activity against a large set of protein targets, including transcription factor complexes, oncoproteins, apoptotic mediators, and metabolic enzymes[85, 87-90]. Ongoing efforts include further optimization of binding affinity and specificity, improvement of bioavailability, and understanding the nature of staple peptides, especially their cell penetration properties.

Studies on Cell Penetrating Peptides

The discovery of potent therapeutic peptides portends a promising future in the treatment of various human diseases. However, one of the major hurdles for peptides reaching the clinic involves poor delivery and low bioavailability, which is highlighted by the development of cell permeable peptide therapeutics. Peptides are generally considered to be non-cell permeable macromolecules because of the hydrophilic nature of the amide main chain. However, the past two decades have witnessed a dramatic increase in our knowledge of cell penetrating peptides (CPPs), a class of small peptides which are able to

translocate across plasma membranes. This line of study was initiated with the discovery in 1988 that the HIV-coded Tat regulatory protein could penetrate into living cells[91]. Three years later, a second cell penetrating protein, the antennapedia homeodomain of *Drosophila*, was discovered to be taken up by cells in a non-receptor mediated manner[92]. A short peptide sequence, namely the third helix of the antennapedia protein, was subsequently identified sufficient for cellular internalization[93]. Since then, extensive studies have been performed regarding 1) the discovery of other polypeptides with cell penetration activity, 2) the investigation of the internalization mechanisms of these cell penetrating peptides, and 3) the application of cell penetrating peptides as drug delivery agents.

So far, hundreds of short peptides possessing cellular uptake ability have been characterized. Generally, these cell-penetrating peptides can be categorized into three different groups as shown in table 1.2[94-95]. The first group of cell penetrating peptides is derived from the sequences of protein transduction domains (PTDs), which are defined as polypeptides that can efficiently cross biological membranes by themselves and can be used to facilitate the delivery of diverse cargo to the interior of mammalian cells. Discovery of these peptides usually starts with the identification of already existing proteins exhibiting cellular uptake properties and subsequently location of the minimal peptide sequence that promotes membrane translocation. In order words, the cell penetrating peptides in this category largely retain their native sequences. Among them, the Tat peptide (48 - 60) derived from the transactivating protein Tat of human immunodeficiency virus-type 1 (HIV-1), the penetratin (or Antp) peptide from the third helix of the *Drosophila* antennapedia homeodomain, and transportan, a fusion peptide with 12 residues from

neuropeptide galanin coupled to the N-terminus of another peptide mastoparan are the most well-studied cell penetrating peptides. These CPPs have been used to deliver a variety of non-permeable macromolecules such as peptides, proteins, and oligonucleotides into cells.

Table 1.2 Examples of typical cell penetrating peptides.

Name	Origin	Sequence
Peptides deriving from protein transduction domains		
Tat (48 - 60)	HIV-1 Tat protein	GRKKRRQRRRPPQ
Penetratin (Antp)	Antennapedia homeodomain	RQIKIWFQNRRMKWKK
Transportan	Galanin-mastoparan	GWTLNSAGYLLGKINLKALAALAKKIL
Amphipathic peptides		
Pep-1	Trp-rich motif-SV40 NLS	KETWWETWWTEWSQPKKKRKV
MPG	HIV-1 GP41-SV40 NLS	GALFLGFLGAAGSTMGAWSQPKKKRKV
MAP	N/A	KLALKLALKALKAALKLA
KALA	N/A	WEAKLAKALAKALAKHLAKALAKALKACEA
Other cell penetrating peptides		
Poly-Arg_8	N/A	RRRRRRRR

NLS: nuclear localization sequence

A second category of cell penetrating peptides is amphipathic peptides, which are largely discovered by *de novo* design and feature little biological homology. Regardless of the specific cell penetration pathway, the first step in uptake should be a strong association with the cell membrane. The major characteristic of a plasma membrane is an amphipathic

phospholipid bilayer with an interior hydrophobic core and a negative net charge owing to the phospholipid headgroups and the embedded proteoglycan molecules. In order to gain a strong interaction with the plasma membrane, peptides are often designed as amphipathic molecules having both polar and non-polar residues in their sequences to best accommodate the hydrophobic yet negatively-charged character. In particular, the amphipathicity of these peptides can result from peptide primary sequences by sequential assembly of a domain of hydrophobic residues with a domain of hydrophilic residues (i.e. Pep-1 and MPG), as well as their secondary structures in which hydrophobic and hydrophilic residues are positioned on opposite sides of the peptide (i.e. MAP and KALA). Indeed, plenty of amphipathic peptides designed using both strategies show robust cell penetration properties. In addition, there also exist several other cell penetrating peptides which have been developed using other criteria. For example, cationic polypeptides such as polyarginine, polylysine, and dendrimeric polycationic peptides emphasize on the role of positive charges in the internalization process.

In order to design next generation cell penetrating peptides with improved cellular uptake properties, it is crucial to understand the mechanisms of penetration. There are several different methods reported for the evaluation of the cell penetration of peptides. The most common method is to label a peptide of interest with a fluorophore and to measure the fluorescence of treated cells. For example, confocal microscopy imaging is used to monitor the presence as well as the subcellular localization of internalized peptides. Fluorescence-activated cell sorting (FACS) is another frequently used method to quantitatively measure the uptake of labeled peptides[56, 89]. The major issue with this method is that the fluorescence analysis cannot discriminate internalized peptides from

those bound at the cell surface, and a majority of cell penetrating peptides are known to interact with the cell membrane and are difficult to completely remove by washing. To this end, fluorophore-free strategies have been applied to study the cellular uptake of peptides. For example, Schepartz and coworkers have coupled peptides with a small molecule, dexamethasone (Dex), that can trigger the dimerization and nuclear accumulation of the glucocorticoid receptor (GR). Treatment of cells expressing a GR-GFP fusion protein with Dex-peptide conjugates leads to rapid cytosol-to-nucleus translocation of the GFP signal if the peptide is able to access the cytoplasm. Therefore, the cell penetration ability can be assessed by determining the ratio of GFP signal in the nucleus versus the cytosol[96]. This method successfully circumvents fluorophore-related problems, but it prevents the study of the dynamics of the internalization process, especially the initial association of the peptides with the cell membrane. On the other hand, different biophysical methods and model systems have been utilized to understand the mechanisms of CPP translocation[97]. For example, the cellular uptake process can be systematically monitored by transmission electron microscopy (TEM), or a large unilamellar phospholipid vesicle (LUV) can be used as model membranes to study lipid-peptide interactions.

These distinct strategies greatly enrich our ability to study cell penetration, but the mechanisms by which CPPs enter cells are still under debate. The controversial results are in part due to the different strategies used in the studies, but are also due to the complicated nature of CPPs[98]. For example, the translocation mechanisms are believed to be different for peptides from different families, and it is entirely possible that one peptide can utilize two or more pathways to enter cells[99]. Generally, there are two major uptake mechanisms: direct penetration and energy-dependent endocytosis, each of which is

supported by a list of observations[97]. Direct penetration is an energy-independent process that may include different pathways, such as inverted micelle formation and pore formation[100-101]. For example, pore-formation penetration starts with interaction between the peptide and the cell membrane, followed by peptide barrel formation in the lipid bilayer in which hydrophobic residues are close to the lipid chains and hydrophilic residues form the central pore. On the other hand, energy-dependent endocytosis is also believed to be employed by several CPPs since their penetration ability decreases dramatically at 4°C or in ATP-depleted cells[102-104]. Endocytosis is an energy-consuming process through which cells absorb molecules by engulfing them. It consists of several pathways including phagocytosis for uptake of particles larger than 0.75 μm in diameter, macropinocytosis, and receptor-mediated endocytosis, such as clathrin- and caveolin-dependent endocytosis[105-106]. The uptake mechanism of CPPs have been extensively investigated using strategies that typically employ small molecule inhibitors to block certain cell uptake pathways which CPPs are believed likely to utilize. However, controversial and often contradictory conclusions are commonly received. For the Tat (48 - 60) peptide, early studies suggested a direct penetration model in which the peptide associates with the plasma membrane through electrostatic interactions, disrupting the membrane enough to allow the peptide to cross the membrane. However, this mechanism has been questioned recently, and a macropinocytosis pathway, in particular clathrin-mediated endocytosis, has been proposed[104, 107-108]. Additionally, it is likely that there are important unidentified factors regulating the intracellular trafficking process. Taken together, hundreds of cell penetrating peptides with little sequence homology exhibit

robust cellular uptake, and there is believed to be no single answer to the mystery of how CPPs traverse the cell membrane.

All-hydrocarbon stapled peptides as a new class of potentially therapeutic molecules have been observed to penetrate the cell membrane at micromolar concentrations through one or more energy-dependent uptake mechanisms that remain unidentified. The work presented in this thesis has focused on systematic elucidation of the cell penetration processes and the development of stapled peptides that hijack an endogenous ubiquitin-proteasome pathway to exhibit improved biological activity.

Reference

1. Hopkins, A. L.; Groom, C. R., The druggable genome. *Nat Rev Drug Discov* **2002,** *1* (9), 727-730.

2. Russ, A. P.; Lampel, S., The druggable genome: an update. *Drug Discov Today* **2005,** *10* (23-24), 1607-1610.

3. Baldwin, A. S., The NF-kappa B and I kappa B proteins: New discoveries and insights. *Annu Rev Immunol* **1996,** *14*, 649-683.

4. Spiegel, A. M.; Weinstein, L. S.; Shenker, A., Abnormalities in G-Protein-Coupled Signal-Transduction Pathways in Human-Disease. *J Clin Invest* **1993,** *92* (3), 1119-1125.

5. Mendonsa, G.; Dobrowolska, J.; Lin, A.; Vijairania, P.; Jong, Y. J. I.; Baenziger, N. L., Molecular Profiling Reveals Diversity of Stress Signal Transduction Cascades in Highly Penetrant Alzheimer's Disease Human Skin Fibroblasts. *Plos One* **2009,** *4* (2).

6. Newman, D. J.; Cragg, G. M., Natural products as sources of new drugs over the last 25 years. *J Nat Prod* **2007,** *70* (3), 461-477.

7. Zhang, J. M.; Yang, P. L.; Gray, N. S., Targeting cancer with small molecule kinase inhibitors. *Nat Rev Cancer* **2009,** *9* (1), 28-39.

8. Leader, B.; Baca, Q. J.; Golan, D. E., Protein therapeutics: A summary and pharmacological classification. *Nat Rev Drug Discov* **2008,** *7* (1), 21-39.

9. Pavlou, A. K.; Reichert, J. M., Recombinant protein therapeutics - success rates, market trends and values to 2010. *Nat Biotechnol* **2004,** *22* (12), 1513-1519.

10. Crews, C. M., Targeting the Undruggable Proteome: The Small Molecules of My Dreams. *Chem Biol* **2010,** *17* (6), 551-555.

11. Hopkins, A. L.; Groom, C. R., Target analysis: a priori assessment of druggability. *Ernst Schering Research Foundation workshop* **2003,** (42), 11-7.

12. Vyas, S. P.; Singh, A.; Sihorkar, V., Ligand-receptor-mediated drug delivery: an emerging paradigm in cellular drug targeting. *Critical reviews in therapeutic drug carrier systems* **2001,** *18* (1), 1-76.

13. Deng, X. M.; Dzamko, N.; Prescott, A.; Davies, P.; Liu, Q. S*., et al.*, Characterization of a selective inhibitor of the Parkinson's disease kinase LRRK2. *Nat Chem Biol* **2011,** *7* (4), 203-205.

14. Jubb, H.; Higueruelo, A. P.; Winter, A.; Blundell, T. L., Structural biology and drug discovery for protein-protein interactions. *Trends Pharmacol Sci* **2012,** *33* (5), 241-248.

15. Arkin, M. R.; Wells, J. A., Small-molecule inhibitors of protein-protein interactions: Progressing towards the dream. *Nat Rev Drug Discov* **2004,** *3* (4), 301-317.

16. Dobson, C. M., Chemical space and biology. *Nature* **2004,** *432* (7019), 824-828.

17. Lipinski, C.; Hopkins, A., Navigating chemical space for biology and medicine. *Nature* **2004,** *432* (7019), 855-861.

18. Verdine, G. L.; Walensky, L. D., The challenge of drugging undruggable targets in cancer: Lessons learned from targeting BCL-2 family members. *Clin Cancer Res* **2007,** *13* (24), 7264-7270.

19. Adhikary, S.; Eilers, M., Transcriptional regulation and transformation by MYC proteins. *Nat Rev Mol Cell Bio* **2005,** *6* (8), 635-645.

20. Rajalingam, K.; Schreck, R.; Rapp, U. R.; Albert, S., Ras oncogenes and their downstream targets. *Bba-Mol Cell Res* **2007,** *1773* (8), 1177-1195.

21. Overington, J. P.; Al-Lazikani, B.; Hopkins, A. L., Opinion - How many drug targets are there? *Nat Rev Drug Discov* **2006,** *5* (12), 993-996.

22. Barker, A.; Kettle, J. G.; Nowak, T.; Pease, J. E., Expanding medicinal chemistry space. *Drug Discov Today* **2013,** *18* (5-6), 298-304.

23. Schreiber, S. L., Molecular diversity by design. *Nature* **2009,** *457* (7226), 153-154.

24. Schreiber, S. L., Target-oriented and diversity-oriented organic synthesis in drug discovery. *Science* **2000,** *287* (5460), 1964-1969.

25. Galloway, W. R. J. D.; Isidro-Llobet, A.; Spring, D. R., Diversity-oriented synthesis as a tool for the discovery of novel biologically active small molecules. *Nat Commun* **2010,** *1*.

26. Dandapani, S.; Marcaurelle, L. A., Current strategies for diversity-oriented synthesis. *Curr Opin Chem Biol* **2010,** *14* (3), 362-370.

27. Dandapani, S.; Marcaurelle, L. A., Accessing new chemical space for 'undruggable' targets. *Nat Chem Biol* **2010,** *6* (12), 861-863.

28. Bradner, J. E.; McPherson, O. M.; Mazitschek, R.; Barnes-Seeman, D.; Shen, J. P.*, et al.*, A robust small-molecule microarray platform for screening cell lysates. *Chem Biol* **2006,** *13* (5), 493-504.

29. Wheeler, G. N.; Field, R. A.; Tomlinson, M. L., Phenotypic Screens with Model Organisms. *Chemical Genomics* **2012**, 121-136.

30. Korn, K.; Krausz, E., Cell-based high-content screening of small-molecule libraries. *Curr Opin Chem Biol* **2007,** *11* (5), 503-510.

31. Erlanson, D. A., Introduction to Fragment-Based Drug Discovery. *Top Curr Chem* **2012,** *317*, 1-32.

32. Congreve, M.; Chessari, G.; Tisi, D.; Woodhead, A. J., Recent developments in fragment-based drug discovery. *Journal of medicinal chemistry* **2008,** *51* (13), 3661-3680.

33. Erlanson, D. A.; McDowell, R. S.; O'Brien, T., Fragment-based drug discovery. *Journal of medicinal chemistry* **2004,** *47* (14), 3463-3482.

34. Erlanson, D. A.; Wells, J. A.; Braisted, A. C., Tethering: Fragment-based drug discovery. *Annu Rev Bioph Biom* **2004,** *33*, 199-223.

35. Bogan, A. A.; Thorn, K. S., Anatomy of hot spots in protein interfaces. *J Mol Biol* **1998,** *280* (1), 1-9.

36. Wells, J. A.; McClendon, C. L., Reaching for high-hanging fruit in drug discovery at protein-protein interfaces. *Nature* **2007,** *450* (7172), 1001-1009.

37. Yang, C. Y.; Wang, S. M., Computational Analysis of Protein Hotspots. *Acs Med Chem Lett* **2010,** *1* (3), 125-129.

38. Wang, W.; Wang, E. Q.; Balthasar, J. P., Monoclonal Antibody Pharmacokinetics and Pharmacodynamics. *Clin Pharmacol Ther* **2008,** *84* (5), 548-558.

39. Zanders, E. D., Biotherapeutics. *Science and Business of Drug Discovery: Demystifying the Jargon* **2011**, 159-177.

40. Cragg, G. M.; Newman, D. J., Natural products: A continuing source of novel drug leads. *Bba-Gen Subjects* **2013,** *1830* (6), 3670-3695.

41. Kaspar, A. A.; Reichert, J. M., Future directions for peptide therapeutics development. *Drug Discov Today* **2013,** *18* (17-18), 807-817.

42. Lien, S.; Lowman, H. B., Therapeutic peptides. *Trends Biotechnol* **2003,** *21* (12), 556-562.

43. Saladin, P. M.; Zhang, B. D. D.; Reichert, J. M., Current trends in the clinical development of peptide therapeutics. *Idrugs* **2009,** *12* (12), 779-784.

44. Garcia-Echeverria, C., Peptides and peptidomimetics as tool compounds and therapeutic agents in oncology. *Int J Pept Res Ther* **2006,** *12* (1), 1-1.

45. Sato, A. K.; Viswanathan, M.; Kent, R. B.; Wood, C. R., Therapeutic peptides: technological advances driving peptides into development. *Curr Opin Biotech* **2006,** *17* (6), 638-642.

46. Vlieghe, P.; Lisowski, V.; Martinez, J.; Khrestchatisky, M., Synthetic therapeutic peptides: science and market. *Drug Discov Today* **2010,** *15* (1-2), 40-56.

47. Latham, P. W., Therapeutic peptides revisited. *Nat Biotechnol* **1999,** *17* (8), 755-757.

48. Moore, S. J.; Cochran, J. R., Engineering Knottins as Novel Binding Agents. *Method Enzymol* **2012,** *503*, 223-251.

49. Gracy, J.; Le-Nguyen, D.; Gelly, J. C.; Kaas, Q.; Heitz, A.; Chiche, L., KNOTTIN: the knottin or inhibitor cystine knot scaffold in 2007. *Nucleic acids research* **2008,** *36* (Database issue), D314-9.

50. Kolmar, H., Alternative binding proteins: biological activity and therapeutic potential of cystine-knot miniproteins. *The FEBS journal* **2008,** *275* (11), 2684-90.

51. Blundell, T. L.; Pitts, J. E.; Tickle, I. J.; Wood, S. P.; Wu, C. W., X-Ray-Analysis (1.4-a Resolution) of Avian Pancreatic-Polypeptide - Small Globular Protein Hormone. *P Natl Acad Sci-Biol* **1981,** *78* (7), 4175-4179.

52. Chin, J. W.; Schepartz, A., Design and Evolution of a Miniature Bcl-2 Binding Protein. *Angew Chem Int Ed Engl* **2001,** *40* (20), 3806-3809.

53. Chin, J. W.; Grotzfeld, R. M.; Fabian, M. A.; Schepartz, A., Methodology for optimizing functional miniature proteins based on avian pancreatic polypeptide using phage display. *Bioorganic & medicinal chemistry letters* **2001,** *11* (12), 1501-1505.

54. Hodges, A. M.; Schepartz, A., Engineering a monomeric miniature protein. *Journal of the American Chemical Society* **2007,** *129* (36), 11024-+.

55. KieberEmmons, T.; Murali, R.; Greene, M. I., Therapeutic peptides and peptidomimetics. *Curr Opin Biotech* **1997,** *8* (4), 435-441.

56. Gracia, S. R.; Gaus, K.; Sewald, N., Synthesis of chemically modified bioactive peptides: recent advances, challenges and developments for medicinal chemistry. *Future Med Chem* **2009,** *1* (7), 1289-1310.

57. Craik, D. J.; Clark, R. J.; Daly, N. L., Potential therapeutic applications of the cyclotides and related cystine knot mini-proteins. *Expert Opin Inv Drug* **2007,** *16* (5), 595-604.

58. Levine, D. P., Vancomycin: A history. *Clin Infect Dis* **2006,** *42*, S5-S12.

59. Borel, J. F., History of the discovery of cyclosporin and of its early pharmacological development. *Wien Klin Wochenschr* **2002,** *114* (12), 433-437.

60. Bullock, B. N.; Jochim, A. L.; Arora, P. S., Assessing helical protein interfaces for inhibitor design. *Journal of the American Chemical Society* **2011,** *133* (36), 14220-3.

61. Lessene, G.; Czabotar, P. E.; Colman, P. M., BCL-2 family antagonists for cancer therapy. *Nat Rev Drug Discov* **2008,** *7* (12), 989-1000.

62. Baldwin, A. S., Jr., The NF-kappa B and I kappa B proteins: new discoveries and insights. *Annu Rev Immunol* **1996,** *14*, 649-83.

63. Blackwood, E. M.; Eisenman, R. N., Max - a Helix-Loop-Helix Zipper Protein That Forms a Sequence-Specific DNA-Binding Complex with Myc. *Science* **1991,** *251* (4998), 1211-1217.

64. Marqusee, S.; Baldwin, R. L., Helix stabilization by Glu-...Lys+ salt bridges in short peptides of de novo design. *Proceedings of the National Academy of Sciences of the United States of America* **1987,** *84* (24), 8898-902.

65. Albert, J. S.; Hamilton, A. D., Stabilization of Helical Domains in Short Peptides Using Hydrophobic Interactions. *Biochemistry-Us* **1995,** *34* (3), 984-990.

66. de Vega, M. J. P.; Garcia-Aranda, M. I.; Gonzalez-Muniz, R., A Role for Ring-Closing Metathesis in Medicinal Chemistry: Mimicking Secondary Architectures in Bioactive Peptides. *Med Res Rev* **2011,** *31* (5), 677-715.

67. Spokoyny, A. M.; Zou, Y. K.; Ling, J. J.; Yu, H. T.; Lin, Y. S.; Pentelute, B. L., A Perfluoroaryl-Cysteine SNAr Chemistry Approach to Unprotected Peptide Stapling. *Journal of the American Chemical Society* **2013,** *135* (16), 5946-5949.

68. Blackwell, H. E.; Grubbs, R. H., Highly efficient synthesis of covalently cross-linked peptide helices by ring-closing metathesis. *Angew Chem Int Edit* **1998,** *37* (23), 3281-3284.

69. Schafmeister, C. E.; Po, J.; Verdine, G. L., An all-hydrocarbon cross-linking system for enhancing the helicity and metabolic stability of peptides. *Journal of the American Chemical Society* **2000,** *122* (24), 5891-5892.

70. Houston, M. E.; Campbell, A. P.; Lix, B.; Kay, C. M.; Sykes, B. D.; Hodges, R. S., Lactam bridge stabilization of alpha-helices: The role of hydrophobicity in controlling

dimeric versus monomeric alpha-helices. *Biochemistry-Us* **1996,** *35* (31), 10041-10050.

71. Scholtz, J. M.; Baldwin, R. L., The Mechanism of Alpha-Helix Formation by Peptides. *Annu Rev Bioph Biom* **1992,** *21*, 95-118.

72. Henchey, L. K.; Porter, J. R.; Ghosh, I.; Arora, P. S., High Specificity in Protein Recognition by Hydrogen-Bond-Surrogate alpha-Helices: Selective Inhibition of the p53/MDM2 Complex. *Chembiochem* **2010,** *11* (15), 2104-2107.

73. Henchey, L. K.; Kushal, S.; Dubey, R.; Chapman, R. N.; Olenyuk, B. Z.; Arora, P. S., Inhibition of Hypoxia Inducible Factor 1-Transcription Coactivator Interaction by a Hydrogen Bond Surrogate alpha-Helix. *Journal of the American Chemical Society* **2010,** *132* (3), 941-+.

74. Patgiri, A.; Jochim, A. L.; Arora, P. S., A Hydrogen Bond Surrogate Approach for Stabilization of Short Peptide Sequences in alpha-Helical Conformation. *Accounts Chem Res* **2008,** *41* (10), 1289-1300.

75. Chapman, R. N.; Dimartino, G.; Arora, P. S., A highly stable short alpha-helix constrained by a main-chain hydrogen-bond surrogate. *Journal of the American Chemical Society* **2004,** *126* (39), 12252-12253.

76. Chang, Y. S.; Graves, B.; Guerlavais, V.; Tovar, C.; Packman, K.*, et al.*, Stapled alpha-helical peptide drug development: A potent dual inhibitor of MDM2 and MDMX for p53-dependent cancer therapy. *Proceedings of the National Academy of Sciences of the United States of America* **2013,** *110* (36), E3445-E3454.

77. LaBelle, J. L.; Katz, S. G.; Bird, G. H.; Gavathiotis, E.; Stewart, M. L.*, et al.*, A stapled BIM peptide overcomes apoptotic resistance in hematologic cancers. *J Clin Invest* **2012,** *122* (6), 2018-31.

78. Verdine, G. L.; Hilinski, G. J., Stapled Peptides for Intracellular Drug Targets. *Method Enzymol* **2012,** *503*, 3-33.

79. Kim, Y. W.; Shim, S. Y.; Kolar, M. J.; Kutchukian, P. S.; Verdine, G. L., i,i+3 Stapling: Highly stereospecific ring-closing metathesis on a-helices. *Abstr Pap Am Chem S* **2010,** *240*.

80. Kim, Y. W.; Kutchukian, P. S.; Verdine, G. L., Introduction of All-Hydrocarbon i,i+3 Staples into alpha-Helices via Ring-Closing Olefin Metathesis. *Organic letters* **2010,** *12* (13), 3046-3049.

81. Kim, Y. W.; Kutchukian, P. S.; Crenshaw, C. M.; Stanton, S. S.; Chang, A.; Verdine, G. L., Stitching a-helical peptides by tandem ring-closing metathesis. *Abstr Pap Am Chem S* **2010,** *240*.

82. Kim, Y. W.; Verdine, G. L., Stereochemical effects of all-hydrocarbon tethers in i,i+4 stapled peptides. *Bioorganic & medicinal chemistry letters* **2009,** *19* (9), 2533-2536.

83. Baek, S.; Kutchukian, P. S.; Verdine, G. L.; Huber, R.; Holak, T. A.; Lee, K. W.; Popowicz, G. M., Structure of the Stapled p53 Peptide Bound to Mdm2. *Journal of the American Chemical Society* **2012,** *134* (1), 103-106.

84. Bernal, F.; Tyler, A. F.; Korsmeyer, S. J.; Walensky, L. D.; Verdine, G. L., Reactivation of the p53 tumor suppressor pathway by a stapled p53 peptide. *Journal of the American Chemical Society* **2007,** *129* (16), 5298-5298.

85. Grossmann, T. N.; Yeh, J. T. H.; Bowman, B. R.; Chu, Q.; Moellering, R. E.; Verdine, G. L., Inhibition of oncogenic Wnt signaling through direct targeting of beta-catenin. *Proceedings of the National Academy of Sciences of the United States of America* **2012,** *109* (44), 17942-17947.

86. Brown, C. J.; Quah, S. T.; Jong, J.; Goh, A. M.; Chiam, P. C.*, et al.*, Stapled Peptides with Improved Potency and Specificity That Activate p53. *Acs Chem Biol* **2013,** *8* (3), 506-512.

87. Moellering, R. E.; Cornejo, M.; Davis, T. N.; Del Bianco, C.; Aster, J. C.*, et al.*, Direct inhibition of the NOTCH transcription factor complex. *Nature* **2009,** *462* (7270), 182-U57.

88. Phillips, C.; Roberts, L. R.; Schade, M.; Bazin, R.; Bent, A.*, et al.*, Design and Structure of Stapled Peptides Binding to Estrogen Receptors. *Journal of the American Chemical Society* **2011,** *133* (25), 9696-9699.

89. Walensky, L. D.; Kung, A. L.; Escher, I.; Malia, T. J.; Barbuto, S.; Wright, R. D.; Wagner, G.; Verdine, G. L.; Korsmeyer, S. J., Activation of apoptosis in vivo by a hydrocarbon-stapled BH3 helix. *Science* **2004,** *305* (5689), 1466-1470.

90. Kim, W.; Bird, G. H.; Neff, T.; Guo, G. J.; Kerenyi, M. A.; Walensky, L. D.; Orkin, S. H., Targeted disruption of the EZH2-EED complex inhibits EZH2-dependent cancer. *Nat Chem Biol* **2013,** *9* (10), 643-650.

91. Frankel, A. D.; Pabo, C. O., Cellular Uptake of the Tat Protein from Human Immunodeficiency Virus. *Cell* **1988,** *55* (6), 1189-1193.

92. Joliot, A.; Pernelle, C.; Deagostinibazin, H.; Prochiantz, A., Antennapedia Homeobox Peptide Regulates Neural Morphogenesis. *Proceedings of the National Academy of Sciences of the United States of America* **1991,** *88* (5), 1864-1868.

93. Derossi, D.; Joliot, A. H.; Chassaing, G.; Prochiantz, A., The 3rd Helix of the Antennapedia Homeodomain Translocates through Biological-Membranes. *J Biol Chem* **1994,** *269* (14), 10444-10450.

94. Heitz, F.; Morris, M. C.; Divita, G., Twenty years of cell-penetrating peptides: from molecular mechanisms to therapeutics. *Brit J Pharmacol* **2009,** *157* (2), 195-206.

95. Deshayes, S.; Morris, M. C.; Divita, G.; Heitz, F., Cell-penetrating peptides: tools for intracellular delivery of therapeutics. *Cell Mol Life Sci* **2005,** *62* (16), 1839-1849.

96. Appelbaum, J. S.; LaRochelle, J. R.; Smith, B. A.; Balkin, D. M.; Holub, J. M.; Schepartz, A., Arginine topology controls escape of minimally cationic proteins from early endosomes to the cytoplasm. *Chem Biol* **2012,** *19* (7), 819-30.

97. Magzoub, M.; Graslund, A., Cell-penetrating peptides: small from inception to application. *Q Rev Biophys* **2004,** *37* (2), 147-195.

98. Richard, J. P.; Melikov, K.; Vives, E.; Ramos, C.; Verbeure, B.; Gait, M. J.; Chernomordik, L. V.; Lebleu, B., Cell-penetrating peptides - A reevaluation of the mechanism of cellular uptake. *J Biol Chem* **2003,** *278* (1), 585-590.

99. Subrizi, A.; Tuominen, E.; Bunker, A.; Rog, T.; Antopolsky, M.; Urtti, A., Tat(48-60) peptide amino acid sequence is not unique in its cell penetrating properties and cell-surface glycosaminoglycans inhibit its cellular uptake. *Journal of controlled release : official journal of the Controlled Release Society* **2012,** *158* (2), 277-85.

100. Plenat, T.; Deshayes, S.; Boichot, S.; Milhiet, P. E.; Cole, R. B.; Heitz, F.; Le Grimellec, C., Interaction of primary amphipathic cell-penetrating peptides with phospholipid-supported monolayers. *Langmuir* **2004,** *20* (21), 9255-9261.

101. Herce, H. D.; Garcia, A. E.; Litt, J.; Kane, R. S.; Martin, P.; Enrique, N.; Rebolledo, A.; Milesi, V., Arginine-Rich Peptides Destabilize the Plasma Membrane, Consistent with a Pore Formation Translocation Mechanism of Cell-Penetrating Peptides. *Biophys J* **2009,** *97* (7), 1917-1925.

102. Lindgren, M.; Hallbrink, M.; Prochiantz, A.; Langel, U., Cell-penetrating peptides. *Trends Pharmacol Sci* **2000,** *21* (3), 99-103.

103. Pooga, M.; Hallbrink, M.; Zorko, M.; Langel, U., Cell penetration by transportan. *Faseb J* **1998,** *12* (1), 67-77.

104. Kaplan, I. M.; Wadia, J. S.; Dowdy, S. F., Cationic TAT peptide transduction domain enters cells by macropinocytosis. *Journal of Controlled Release* **2005,** *102* (1), 247-253.

105. Marsh, M.; McMahon, H. T., The structural era of endocytosis. *Science* **1999,** *285* (5425), 215-220.

106. Simons, K.; Ikonen, E., Functional rafts in cell membranes. *Nature* **1997,** *387* (6633), 569-572.

107. Richard, J. P.; Melikov, K.; Brooks, H.; Prevot, P.; Lebleu, B.; Chernomordik, L. V., Cellular uptake of unconjugated TAT peptide involves clathrin-dependent endocytosis and heparan sulfate receptors. *J Biol Chem* **2005,** *280* (15), 15300-15306.

108. Brooks, H.; Lebleu, B.; Vives, E., Tat peptide-mediated cellular delivery: back to basics. *Adv Drug Deliver Rev* **2005,** *57* (4), 559-577.

Chapter II Targeted β-catenin Ubiquitination and Degradation Using Bifunctional Stapled Peptides

The Canonical Wnt Signaling Pathway

The Wnt (**W**ingless and I**nt**-1) signaling cascade regulates a large number of biological activities from early development to adult life in all animals. The discovery of Wnt signaling was initiated in 1982 by identification of the *Wnt1* gene (originally named *Int-1*), a proto-oncogene encoding a secreted, cysteine-rich protein which is activated upon integration of mouse mammary tumor virus in virally induced breast tumors[1]. The homolog of *Wnt-1* gene in *Drosophila melanogaster* was discovered five years later in 1987[2]. It was determined to be the previously characterized *Drosophila* gene known as *Wingless*, which controls segment polarity during larval development[3]. Since then, a variety of genes have been identified as core components in the Wnt signaling cascade, and significant progress has been made toward understanding the mechanism of the Wnt regulation in health and disease[4-5].

The term "Wnt signaling" does not simply stand for a single purpose signal transduction pathway. Rather, it refers to a diverse collection of pathways triggered by Wnt ligand-receptor interactions that regulate cell behavior in multiple ways, such as cell polarity, proliferation, differentiation, survival and self-renewal[6]. Diversity in Wnt signaling is derived from the large number of its components, including 19 Wnt ligands, 10 receptors, as well as its signaling transduction components[7]. The most well-known Wnt pathway is

the highly conserved canonical Wnt/β-catenin signaling pathway, which regulates the stability of the transcription coactivator β-catenin and subsequent β-catenin-dependent gene expression[8].

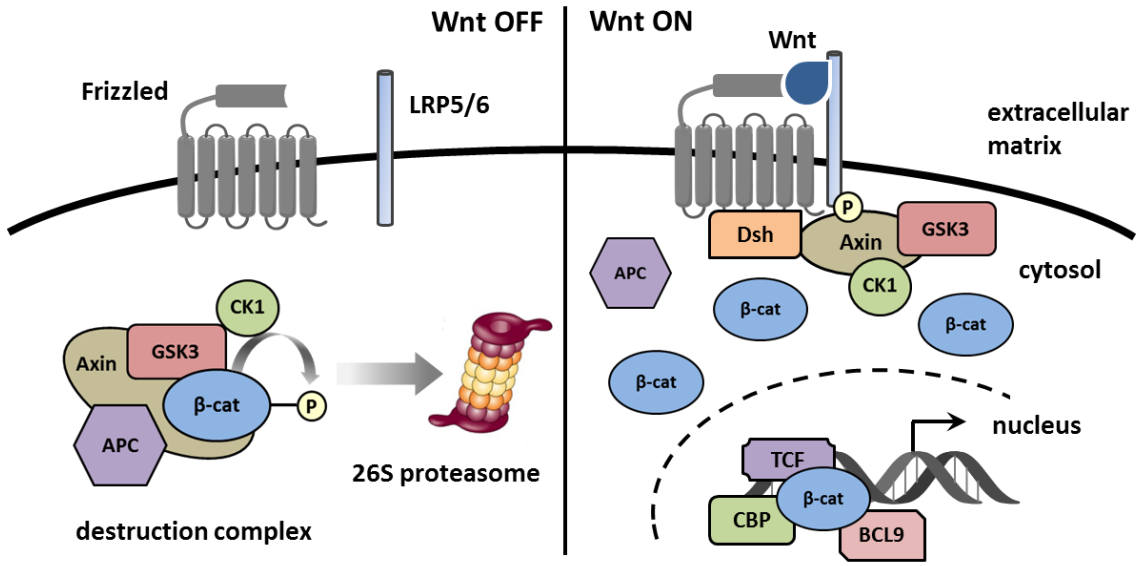

Figure 2.1 The canonical Wnt signaling pathway with its major components in the "Wnt OFF" (Left) and "Wnt ON" (Right) states. BCL9 and CBP are transcriptional coactivators.

The canonical Wnt signaling pathway initiates following the engagement of secreted Wnt proteins with the receptors at cell membrane, which causes an accumulation of β-catenin in the cytoplasm and its eventual translocation into the nucleus to activate transcription factors belonging to the T cell factor/lymphoid enhancer factor (TCF/LEF) family and thereby enhances downstream gene expression[9]. In this manner, β-catenin serves as a hub to connect the canonical Wnt signal from the plasma membrane to the nucleus. In the absence of Wnt ligands, the cytosolic β-catenin protein level is kept low due to phosphorylation-dependent ubiquitination and degradation. A multicomponent destruction complex for β-catenin is assembled by the association of scaffolding protein Axin, tumor suppressor protein adenomatous polyposis coli (APC), casein kinase 1 (CK1)

and glycogen synthase kinase 3 (GSK3). Phosphorylation of β-catenin is performed by the sequential action of CK1 and GSK3 on residues Ser45 and Ser33, Ser37, Thr41, respectively. Phosphorylated β-catenin is then recognized by β-Trcp, an E3 ubiquitin ligase subunit, and is ubiquitinated and degraded through the ubiquitin-proteasome pathway (Figure 2.1 Left)[10-11].

Upon Wnt stimulation, the Wnt proteins associate with a heterodimeric receptor complex consisting of two distinct membrane bound proteins. One belongs to the Frizzled (Fz) family of serpentine proteins, and the other is low-density-lipoprotein receptor related protein LRP5/6. The binding of Wnt ligands to the LRP receptor induces phosphorylation on the cytoplasmic tail of LRP protein, which provides a docking site for Axin association. Meanwhile the intracellular domain of Wnt ligand bound the Fz receptor interacts with Dishevelled (Dsh) protein, facilitating the interaction between the LRP tail and Axin. The engagement of Axin to the plasma membrane via LRP disrupts the β-catenin destruction complex, resulting in the inhibition of β-catenin phosphorylation and its subsequent degradation. Consequently, the accumulated β-catenin undergoes translocation to the nucleus, where it recruits powerful transcription coactivators, such as CREB-binding protein (CBP) and B-cell lymphoma 9 protein (BCL9) to DNA-bound transcription factors of the TCF/LEF family and eventually activates downstream gene expression (Figure 2.1 Right)[12-13].

Activated Wnt signaling serves a critical role in many tissue types during embryonic development[14]. In adults, activated Wnt signaling also has an essential function in stem cell maintenance and tissue regeneration[15]. Given the importance of Wnt signaling in stem cell

biology, it is not surprising that inappropriate activation of Wnt signaling is strongly implicated in the initiation and progression of several types of cancer[16]. For example, approximately 90% of colorectal cancers are associated with high-level of constitutive activation of Wnt signaling[17]. In most cases, aberrant activation of the Wnt signaling pathway results from the reduced ability of the destruction complex to recruit and degrade β-catenin. Mutations and truncations have been found in APC, Axin and β-catenin itself to prevent formation of the destruction complex[5]. Recent studies reveal that malfunctioning of the Wnt signaling pathway is not only involved in the onset of numerous cancers, but also results in many other diseases, for example, metabolic disease, bone disease, and *etc*.[18-19] Therefore, targeting the Wnt signaling pathway is of particular interest in treatment of human diseases.

β-catenin - an Appealing Target in Drug Discovery

The broad involvement of Wnt signaling in disease has driven extensive research efforts at targeting the Wnt pathway with small molecules. Several compounds, as listed in Table 2.1, have been reported to inhibit Wnt-dependent signaling by phenotypic screening of small molecule libraries[20-25]. Among them, the most promising compounds so far either inhibit tankyrase, an Axin destabilizer (XAV939 and IWR-1), or activate CK1α (pyrvinium), which affect Wnt signaling primarily by stimulating the activity of the β-catenin destruction complex. Although these efforts have provided valuable tool compounds, the therapeutic utilities are limited by the fact that most disease-causing mutations are either in APC or in pathway components downstream of the destruction complex[26]. Additionally, tankyrase

and CK1α are involved in many other cellular processes, increasing the risk of undesirable off-target effects. The most effective target in the canonical Wnt signaling pathway is β-catenin, since it serves as a critical junction in signaling and operates downstream gene expressions. However, direct targeting of β-catenin protein has yielded limited success thus far.

Table 2.1 Small molecule inhibitors in the canonical Wnt signaling pathway.

Small Molecule	Target	Reference
XAV939	tankyrase	20
IWR-1	Axin	21
IWP	Porcupine	22
Pyrvinium	CK1	23
PKF115-584	TCF/β-catenin	24
ICG-001	CREB-binding protein	25

The β-catenin protein is a conserved dual function protein exerting a crucial role in developmental and homeostatic processes. Besides its function in signal transduction in canonical Wnt signaling cascade as discussed above, β-catenin plays a second role in regulating the coordination of cell-cell adhesion by association with the cytoplasmic tail of cadherin family proteins[27]. Human β-catenin is a protein with 781 residues, consisting of a central region (residues 141-664) made up of 12 Armadillo (ARM) repeats, which is flanked by distinct N- and C-terminal domains, NTD and CTD respectively. A conserved helix-C (residues 667-683) is located proximally to the CTD, adjacent to the last ARM repeat[28]. The NTD and the CTD are structurally flexible, but the central armadillo domain is

a relatively rigid scaffold, which serves as an interaction platform for many binding partners, and thereby involved in diverse cellular processes (Figure 2.2).

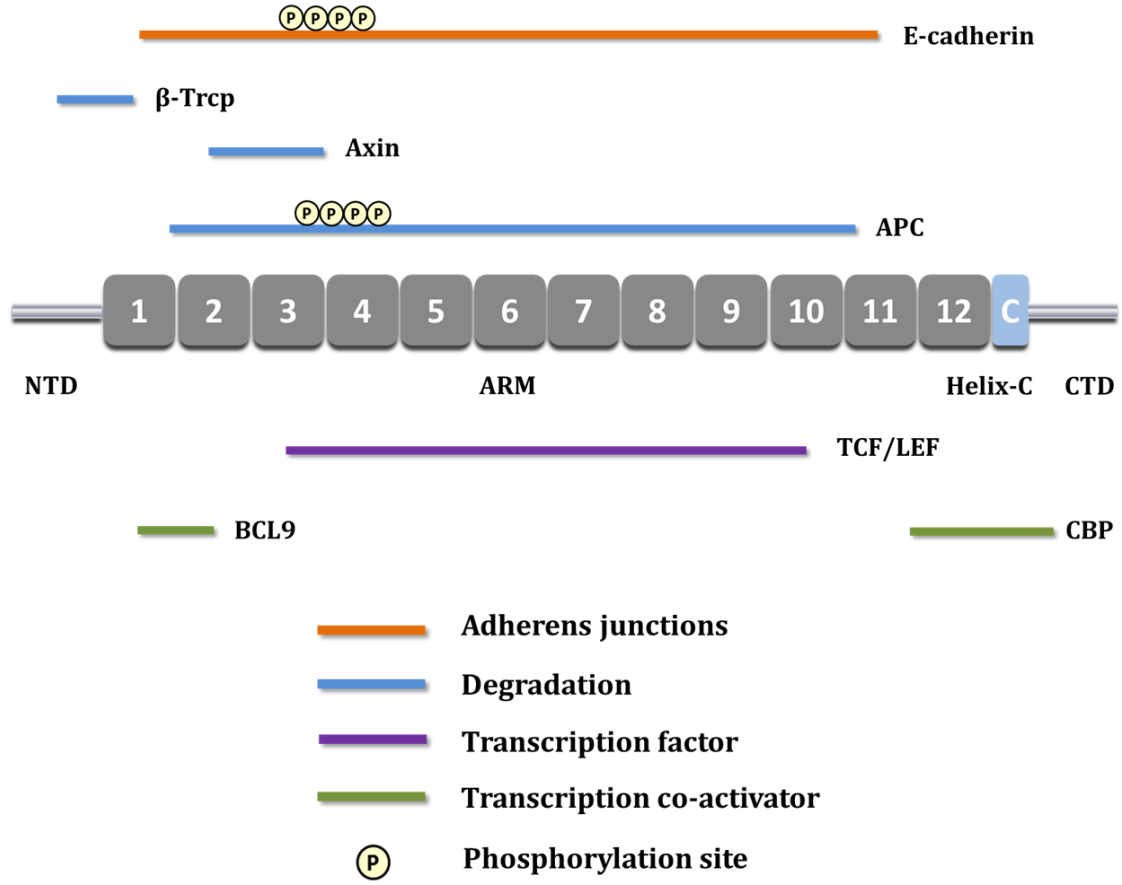

Figure 2.2 Schematic illustration of β-catenin and its interacting partners in adherens junctions, cytoplasm and nucleus. β-catenin is shown as 12 Armadillo repeats flanked by N- and C-terminal domains. The interacting proteins are colored in different categories according to their biological activities. The disposition of each interacting partner represents the binding region on β-catenin protein.

From the perspective of blocking Wnt signaling in cancer, the most obvious approach would be to target the β-catenin and TCF/LEF interface directly. However, as shown in Figure 2.3, TCF associates with β-catenin protein with an extended binding interface of approximately 60 Å in length[29]. The lack of a deep hydrophobic pocket in β-catenin, the typical region of intervention for a small molecule inhibitor, has resulted in

limited success with inhibitors from this class. Although several compounds, such as PKF115-854, have been suggested to disrupt β-catenin and TCF/LEF interaction, their specificity and efficacy are yet to be characterized (Table 2.1)[24]. Therefore, direct targeting β-catenin at the TCF/LEF binding surface is an appealing challenge in the inhibition of the canonical Wnt signaling pathway.

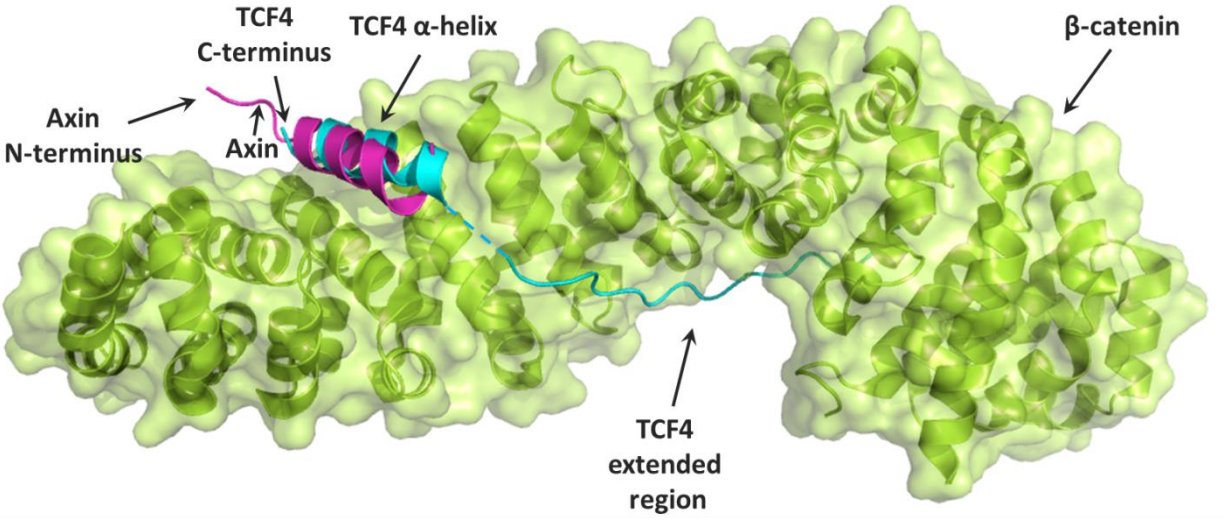

Figure 2.3 Superimposed crystal structure of the β-catenin armadillo domain bound to the β-catenin-binding-domain (CBD) of Axin (PDB 1QZ7) and TCF4 (PDB 2GL7). The CBD of Axin and TCF4 helical region overlap the binding surface with opposite orientations.

Stapled Peptides as Direct Inhibitors Targeting β-catenin Protein

The Verdine Lab at Harvard University has developed and applied the all hydrocarbon stapled α-helical peptide technology to target several intracellular proteins, including apoptotic mediators[30], and multi-protein transcription factor complexes[31]. Given the difficulty in the identification of small molecule antagonists to target β-catenin and TCF/LEF interface, we saw the potential utility of stapled peptides in this system. This

strategy was further rationalized by the presence of the requisite α-helical peptide at the binding surface (Figure 2.3)[32]. As a result, we took advantage of the fact that the β-catenin-binding-domain (CBD) of Axin protein overlaps the binding surface with TCF helical region, characterized stapled Axin-derived (StAx) peptides that function as direct β-catenin antagonists *in vitro* and in cultured cells through a systematic approach including screening of candidate stapling positions, affinity optimization via phage display, and introduction of residues that promote cell penetration. The crystal structure of β-catenin/StAx complex revealed that the stapled Axin peptide binds at the same site as Axin-CBD and the TCF helical region. Moreover, these peptides, but not closely related negative control molecules, interfered specifically with transcriptional activation of canonical Wnt pathway genes. In addition, the most active stapled peptide induced growth inhibition of Wnt-dependent cancer cells, but did not affect the growth of cancer cells that do not rely on deregulated Wnt signaling pathway[33].

Bifunctional Stapled Peptides as Improved β-catenin Antagonists

In order to further improve the biological activity of stapled Axin peptide inhibitors (StAx), a bifunctional stapled peptide strategy that additionally harnesses the regulation of protein homeostasis by ubiquitin-proteasome system was employed to improve antagonistic efficiency in targeting β-catenin (Figure 2.4).

Ubiquitin is a small, highly conserved protein that is attached to lysine residues on proteins targeted for degradation through the sequential actions of ubiquitin-activating

enzymes (E1), ubiquitin-conjugating enzymes (E2), and ubiquitin ligase (E3). Successive conjugation of ubiquitin to previously attached ubiquitin molecules on the substrate protein results in a polyubiquitin chain that is recognized by the 26S proteasome, ultimately leading to degradation of the target protein[34].

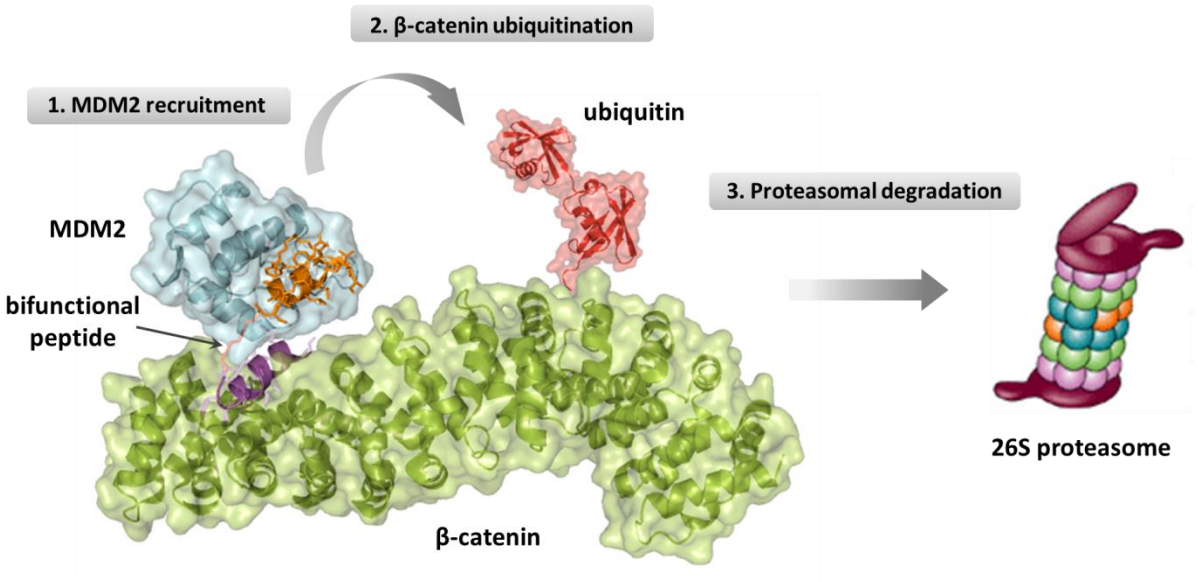

Figure 2.4 Schematic diagram of β-catenin ubiquitination and degradation by bifunctional stapled peptides. The β-catenin binding part in the bifunctional peptide is colored in purple, whereas the MDM2 binding part is colored in orange. The process starts with MDM2 recruitment to β-catenin, followed by poly-ubiquitination of β-catenin protein, which is eventually recognized and degraded by 26S proteasome.

In this approach, StAx peptides were proposed to conjugate with a second stapled peptide which can recruit an endogenous ubiquitin ligase to β-catenin protein. In doing so, the new bifunctional stapled peptides would not only inhibit β-catenin activity by interfering with β-catenin/TCF interactions, but would also trigger its ubiquitination and subsequent fast degradation by the proteasome system inside cells. In addition, given that stapled peptides are usually resistant to intracellular proteolysis, the bifunctional stapled peptides may be considered catalytic β-catenin antagonists, since they can facilitate the ubiquitination and proteasomal degradation process in multiple turnovers.

The concept of bifunctional molecules that specifically bring two or more proteins together for improved or novel biological effect has been established for decades. A bifunctional small molecule can be as simple as a natural product that interacts with two proteins simultaneously. For example, FK506 and rapamycin are macrocyclic immunosuppressive molecules bound to the same immunophilin, FKBP, with similar structural elements, which compose half of the macrocycle. The distinct chemical moieties from the other half of the macrocycle endow them a unique binding surface for a second protein partner: calcineurin for the FK506-FKBP complex, and mTOR for the rapamycin-FKBP complex. It is through this second interaction that these molecules derive different biological activities[35-36]. Subsequently, variants of these molecules have been engineered to bind to orthogonal proteins known as "chemical inducers of dimerization"[37]. Since then, the field has expanded with new molecules and new applications in chemical genetics and cell biology[38]. In particular, the Deshaies and Crews lab developed a novel class of bifunctional molecules named as the PROTACS (proteolysis targeting chimeric) molecules, designed to exploit the ubiquitin-proteasome system and selectively degrade targeted proteins[39]. Typically, a PROTAC molecule is made up of two ends, one of which can be recognized by an E3 ubiquitin ligase, while the other binds to a protein target. Therefore, the targeted protein is recruited to the E3 ligase for ubiquitination and followed by proteasomal degradation. So far, this approach has been successfully applied to several protein targets by distinct E3 ligases[40-41]. Unlike the common gene knockout or RNAi technology, this method provides a useful research tool for study of protein function through controlled knockdown of target proteins at the post-translational stage, thereby avoiding many issues related with classic genetic approaches. Despite the potential of PROTAC technology as an

investigative toolkit, the poor cell penetration limits its widespread application. In this study, bifunctional stapled peptides are also generated with the intention of hijacking ubiquitin-proteasome system, but have the potential to exhibit better cellular and *in vivo* activity, as stapled peptides have been demonstrated to efficiently cross the cell membrane.

The Design and Synthesis of Bifunctional Stapled Peptides

As discussed above, the goal of this project is to synthesize **bi**functional **s**tapled **Ax**in (Bisax) peptides by conjugation of β-catenin binding StAx peptides with another stapled peptide which can recruit an E3 ubiquitin ligase to β-catenin and thereby induce the ubiquitination and degradation via endogenous ubiquitin-proteasome system. StAx-35 was used in this study as a β-catenin binder because it exhibits the best binding affinity to β-catenin in a panel of stapled axin peptides with a dissociation constant of low nanomolar range.

Table 2.2 Stapled Axin (StAx) and SAH-p53-8 peptides and their respective negative controls.

Peptide	Sequence
StAx-35	RRWPQ-S5-ILD-S5-HVRRVWR
StAx-Neg	RR**A**PR-S5-IL**H**-S5-**D**VRRV**A**R
SAH-p53-8	QSQQTF-R8-NLWRLL-S5-QN
SAH-p53-8-Neg	QSQQT**A**-R8-NLWRLL-S5-QN

For an E3 ubiquitin ligase binder, a stapled peptide SAH-p53-8 which derived from the tumor suppressor p53 protein, was demonstrated to bind to MDM2, an E3 ubiquitin ligase with high affinity and specificity according to our previous results[42]. Therefore, SAH-p53-8 was chosen to conjugate with StAx-35 peptide to recruit the E3 ligase MDM2 to β-catenin

target. In addition, negative control stapled peptides for StAx-35 and SAH-p53-8 were also included here as building blocks for negative control bisax peptides which could not bind to either protein (Table 2.2).

a)

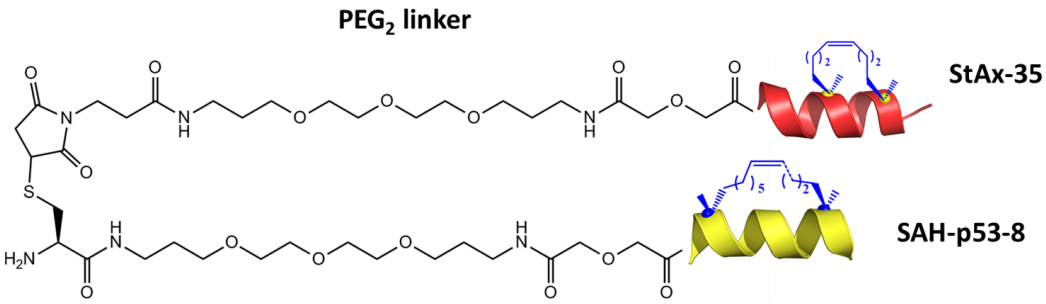

b)

Bisax	StAx-35 – SAH-p53-8	Linker
5	N–N	2 × PEG_2
8	N–C	2 × PEG_2
11	C–N	2 × PEG_2
14	C–C	2 × PEG_2
20F	N–N	2 × PEG_2
21S	N–N	2 × PEG_1
22L	N–N	4 × PEG_2
23S	N–C	2 × PEG_1
24L	N–C	4 × PEG_2
25	X–X	2 × PEG_2

Figure 2.5 Bifunctional stapled Axin (Bisax) peptides. (a) Schematic illustration of the linkage of bisax. (b) Bisaxes used in this study with varied orientation and linker length, where "f" means FITC-labeled, "S" and "L" mean short and long linker, respectively, and "X" means negative control peptides.

Unlike bifunctional small molecules that can rotate freely around the central linker to accommodate themselves in the binding pockets of protein targets, the binding of bifunctional peptides to their targets is more constrained by the peptide orientation. Improper orientation around the linker, as well as suboptimal linker lengths may cause unexpected steric clashes between the two binding proteins. Due to the lack of crystal

structure information for full length β-catenin or MDM2, it is difficult to completely rationalize the optimal peptide orientations and linker length based on their partial structures. Therefore, bisax peptides were made with all four possible orientations and with a linker length varied from approximately 25 Å (2 × PEG_1) to 100 Å (4 × PEG_2). In doing so, we aimed to screen for the best combinations as determined by biological activity *in vitro* and in cell-based assays (Figure 2.5).

For the conjugation, a thiol-malaimide Michael addition was used to link the two stapled peptides together because it is a fast and high yield reaction and most importantly in this study, it creates a non-cleavable covalent bond between the two peptides, which keeps the bisax peptide intact in *in vitro* assays and inside cells[43]. Specifically, a cysteine residue was coupled at either N- or C-terminus of the StAx peptides, whereas a maleimide moiety was appended on SAH-p53-8 peptides. These were synthesized and HPLC purified separately. The final product was obtained by in-solution Michael addition of the two peptide precursors and followed by a second round of HPLC purification. As a result, a total of 10 bisax peptides with varied orientations and linker length were synthesized with >95% purity as verified by LC/MS (Figure 2.5).

Analysis of Binding of Bifunctional Stapled Peptides

In order to confirm that the bifunctional stapled Axin (Bisax) peptides retain the binding affinity to both β-catenin and MDM2 proteins, an *in vitro* fluorescence polarization (FP) assay was performed. FP assay measures the polarization of light emitted by

fluorophore labeled molecules at unbound and bound states. Typically, the fluorophore labeled compound is usually small and rotates rapidly, which generates low polarization. Upon binding to a larger molecule, its rotation slows down dramatically, and a high polarization signal can be observed. Thus, dissociation constant (K_d) can be calculated when fitting the polarization values into a sigmoidal curve[44]. In this study, a fluorescein isothiocyanate (FITC) labeled bisax-20F was prepared by coupling a FITC label at SAH-p53-8 end of bisax-5 peptide. N-terminal FITC labeled StAx-35 and SAH-p53-8 were synthesized as previously reported[33, 42]. Human β-catenin and MDM2 full length proteins were expressed in *E. coli* and purified using a modified version of reported protocols[28, 45]. (Details in Experimental Methods)

The fluorescence polarization assays were carried out in triplicates. The raw data were imported into GraphPad Prism (GraphPad software), and were subjected to normalization where 0% bound stands for non-bound state, and 100% bound indicates a fully bound state. The normalized data were then plotted and fitted to Hill equation with simultaneous weighting of the standard deviations of each data point.

$$\text{Hill equation: } y = m1 + (m2 - m1)/\{1 + [\frac{m3}{x}]^{m4}\}$$

The Hill equation for binding is listed above, where m1 is the polarization at the unbound state, m2 is the polarization at the saturated bound state, m3 is the dissociation constant (K_d), and m4 is the Hill coefficient, which usually indicates the cooperativity of the binding interaction.

Figure 2.6 shows the fluorescence polarization results. As expected, StAx-35 binds to β-catenin protein with a K_d of approximate 40 nM, which is consistent with previous reports, whereas SAH-p53-8 stapled peptide shows no quantifiable binding to β-catenin. Bisax-20F is a fluorescein labeled peptide where StAx-35 and SAH-p53-8 are conjugated through N-terminus-N-terminus linkage. It exhibits a binding affinity of approximate 60 nM when incubated with β-catenin protein, an affinity close to that of StAx-35 stapled peptide. (Figure 2.6a) Similar results were observed when these FITC labeled peptides were incubated with the MDM2 protein. SAH-p53-8 and bisax-20F bind to the MDM2 protein tightly, with K_d values of 34 and 38 nM respectively. However, StAx-35 could not bind to MDM2 protein at all (Figure 2.6b). Taken together, FP binding assay results show that bisax peptides can bind to β-catenin and MDM2 protein separately, and the binding affinity of bsax-20 is comparable to StAx-35 and SAH-p53-8 alone.

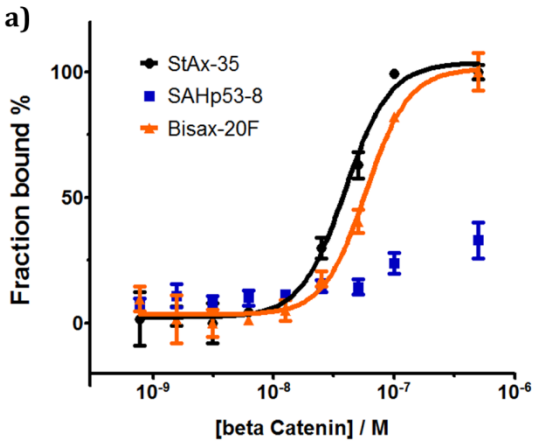

Compound	K_d (nM)
StAx-35	39.3 ± 2.7
SAHp53-8	N. D.
Bisax-20F	58.4 ± 5.2

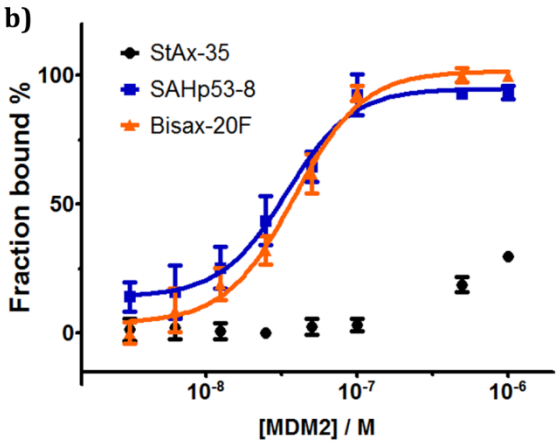

Compound	K_d (nM)
StAx-35	N. D.
SAHp53-8	34.2 ± 5.5
Bisax-20F	38.4 ± 3.5

Figure 2.6 Fluorescence polarization assays showing that bifunctional stapled peptide retains binding affinity to β-catenin and MDM2 proteins. a) Bisax-20F binds to β-catenin protein with similar affinity as StAx-35. b) Bisax-20F binds to the MDM2 protein with similar affinity as SAH-p53-8.

The fluorescence polarization assay above raised several questions regarding to the binding abilities of bisax peptides. For example, only bisax-20F with N-terminus-N-terminus linkage and two polyethylene glycol spacers was tested, the binding properties for the rest of bisax peptides with different orientations and varied linker length are still unknown. In addition, although bisax-20F has similar binding affinity to β-catenin and MDM2 protein as StAx-35 and SAH-p53-8 respectively, it is unclear from these results whether it binds at the same sites of the target proteins.

In order to address these questions, a competition fluorescence polarization assay was carried out. FITC-labeled StAx-35 (or SAH-p53-8) was pre-incubated with β-catenin (or MDM2) protein to generate a bound state which produces a high fluorescence polarization signal. The concentration of β-catenin (or MDM2) protein was chosen based on the FP assay where 80% of the protein was bound to the FITC-labeled peptide. Then non-labeled bisax peptides were then added at increasing concentrations, aiming to compete with the bound FITC-StAx-35 (or FITC-SAH-p53-8). If they bind at the same sites, FITC-StAx-35 (or FITC-SAH-p53-8) will be displaced, resulting in a low polarization unbound state. However, if non-labeled bisax peptides could not bind to the target proteins or they bind at a different site, the polarization signal will stay high. Polarization values were plotted and fitted into sigmoidal curve to yield an IC_{50} which can be used to compare the binding affinity for different bisax peptides.

As shown in Figure 2.7, the active compound bisax-8 can bind to β-catenin (and MDM2) protein tightly and competes with FITC-StAx-35 and FITC-SAH-p53-8 which causes decrease in polarization signal with IC_{50} values of 0.285 ± 0.014 μM and 0.242 ± 0.016 μM

respectively. However, the negative control peptide bisax-25 cannot compete either of the FITC-labeled peptides at all. This *in vitro* competition FP assay confirms the bind ability of bisax peptides to both β-catenin and MDM2 protein, and indicates that they bind at the same site on target proteins as StAx-35 and SAH-p53-8.

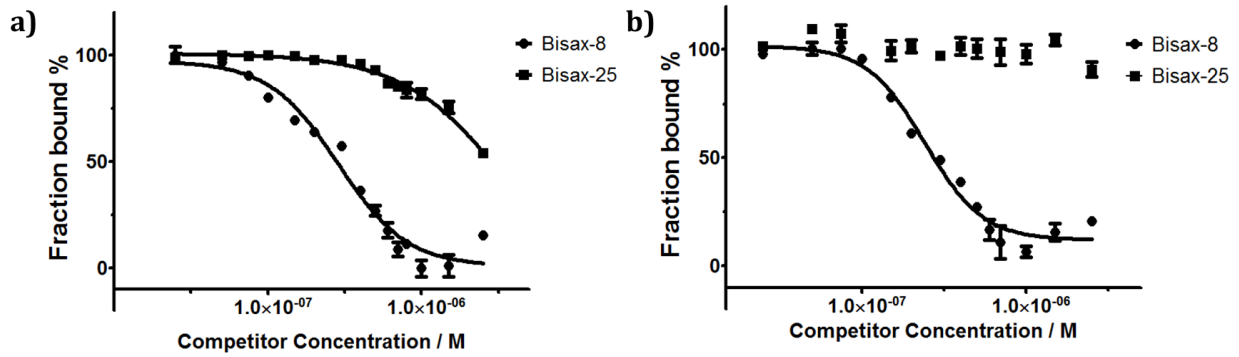

Compound	IC_{50} (μM)
Bisax-8	0.285 ± 0.014
Bisax-25	> 5

Compound	IC_{50} (μM)
Bisax-8	0.242 ± 0.016
Bisax-25	N. D.

Figure 2.7 Competition fluorescence polarization assay with increasing amount of bifunctional stapled peptides against a) β-catenin and b) MDM2 protein. The active bisax-8 peptide competes with both StAx-35 and SAH-p53-8 peptides, whereas the negative bisax-25 cannot, which indicates that bifunctional peptides bind at the same site on target proteins as each of the un-ligated peptides.

In order to compare the binding affinity for all bisax peptides and thereby analyzing the effect of peptide orientations and linker length, the competition FP assay was applied to all the bisax peptides against β-catenin. In particular, bisax-5, 8, 11 and 14 are compounds with all four possible orientations and the same 2 × PEG_2 linker (~ 50 Å). With this linker, the peptide orientation did not have any significant effect with regard to their binding properties. All of the four bifunctional peptides exhibited similar binding affinities to β-catenin, ranging from 0.285 to 0.593 μM (Figure 2.8a). Similarly, the linker length does not appear to affect the measured binding properties either. As shown in Figure 2.8b, bisax-8,

23 and 24 are peptides with N-terminus of StAx-35 linking to C-terminus of SAH-p53-8, whereas the linker length varies from approximately 25 Å to 100 Å. However, they can efficiently compete with FITC-StAx-35 with similar IC_{50} values.

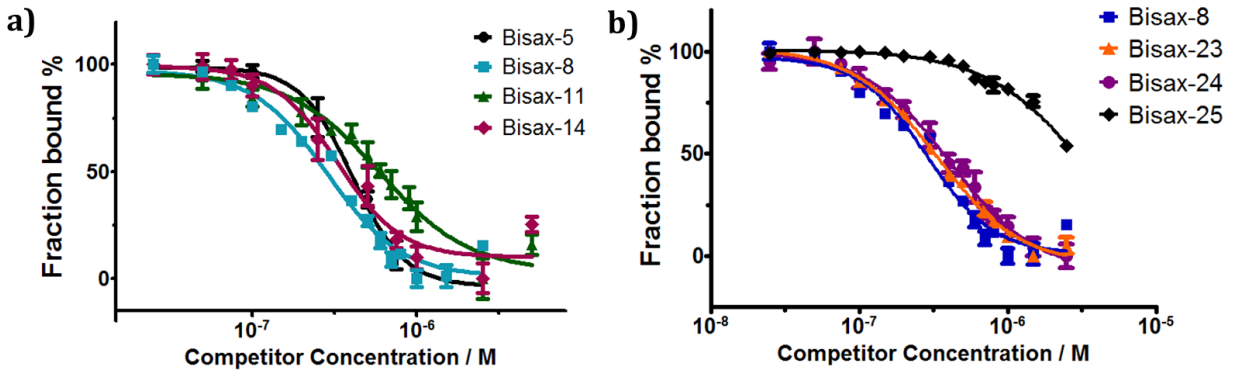

Compound	IC_{50} (μM)
Bisax-5	0.407 ± 0.020
Bisax-8	0.285 ± 0.014
Bisax-11	0.593 ± 0.071
Bisax-14	0.326 ± 0.031

Compound	IC_{50} (μM)
Bisax-8	0.285 ± 0.014
Bisax-23S	0.333 ± 0.010
Bisax-24L	0.410 ± 0.020
Bisax-25	> 5

Figure 2.8 Competition fluorescence polarization assays using bisax peptides with a) different orientations and b) varied linker length showing that both peptide orientation and linker length do not appear to affect the measured binding properties.

Based on competition FP assay results, a better understanding of the binding properties for bisax peptides can be achieved. 1) All bisax peptides, except the negative control bisax-25, retain their binding ability to target proteins individually. 2) Binding is minimally influenced by peptide orientation and linker length. 3) Bisax peptides bind at the same site of β-catenin (or MDM2) protein as StAx-35 (or SAH-p53-8) stapled peptides.

Evaluation of MDM2 Recruitment to β-catenin

According to the *in vitro* FP and competition FP assay results, bisax peptides can bind to β-catenin and MDM2 protein separately with high affinity. Next, we wanted to determine whether bisax peptides were able to recruit MDM2 to β-catenin. A pull-down assay was employed to address this question. The *in vitro* pull-down assay is a useful biochemistry technique to determine physical interactions between two or more components. Typically, a "bait" protein is tagged and captured on an immobilized affinity ligand specific for the tag, which is then incubated with a protein source containing putative "prey" proteins, such as a cell lysate. After rigorous wash, the bound proteins are eluted, separated by SDS-PAGE gel and confirmed by western blotting[46]. In this study, the prediction is that bisax peptide will recruit the MDM2 protein to β-catenin, generating a β-catenin-bisax-MDM2 interacting complex. To assay for such a complex, the β-catenin was expressed as N-terminal GST fusion protein and immobilized on glutathione coated agarose resin as a "bait" protein. The "prey" MDM2 protein was from HEK293T cell lysate instead of purified MDM2 protein to mimic a cellular environment. Given the MDM2 protein expression level in mammalian cells is usually low, a stable HEK293T cell line which can constitutively overexpress N-terminal myc-tagged human MDM2 full length protein was generated by transiently transfection of a mammalian expressing neomycin-resistant plasmid encoding MDM2 protein followed by G418 selection. Cell lysate from this stable HEK293T cell line were incubated with bisax peptides at increasing concentrations in order to analyze the complex formation in dose-dependent manner. The bound MDM2 protein was eventually eluted after three rounds of washing and visualized by western blotting following standard protocol (Details in Experimental Methods).

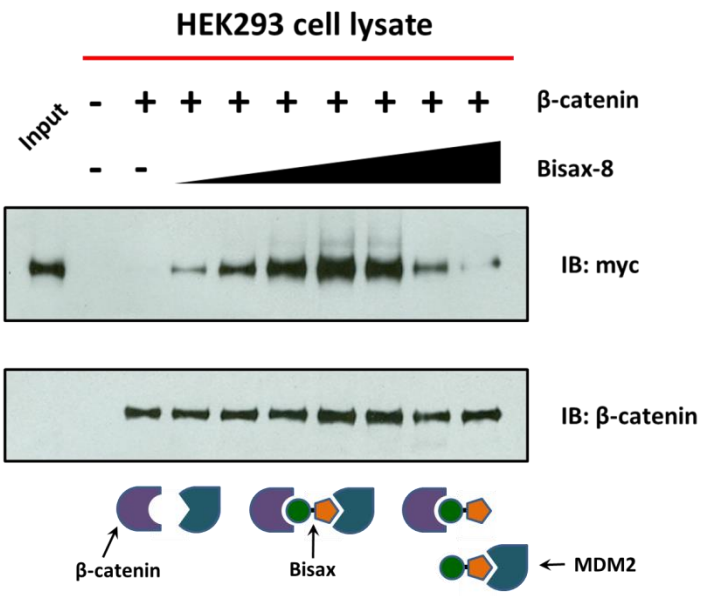

Figure 2.9 *In vitro* pull-down assay shows bisax-8 recruits MDM2 protein to beads immobilized β-catenin in dose-dependent manner.

The pull-down assay result using bisax-8 is shown in Figure 2.9. Lane 1 shows that myc-tagged MDM2 full length protein expressed well in HEK293T cells. When no β-catenin or bisax-8 was added in the mixture, MDM2 protein cannot be visualized on the gel (Lane 2 and 3), indicating that there is no non-specific binding between MDM2 protein and glutathione beads or β-catenin protein, and therefore all the MDM2 signals observed in following lanes result from specific bisax recruitment. Interestingly, when increasing amount of bisax-8 were added into the mixture, bound MDM2 was first increased (Lane 4 - 7) to reach a plateau and then decreased afterwards with a threshold approximately 500 nM. To rationalize the result, the immobilized β-catenin is not saturated with bisax-8 up to 500 nM, so all bisax-8 peptide is supposed to bind to β-catenin protein and thereby increasing the amount of bound MDM2 protein from cell lysate. However, the immobilized β-catenin is saturated by bisax-8 at concentration of approximately 500 nM. If bisax-8 concentration continues to increase, the leftover non-bound bisax-8 will compete with β-

catenin bound peptide in MDM2 binding, causing a decrease in MDM2 association. When bisax-8 concentration is high enough to saturate both immobilized β-catenin and MDM2 protein from cell lysate, no signal can be observed, which is shown in Lane 10, where the majority of MDM2 protein is competed off at highest concentration of 10 μM. In addition, it is noteworthy that the result was based on the equal amount of immobilized β-catenin in all experiments according to immunoblotting of β-catenin loading control.

The pull-down assay above shows that bisax-8 can efficiently recruit MDM2 protein to β-catenin target in the context of HEK293T cell lysate. The same experiment was carried out for all bisax peptides in order to investigate the effects of varied peptide orientations and linker length. In this experiment, the concentration of bisax peptides was chosen as 500 nM based on the maximum MDM2 signal in bisax-8 pull-down assay.

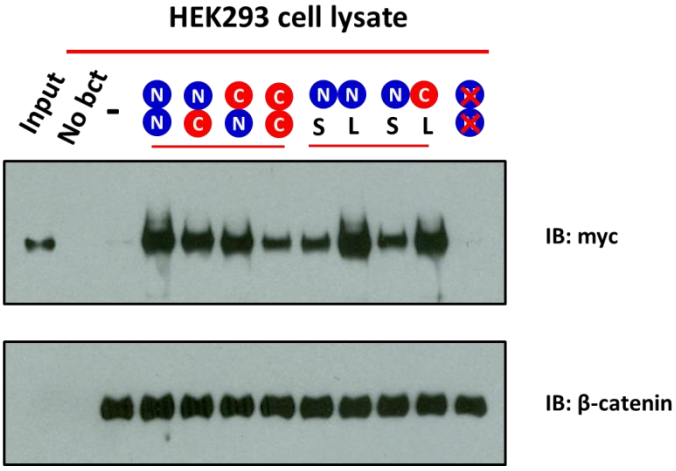

Figure 2.10 Bifunctional stapled peptides with varied orientations and linker length exhibit different pull-down activity, where "S" and "L" stand for short and long linker, respectively, and "X" means negative control peptides.

As shown in Figure 2.10, these bisax peptides indeed exhibit different pull-down activities. Lanes 4 – 7 are peptides with the same 2 × PEG_2 linker but different orientations.

It turns out that all of four possible linkage can recruit MDM2 to β-catenin protein, but bisax-5 with N-N linkage is the most efficient, followed by bisax-8 and 11 with either N-C or C-N linkage which have similar activity in MDM2 pull-down, whereas bisax-14 with C-C orientation is the worst. It is possible that the C-C linkage with this 2 × PEG_2 linker causes steric clashes between β-catenin and MDM2 protein, and the N-N linkage is the best to accommodate the two proteins. As for the different linker length, the longer linker always shows better pull-down activity (Lane 8, 9 and 10, 11), which could be attributed to the larger number of degrees of freedom to fit both proteins together. Importantly, the negative bisax-25 peptide shows no activity in MDM2 pull-down since it cannot bind to either β-catenin or MDM2 protein (Lane 12).

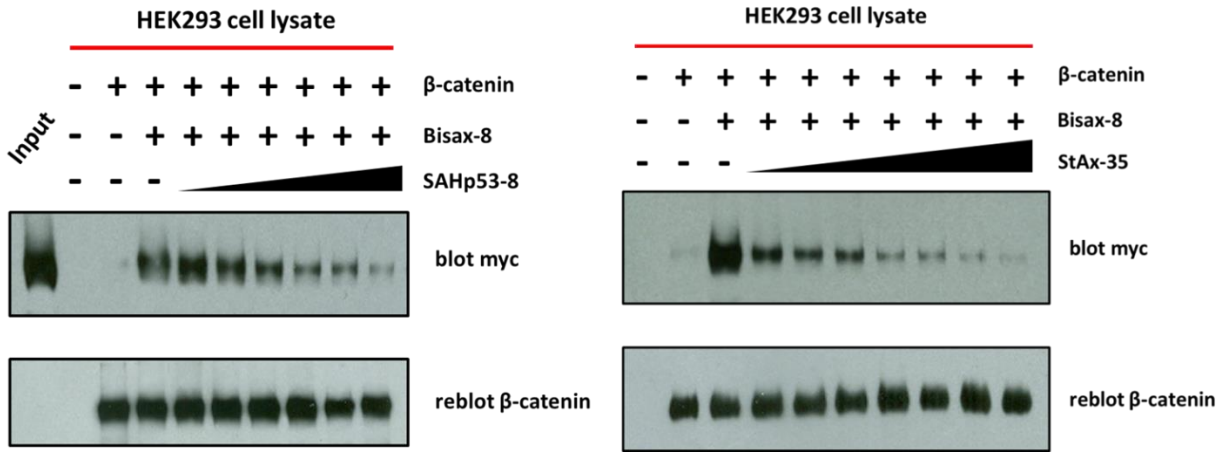

Figure 2.11 SAH-p53-8 and StAx-35 can compete with bisax peptides in MDM2 pull-down assay, indicating the recruitment of MDM2 to β-catenin is a reversible process and both SAH-p53-8 and StAx-35 contribute to the binding.

In order to confirm the pull-down assays results, as well as to verify that MDM2 recruitment is reversible in the cell lysate context, a competition pull-down assay was performed, in which increased concentrations of StAx-35 or SAH-p53-8 stapled peptide was added into the incubation mixture to compete with bisax peptides. As a result, both

SAH-p53-8 (Figure 2.11 Left) and StAx-35 (Figure 2.11 Right) can efficiently compete with bisax-8 in MDM2 protein pull-down in dose-dependent manner. Taken together, the *in vitro* pull-down assays indicate that 1) bisax peptides can efficiently recruit the MDM2 ligase to β-catenin protein, and this process is concentration-dependent, 2) the peptide orientation and linker length indeed play a significant role in forming this β-catenin-bisax-MDM2 complex, and in current study, the N-N linkage with the longest 4 × PEG_2 spacer is the best combination, 3) the recruitment of MDM2 to β-catenin is reversible, which can be disrupted by incubation with either StAx-35 or SAH-p53-8 stapled peptide.

Assessment of *in vitro* Activity of Bisax Peptides

The biochemistry assays above show that bisax peptides can bind to β-catenin and MDM2 protein simultaneously and thereby recruit the MDM2 protein to β-catenin target. We next wanted to verify that MDM2 can ubiquitinate β-catenin when the two proteins are in close proximity. Given that this is a new system and β-catenin and MDM2 proteins are not native ubiquitination partners, several questions needed to be addressed when analyzing the activity of bisax peptides. 1) Is an E3 ligase still functional on a non-native substrate if they are brought into close enough proximity? The majority of previous studies have tested ubiquitination reactions of an E3 ligase with its native substrates, and little is known about the activity of an E3 ligase on a non-related substrate[47-48]. As far as we know, the β-catenin protein does not have any specific interaction with MDM2, and β-catenin is not in the known substrate list of MDM2 ligase. However, in this study, bisax peptides can bind to both β-catenin and MDM2 protein simultaneously to form a β-catenin-bisax-MDM2

complex, which creates an association between the two proteins. In this case, MDM2 has the potential to be active on β-catenin protein even though they are not native ubiquitination partners. 2) Does β-catenin have any lysine residues that can be ubiquitin-modified near the interacting MDM2 ligase? In the ubiquitination process, a ubiquitin molecule is covalently conjugated to a certain lysine side chain through an isopeptide bond. In this case, the target protein at least needs to have a lysine residue near the E3 ligase binding site as a ubiquitin receptor. The β-catenin protein has 26 lysine residues in total, which are spread over different domains according to crystal structure data[28]. Thus, it is entirely possible that at least some of the lysine residues will be near the MDM2 binding site, although it is difficult to predict the exact binding region in β-catenin due to the lack of a full-length MDM2 protein structure. To address this problem, a panel of bisax peptides was synthesized with varied orientations and linker length in order to figure out the peptide with optimal composition. 3) What is the ubiquitination pattern if MDM2 can ubiquitinate β-catenin target? Ubiquitination reactions have two different patterns: poly-ubiquitination and mono-ubiquitination[49]. Both of them occur natively in cells, and each of them has distinct biological activities. However, the mechanism by which it is decided that a substrate is mono- or poly-ubiquitinated is still not clear. In order for β-catenin to be degraded by 26S proteasome, it needs to be poly-ubiquitinated with a ubiquitin chain consisting of at least four ubiquitin molecules.

With these concerns in mind, an *in vitro* ubiquitination assay was developed based on previous protocols[50]. In detail, human UBA1 full length protein and UbcH5c were chosen as ubiquitin E1 and E2 enzymes respectively, and were expressed and purified from *E. coli* as N-terminal His_6-tagged proteins. The E3 ligase human MDM2 protein and MDM2

inactive C464A mutant were purified using the same protocol as previously used for FP assays. The β-catenin protein with a C-terminus AviTag, a BirA biotin ligase recognition sequence, was coexpressed with BirA biotin ligase, *in situ* biotinylated in *E. coli*, and purified following the same protocol as the β-catenin protein used in the FP assays. The biotinylated β-catenin was immobilized on streptavidin agarose resin during the ubiquitination reaction with addition of all required enzymes, which then underwent stringent washing to remove all the other components. The advantage of this method is that the ubiquitinated protein can be visualized using both β-catenin and ubiquitin antibodies, whereas in previous protocol the bands observed using ubiquitin antibody might also come from the reaction of other components, particularly the autoubiqutination of E3 ligase.

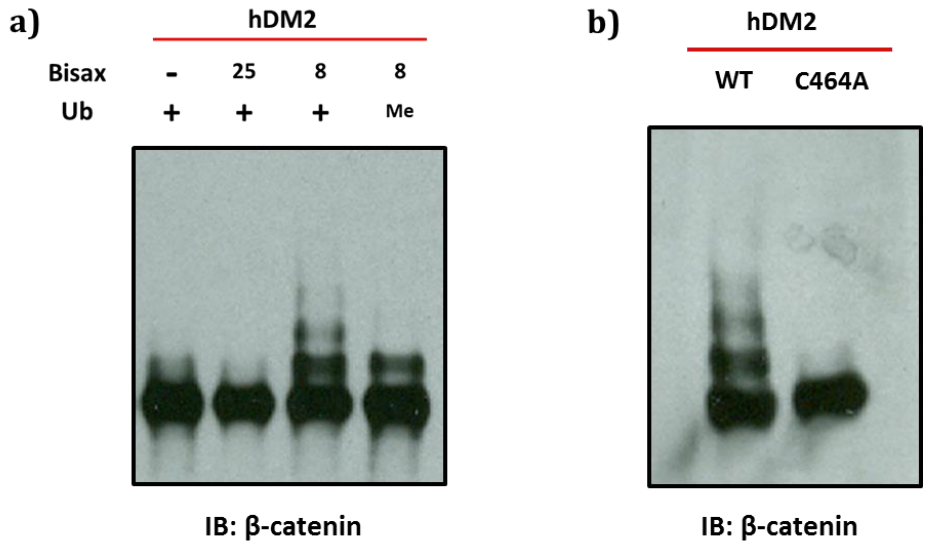

Figure 2.12 *In vitro* ubiquitination assay shows bisax-8 can induce β-catenin poly-ubiquitination by recruiting E3 ubiquitin ligase MDM2. a) The ubiquitination reaction only occurs in presence of active bisax-8 peptide, and the reaction with Me-Ub confirms the formation of poly-ubiquitination chain on β-catenin. b) Inactive MDM2 mutant C464A cannot produce poly-ubiquitinated β-catenin, highlighting the significance of MDM2 in the process.

Shown in Figure 2.12 are the *in vitro* β-catenin ubiquitination assay results. Promisingly bisax-8 could successfully induce the ubiquitination of β-catenin as visualized from β-catenin blotting, whereas the negative control bisax-25 could not (Figure 2.12a, Lane 2 and 3). In addition, no ubiquitination occurred when no bifunctional peptide was added into the reaction, confirming that the ubiquitination reaction was mediated by bisax peptide, not the non-specific interactions between the two proteins (Figure 2.12a Lane 1). However, a ubiquitination ladder shown in lane 3 does not necessarily indicate poly-ubiquitination because mono-ubiquitination at multiple sites on β-catenin protein would also generate the same pattern on gel. In order to address this question, the wide-type ubiquitin protein was replaced by methylated ubiquitin in the ubiquitination reaction. The methylated ubiquitin has all seven lysine residue capped by methyl group and therefore is unavailable to form polyubiquitin chains[51], which is widely used in ubiquitination assays to determine different ubiquitination patterns. In this study, only a single ubiquitinated β-catenin band can be observed in the presence of methylated ubiquitin, indicating a poly-ubiquitination reaction of β-catenin protein (Figure 2.12a Lane 4). In addition, to confirm the importance of MDM2 ligase in β-catenin ploy-ubiquitination, MDM2 C464A mutant protein was used as E3 source in *in vitro* ubiquitination assay. This MDM2 mutant has a cysteine to alanine mutation at the catalytic RING domain, which is unable to chelate to the Zn^{2+} ion and hence loses the ubiquitin ligase activity[47]. As expected, no reaction was observed, which indicates that the poly-ubiquitination of β-catenin target is dependent on recruited MDM2 ligase as well (Figure 2.12b).

According to our *in vitro* ubiquitination assay, the β-catenin ubiquitination reaction depends on the presence of both bisax peptides and MDM2 protein. A specificity assay was

performed to confirm that MDM2 protein can only ubiquitinate β-catenin target with this panel of bifunctional peptides. The same experiment was repeated using KRas or c-myc protein as substrate instead of β-catenin. KRas, c-myc and β-catenin proteins are different in size and tertiary structures, and none of them are the native ubiquitination substrate of MDM2 ligase[52-53]. However, they have comparable number of lysine residues, which is adequate for potential ubiquitin modification. Neither KRas nor c-myc protein exhibited ubiquitination activity even though the amount of MDM2 protein was three times that used in β-catenin ubiquitination assay (Figure 2.13). Therefore, we can conclude from this *in vitro* ubiquitination assay that MDM2 could specifically poly-ubiquitinate β-catenin substrate only in the presence of bisax peptides.

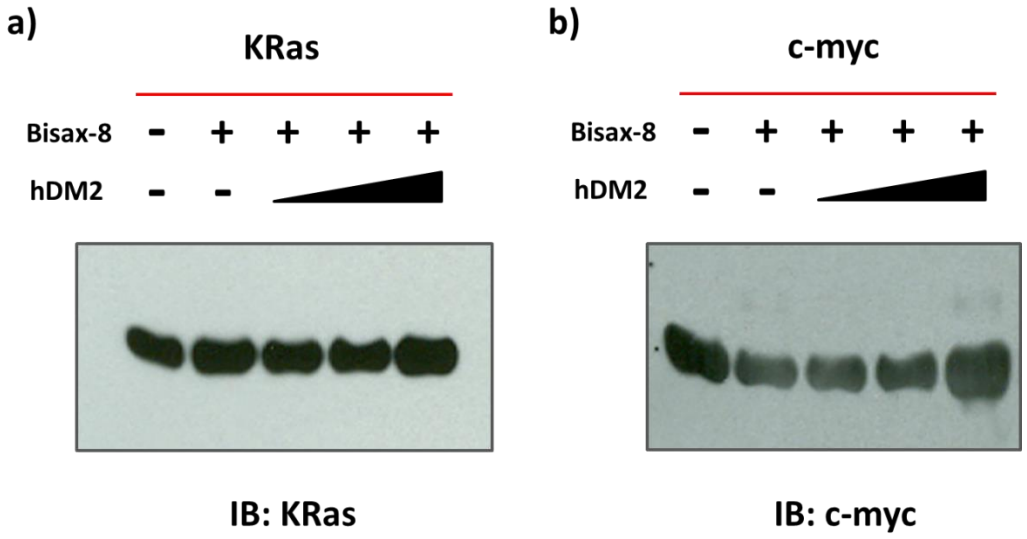

Figure 2.13 *In vitro* ubiquitination assays using a) KRas and b) c-myc protein as substrates indicate that bifunctional peptides promote the ubiquitination of β-catenin specifically.

Next I examined the different activities in mediating β-catenin ubiquitination for the entire panel of bisax peptides. As shown in Figure 2.14, there was no ubiquitination reaction without bisax peptides or with negative control bisax-25. All the other bisax

peptides exhibited similar activities except for bisax-14, which has the least competency to produce ubiquitinated β-catenin. Recall from the *in vitro* pull-down assay that bisax-14 is the peptide that pulls down the least amount of MDM2 protein from HEK293T lysate. This suggests that the ubiquitination activity is correlated with the ability to recruit MDM2 to β-catenin protein.

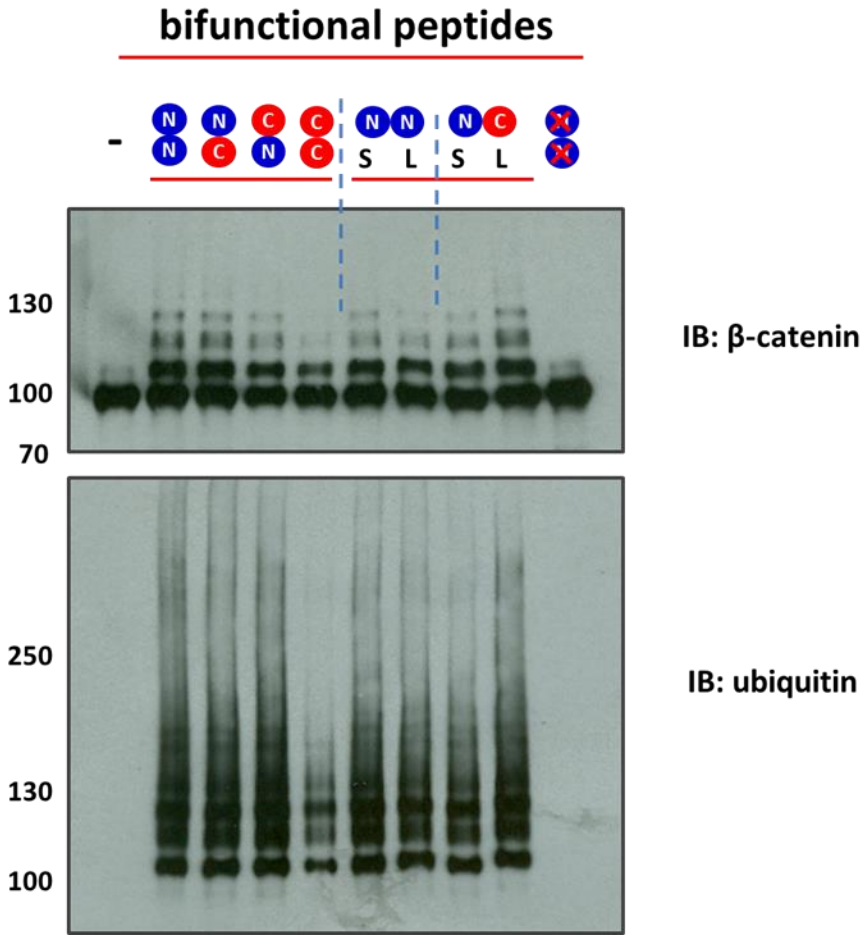

Figure 2.14 *In vitro* β-catenin ubiquitination assay using bisax peptides with varied orientations and linker length, where "S" and "L" stand for short and long linker, respectively, and "X" means negative control peptides.

Analysis of Cell Penetration of bisax peptides

The *in vitro* assays show bisax peptides can not only recruit MDM2 protein to β-catenin target with high affinity, but also trigger specific poly-ubiquitination of β-catenin protein. The logical next step would be to study the activity of these bifunctional peptides in cell-based assays to determine whether they could induce β-catenin degradation and regulate downstream gene expression. Before performing any cell-based experiments to address these questions, we verified the cell penetration properties of bisax peptides. In previous studies, both StAx-35 and SAH-p53-8 peptide are good cell penetrators and are biological active in mammalian cells[33, 42]. But the bisax peptides in this study are doubled in size and molecular weight, thus, it is necessary to assure their cell permeable abilities and compare with StAx-35 and SAH-p53-8 stapled peptides.

As shown in Figure 2.15, a concentration-dependent cell penetration assay was performed for StAx-35, SAH-p53-8 and Bisax-20F by treatment of HeLa cells for 4 hours at 37°C. StAx-35 and SAH-p53-8 showed good cell permeability starting at 5 μM, which is consistent with published results. Interestingly, bisax-20F starts to penetrate cells at 1 μM, and the penetration ability at 5 and 10 μM are similar as the two stapled peptides. This result indicates that the double-sized bisax peptides can efficiently translocate the cell membrane and exhibit even better permeation at lower concentrations than the stapled peptide counterparts.

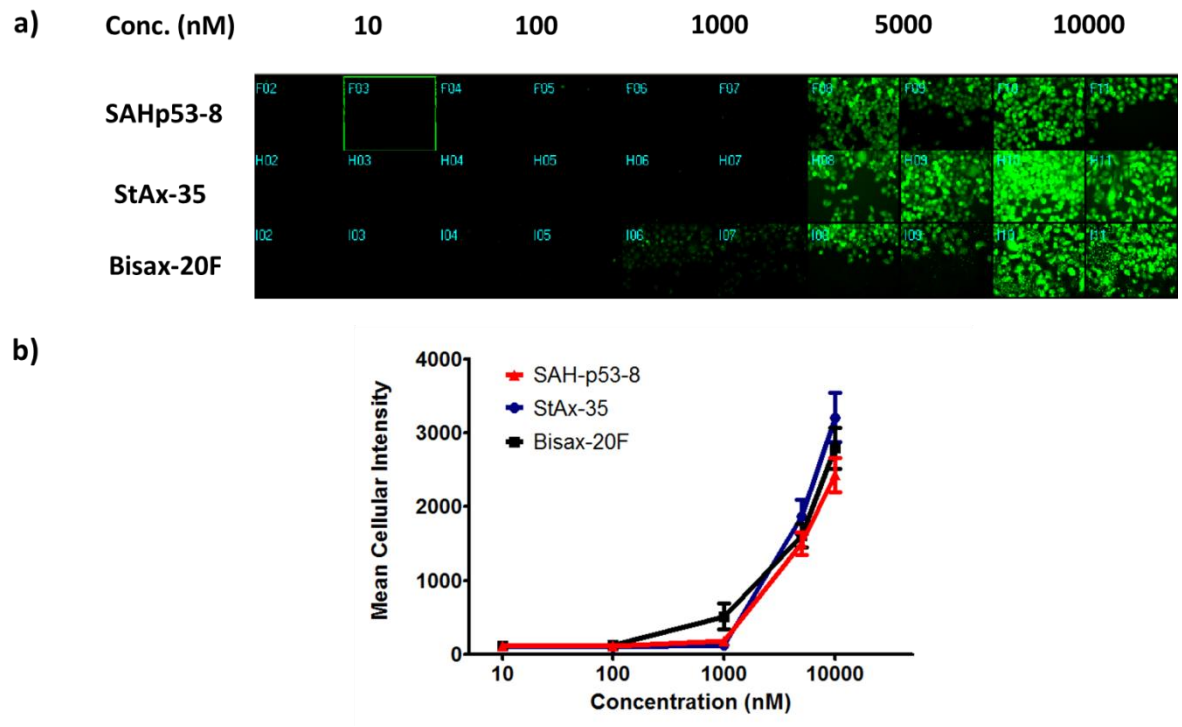

Figure 2.15 Cell penetration study of bifunctional stapled peptides. (a) Image view and (b) quantitative measurement of cell penetration show that bifunctional peptides can efficiently cross cell membrane and exhibit better penetration that each un-ligated stapled peptide at 1 μM.

Endogenous β-catenin Knockdown in SW480 Cells

With the confirmation of cell penetration for the bisax peptides, a cell-based assay was carried out to determine the cellular activity of these bifunctional peptides. Human colorectal cancer line SW480 was used in this study, which have a high level of endogenous β-catenin expression levels due to APC truncation, resulting in the failure to form the β-catenin destruction complex[54]. Total β-catenin protein was visualized by western blotting after treatment of SW480 cells with bisax peptides, and the results are shown in Figure 2.16. Bisax-11 exhibits a dose-dependent knockdown of β-catenin protein in SW480 cells with an IC_{50} approximately 50 μM, whereas the negative control bisax-25 shows no

reduction in β-catenin level at a concentration as high as 100 μM. The result is very promising, indicating the efficacy and specificity of bisax peptides in cancer cell lines. However, one can argue that the activity observed from this assay might result from StAx-35 alone, because StAx-35 can bind to β-catenin specifically with high affinity and exhibits modest intracellular activity according to previous experience.

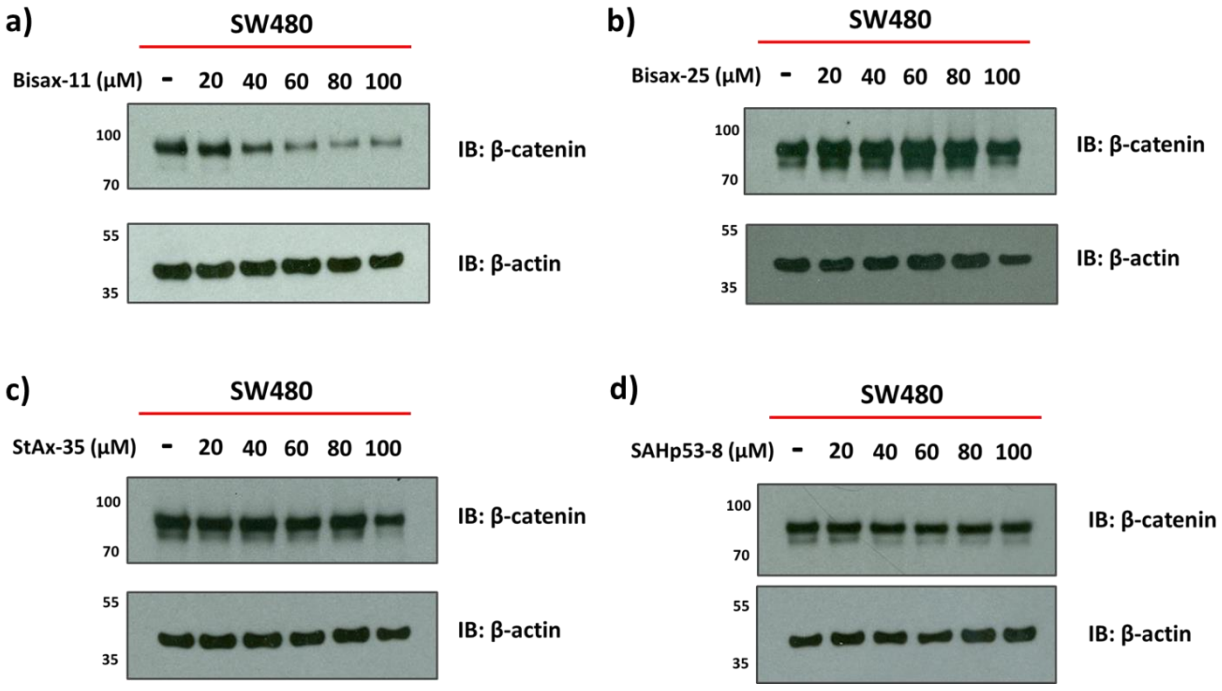

Figure 2.16 Bifunctional peptides can specifically knockdown endogenous β-catenin protein levels in SW480 cells as visualized by western blotting the β-catenin amounts upon treatment of (a) bisax-11, (b) bisax-25, (c) StAx-35 and (d) SAH-p53-8.

In order to confirm that both StAx-35 and SAH-p53-8 fragments in bisax peptides are indispensable in acquiring their cellular activities, the same experiment was performed with treatment of only StAx-35 or SAH-p53-8. SAH-p53-8 does not appear to have any activity in knockdown of endogenous β-catenin level even at a concentration of 100 μM. StAx-35 does not show any activity below 100 μM, and a modest activity can be observed as the concentration reaches 100 μM. Taken together, these results indicate that bisax

peptides exhibit improved cellular activity in knockdown of intracellular β-catenin proteins, and this activity depends on both StAx-35 and SAH-p53-8 fragments.

Luciferase Activity Suppression

As discussed above, β-catenin protein acts as a transcriptional coactivator in the canonical WNT signaling pathway. The accumulated cytosolic β-catenin migrates into nucleus, binds to TCF/LEF transcription factors, recruits other transcriptional coactivators and initiates downstream gene expression. In order to further characterize the biological activity of bisax peptides inside mammalian cells, a luciferase reporter gene assay was performed as a simplified model to analyze β-catenin-dependent gene expressions. SW480 cells were transiently transfected with a plasmid encoding the firefly luciferase gene driven by a promoter containing four tandem TCF binding sites. Therefore, its expression was dependent on cellular β-catenin levels and is variable in different experiment conditions. Meanwhile, SW480 cells were also cotransfected with a renilla luciferase gene driven by a constitutive CMV promoter for signal normalization. Upon treatment of bisax peptides for 24 hours, luciferase levels were determined by measuring the emitted luminescence after incubation with their individual substrates. The ratio of firefly/renilla luciferase level indicated the relative gene expression profile due to bisax peptide treatment and could be compared among different experiments.

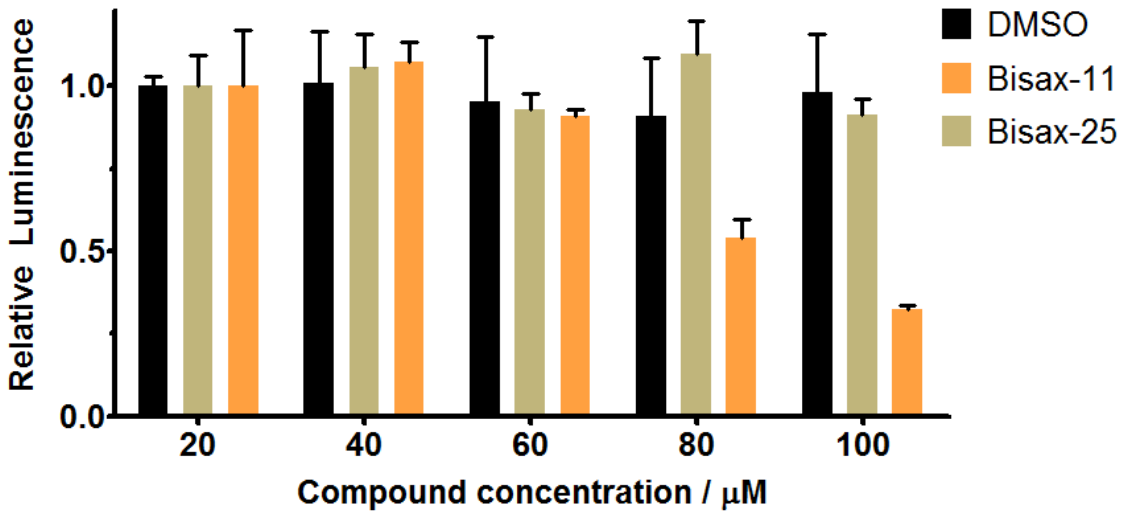

Figure 2.17 Luciferase reporter gene assay showing suppression of luciferase upon treatment of bisax-11 peptide in a dose-dependent manner. However, the negative bisax-25 does not have any suppression activity.

As shown in Figure 2.17, treatment of bisax-11 exhibits a dose-dependent decrease in downstream firefly luciferase with an IC_{50} of approximately 60 μM, which is similar as the inhibition activity in knockdown of endogenous β-catenin protein in SW480 cells. Negative control peptide bisax-25 did not suppress the luciferase expression at a concentration as high as 100 μM. Given that StAx-35 can bind to β-catenin target with high affinity and specificity by competing the binding with TCF/LEF transcription factor, we wanted to rule out the possibility that the luciferase suppression observed in this assay is resulted from StAx-35 alone. To address this question, the same experiment was carried out by incubation of SW480 cells with only SAH-p53-8 or StAx-35 peptide. As shown in Figure 2.18, SAH-p53-8 exhibits no effect on luciferase levels, whereas StAx-35 shows modest luciferase suppression only at the highest concentration of 100 μM. At first glance, this result is not consistent with our previous experiments where StAx-35 could efficiently inhibit β-catenin mediated transcriptional activity in luciferase reporter assay. However, in

our previous study, HeLa cells were stimulated with Wnt3a conditioned medium to increase intracellular β-catenin levels, resulting in a highly robust expression of downstream genes. The observed luciferase suppression activity of StAx-35 was based on attenuation of the artificially elevated β-catenin which is much more abundant than that in Wnt-dependent cancer cells. The experiment in this study was more stringent, which assesses the knockdown of endogenous β-catenin in SW480 cells without any manipulation. Therefore, the data shown here indicated that bisax peptides have a better biological activity than StAx-35 in the environment of a beta-catenin driven cancer line, and the activity is gained from induced ubiquitination and proteasomal degradation by recruitment of MDM2 ligase.

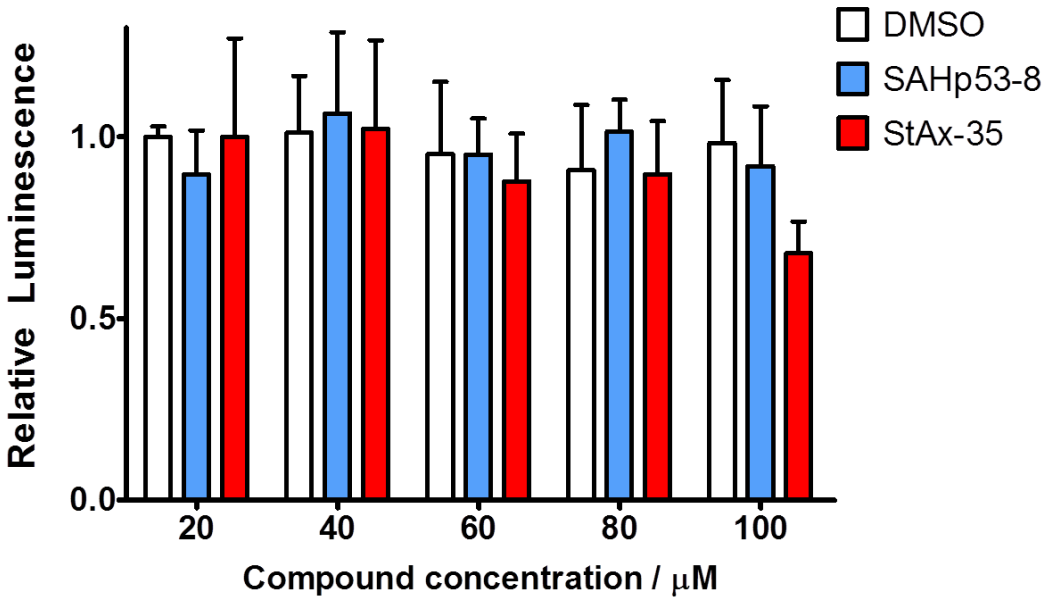

Figure 2.18 Luciferase reporter gene assays with SAH-p53-8 and StAx-35 indicate that the suppression of luciferase by bifunctional peptides requires both un-ligated stapled peptides.

Conclusion

In this study, a bifunctional stapled peptides strategy was employed to target the β-catenin protein for ubiquitination and proteasomal degration, which is a key regulator in the canonical WNT signaling pathway. I designed and synthesized a panel of bifunctional stapled Axin (bisax) peptides and demonstrated through biochemical assays that they can recruit the MDM2 protein, a ubiquitin E3 ligase, to the β-catenin target. I also developed an *in vitro* ubiquitination assay to show a specific β-catenin poly-ubiquitination mediated by bisax peptides. Furthermore, treatment of bisax peptides in human colorectal cancer line SW480 showed knockdown in endogenous β-catenin levels in a concentration-dependent manner. In addition, a dose-dependent decrease in luciferase expression was observed in luciferase reporter gene assay as well, indicating that bisax peptides can downregulate downstream gene expression in the WNT signaling pathway. These data suggest that bisax peptides may serve as a potential drug candidate in treatment of WNT-addicted cancers in a pathway specific manner, and can also be a useful research tool for better understanding the WNT signaling pathway by targeted knockdown of β-catenin at protein level.

Future Directions

The work in this study shows promising results in the development and application of bifunctional stapled peptides as potential drug candidates as well as unique research tools in WNT-dependent diseases. In order to further optimize the system and apply this technology to other challenges, future studies should be focused on the following aspects.

1) Introduction of cooperative binding to β-catenin and MDM2 proteins. The work in this study is based on the strategy that bisax peptides can recruit MDM2 protein to β-catenin target by binding to both proteins simultaneously. We varied the peptide orientations and linker length, and demonstrated their binding abilities to both proteins. Following studies can be performed to optimize the peptide sequences as well as linker length to introduce a cooperative binding to β-catenin and MDM2 proteins, which would facilitate the recruitment of the MDM2 protein to β-catenin targets.

2) Identification of ubiquitination sites on β-catenin protein. This study shows that bisax peptides can efficiently poly-ubiquitinate β-catenin protein by recruitment of MDM2 ligase. Future studies should identify the ubiquitination sites on β-catenin target. This can be accomplished by mass spectrometry studies together with an *in vitro* ubiquitination assay with β-catenin mutants. Once the ubiquitination sites are identified, efforts may be directed towards distinguishing the differences between induced ubiquitination in this study and its native ubiquitination by the native β-Trcp ubiquitin ligase. Furthermore, we also need to figure out the effect of bisax peptides with varied orientations and linker length. For example, do they trigger the ubiquitination reaction on the same sites? If not, what sites are preferred in proteasomal degradation? Can we further optimize the activity of bifunctional peptides by adjusting its ubiquitination sites? Studies on these questions will definitely improve our understanding of bifunctional stapled peptide strategy.

3) Assessment of downstream gene expression in the WNT signalling pathway. In this study, bisax peptides could knockdown endogenous β-catenin levels in human colorectal cancer line SW480 cells and suppress luciferase gene expression in luciferase reporter

assay. However, the downstream gene expression profiles in the WNT signalling pathway were untested. An RT-PCR or microarray experiment needs to be carried out to determine the effect of bisax peptides on β-catenin-dependent gene expressions. In addition, a pathway specificity assay is also needed to confirm that bisax peptides only show activity on the WNT signalling pathway.

4) Test the activity of bifunctional stapled peptides in animal models. If bisax peptides exhibit good activity in above assays, an *in vivo* assay needs to be performed to determine their efficacy in animal models.

5) Optimization of bifunctional stapled peptides. In order to further improve the biological activity of bisax peptides, optimizations need to be performed, which can be based on the following strategies: a) increase the reactivity in polyubiquitination by adjusting peptide orientations and linker length, b) enhance the cell penetration ability by peptide sequence modification, c) employ other β-catenin binding peptides or recruit other E3 ligases to ubiquitinate β-catenin protein with better efficiency.

6) Application of bifunctional stapled peptides strategy to other protein targets. Our bifunctional stapled peptide strategy provides a useful research tool to manipulate the phenotype of cells by targeted knockdown of specific proteins. This study established a platform and performed initial tests using β-catenin as substrate and MDM2 as E3 ubiquitin ligase. However, it can be easily expanded to other protein targets if a stapled α-helix peptide binder can be discovered. Moreover, given the large number of ubiquitin ligases in human genome, it is entirely achievable to develop multiple bifunctional stapled

peptides to target a single protein to allow for optimization of target ubiquitination and proteasomal degradation.

Materials and Methods

Plasmids.

1. **pET28a-UBA1.** Human UBA1 gene sequence was generated by PCR amplification using reverse transcribed cDNA pool from HEK293T cells as template. The primers are: 5'BamHIE1, GGGGATCCATGTCCAGCTCGCCGCTGTCCAAGAAACG, and 3'NotIE1, GCTTAT GCGGCCGCTCAGCGGATGGTGTATCGGACATAGGG. PCR products were subcloned into pET28a vector (Novagen) using BamHI and NotI cleavage sites. The resulting construct contains an N-terminal hexahistidine tag.
2. **pMCSG7-TEV-UBE2D3.** Human UBE2D3 gene (UbcH5c) sequence was generated by PCR amplification using reverse transcribed cDNA pool from HEK293T cells as template. The primers are: 5'KpnITEVE2, CTAGGGTACCGAGAACCTGTACTTCCAATCCATGGCGCTG AAACGGATTAATAAGGAAC, and 3'EcoRIE2, CTACGAATTCTCACATGGCATACTTCT GAGTCCATTCCC GAG. PCR products were subcloned into pMCSG7 vector (Verdine lab DNA database #1426) using KpnI and EcoRI cleavage sites. The resulting construct contains a TEV cleavage site between N-terminal hexahistidine tag and UbcH5c protein.
3. **pMAL-TEV-bCat.** Human β-catenin DNA sequence was generated by PCR amplification using pET28b-β-catenin (Verdine Lab DNA database #2558) as template. The primers are: 5'BamHIbCat, GTGCGGATCCATGGCTACTCAAGCTGATTTGATGG, and 3'SalIbCat, GGCGGTCGACTTACAGGTCAGTATCAAACCAGGC. PCR products were subcloned into pMAL-TEV vector (Verdine Lab DNA database #1721) using BamHI and XhoI cleavage sites. The resulting construct encodes MBP fusion human β-catenin full length protein with a TEV cleavage site between N-terminal MBP tag and β-catenin protein.
4. **pMAL-TEV-bCat-AVI.** This construct is a gift from Dr. Johannes Yeh.

5. **pGEX-5x-bCat.** This construct is a gift from Dr. Johannes Yeh.
6. **pMAL-TEV-myc-MDM2.** Human MDM2 gene sequence was PCR amplified using pcDNA3.1(+)-HA-hDM2 (Verdine lab DNA database #1716) as template. The primers are: 5'BamHImycMDM2, GCGGGATCCGAACAAAAACTTATTTCTGAAGAAGATCTGGGTGG TATGGTGAGGAGCAGG, and 3'XhoIMDM2, GGCTCGAGCTAGGGGAAATAAGTTAGCAC AATC. PCR products were subcloned into pMAL-TEV vector (Verdine Lab DNA database #1721) using BamHI and XhoI cleavage sites. The resulting construct contains a TEV cleavage site between N-terminal MBP tag and myc-tagged MDM2 protein.
7. **pMAL-TEV-myc-MDM2 C464A.** This MDM2 mutant was generated by site-directed mutagenesis (QuikChange II XL kit from Stratagene) using pMAL-TEV-myc-MDM2 as template. The primers are: C464A forward, CTTATGGCCTGCTTTACAGCTGCAAAGAAGC TAAAG, and C464A reverse, CTTTAGCTTCTTTGCAGCTGTAAAGCAGGCCATAAG.
8. **pCMV-myc$_3$-MDM2.** This mammalian cell expressing construct was purchased from Addgene (Plasmid 20935). It encodes human MDM2 full length protein with a 3 × myc tag at N-terminus.
9. **pGL-TOPflash.** This mammalian cell expressing construct encodes firefly luciferase gene driven by a promoter containing four tandem TCF DNA binding sequences. It is from Verdine lab DNA database #2561.
10. **pGLTK-renilla Luciferase.** This construct is from Verdine lab DNA database #2174, which constitutively expresses renilla luciferase in mammalian cells.

Stapled Peptide Synthesis. All peptides were synthesized following an established protocol using standard Fmoc-peptide chemistry on Rink amide MBHA resin in NMP[55]. Briefly, Fmoc deprotection of the N-terminal amine was carried out in 25% piperidine in NMP for 2 × 10 minutes with nitrogen bubbling. After deprotection, the resin was washed with NMP 3 × 2 minutes. The coupling reaction was generally performed by adding a mixture of 10 equivalents of the amino acids, 9.9 equivalents of HCTU and 20 equivalents of DIPEA in NMP. The reactions were allowed to proceed for one hour generally or longer if coupling an amino acid with difficult stretch of residues. Coupling of non-natural amino acids (S_5, R_8 or PEG linker) was performed with 4 equivalents of the amino acid, 3.9 equivalents of HCTU and 10 equivalents of DIPEA in NMP for two hours. The metathesis reaction of olefin containing non-natural amino acid was generally performed using Grubbs-I catalyst (benzylidene-bis(tricyclohexylphosphine)-dichlororuthenium) dissolved to approximately 10 mg/mL in dichloroethane (DCE) for two hours under nitrogen bubbling. After olefin metathesis, resin was wash extensively with DCE to remove excess Grubbs-I catalyst. Stapled peptides were then N- or C-terminal modified following standard coupling procedures with a variety of functional moieties, including fluorescein isothiocyanate (FITC), acetic anhydride, and maleimidopropionic acid. Upon completion, peptides were simultaneously cleaved from resin and deprotected using a cleavage cocktail containing 95% TFA, 2.5% water and 2.5% TIS. Peptides were cleaved at room temperature with gentle rotating for 3 hours. The resin was dried through nitrogen flow. An excess of cold diethyl ether was added to the acidic resin and peptide slurry to precipitate the peptide. The pellet was collected after centrifuge at 3500 rpm for 20 minutes, and washed with cold diethyl ether one more time. The resulting crude peptide

precipitate was dried , dissolved in 50% acetonitrile/water, passed through a 0.2 μm syringe filter and were generally purified with a 10% - 70% linear acetonitrile gradient in water containing 0.1% TFA over 20 minutes by reverse phase HPLC using a C-18 column (Agilent, Palo Alto, CA). Compound identification and purity was assessed using coupled LC/MS (Agilent, Palo Alto, CA). Purified fractions were pooled and evaporated to remove acetonitrile and trace TFA by speedvac. The resulting liquid was lyophilized to dryness and stored as dry stock at 4°C. For biochemical and cell-based assay usage, peptides were dissolved in DMSO and quantified by absorbance at 280 nm if Tryptophan is present or at 494 nm when FITC labeled. Following quantification, peptides were stored as DMSO stocks at -20°C until use.

Bisax Peptide Synthesis. Bifunctional stapled Axin (Bisax) peptides were generated by Michael addition of terminal Cysteine in SAH-p53-8 peptides and maleimide group in StAx peptides. The two peptides were synthesized and HPLC purified separately and stored as DMSO stock solution at -20°C. The reaction proceeded as 1:1 mixture of these two peptides in 50 % acetonitrile/PBS at room temperature for 1 hour. In some cases, a 1.5 equivalent of TCEP was first incubated with Cysteine containing SAH-p53-8 peptides at room temperature for 15 minutes followed by adding maleimide containing StAx peptides. The crude product was purified by reverse phase HPLC following the same protocol as each individual peptide (Figure 2.19). The purity of bisax pepides was tested >95% according to the LC/MS results (Table 2.3). The purified bisax peptides were dissolved in DMSO, quantified by 280 nm absorbance and stored at -20°C until use.

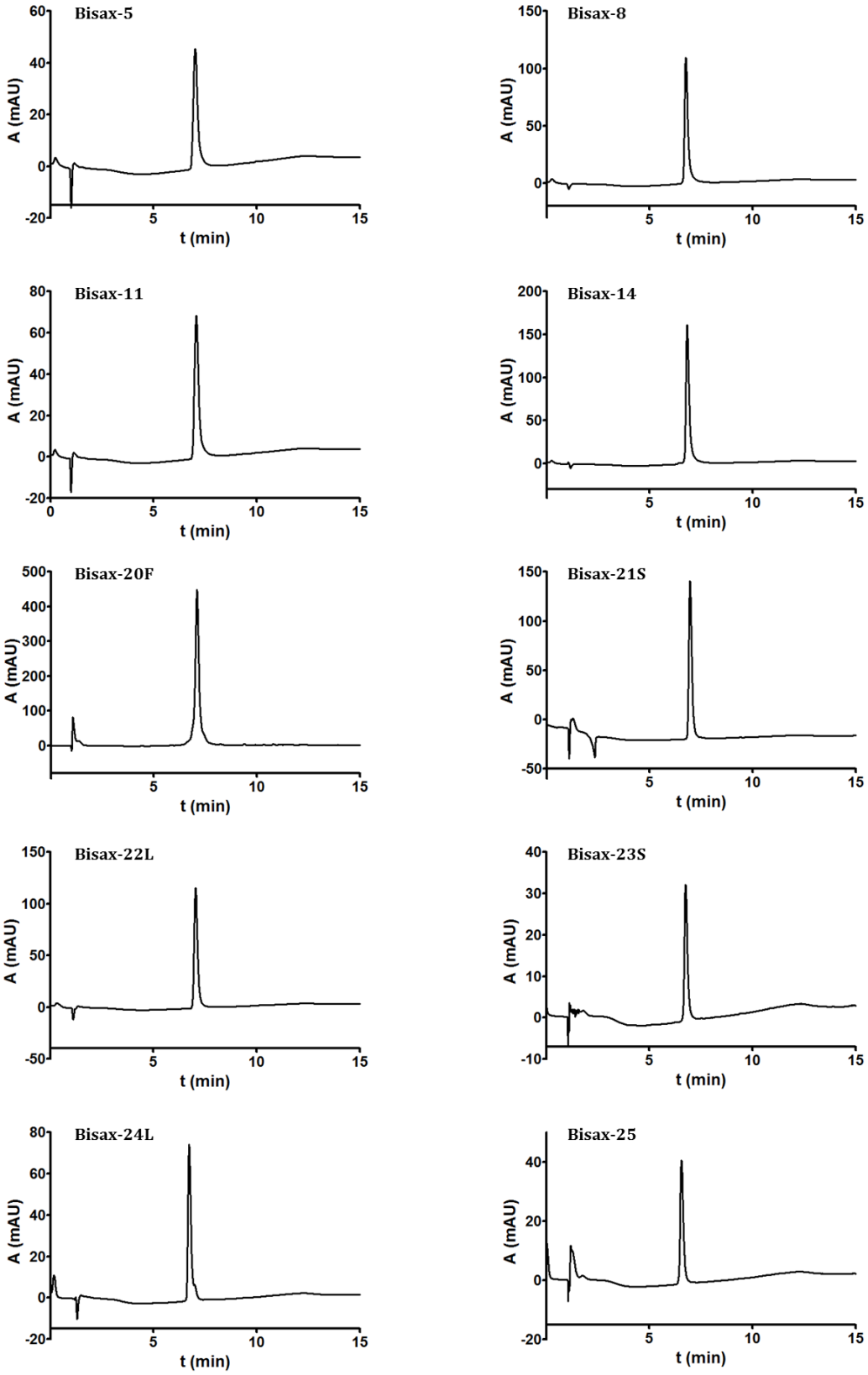

Figure 2.19 HPLC trace of purified bisax peptides measured at 280 nm.

Table 2.3 List of bisax peptides with their chemical formula, molecular weight, calculated and found mass.

Bisax	Chemical Formula	Molecular Weight	Calculated m/z	Found m/z
5	$C_{243}H_{386}N_{70}O_{60}S$	5280.2	1761.1/1321.1/1057.0/881.0/755.3/661.0	1761.1/1321.2/1057.1/881.1/755.4/661.1
8	$C_{251}H_{400}N_{72}O_{62}S$	5450.4	1817.8/1363.6/1091.1/909.4/779.6/682.3	1818.8/1363.5/1091.3/909.5/779.5/682.4
11	$C_{251}H_{400}N_{72}O_{62}S$	5450.4	1817.8/1363.6/1091.1/909.4/779.6/682.3	1818.3/1363.6/1091.1/909.4/779.7/682.3
14	$C_{259}H_{414}N_{74}O_{64}S$	5620.6	1874.5/1406.2/1125.1/937.8/804.0/703.6	1874.2/1406.1/1125.0/937.7/803.9/703.7
20F	$C_{276}H_{421}N_{75}O_{67}S_2$	5925.9	1976.3/1482.5/1186.2/988.7/847.6/741.8	1976.0/1482.4/1186.2/988.7/847.6/741.7
21S	$C_{227}H_{356}N_{68}O_{54}S$	4933.7	1645.6/1234.4/987.8/823.3/705.8	1645.4/1234.4/987.7/823.3/705.9
22L	$C_{271}H_{438}N_{74}O_{72}S$	5916.9	1973.3/1480.2/1184.4/987.2/846.3/740.6	1973.2/1480.1/1184.3/987.1/846.3/740.5
23S	$C_{235}H_{370}N_{70}O_{56}S$	5103.9	1702.3/1277.0/1021.8/851.7/730.1	1702.6/1277.0/1021.6/851.5/730.2
24L	$C_{279}H_{452}N_{76}O_{74}S$	6087.1	1522.8/1218.4/1015.5/870.6/761.9	1522.8/1218.3/1015.5/870.5/761.8
25	$C_{222}H_{376}N_{70}O_{59}S$	5001.9	1668.3/1251.5/1001.4/834.7/715.6/626.2	1667.8/1251.5/1001.4/834.6/715.5/626.2

Protein Expression and Purification.

1. His_6-UBA1. N-terminal His_6-tagged human UBA1 full length protein was expressed in *Escherichia coli* strain BL21(DE3) pLysS (Stratagene) using construct pET28a-UBA1. Transformed bacteria was grown at 37°C until an OD600 = 0.4 was reached, at which point the culture was induced with a final concentration of 0.4 mM isopropyl β-D-1-thiogalactopyranoside (IPTG). Induced cells were grown at 16°C for 16 hours, before harvest by centrifugation at 3500 rpm/4°C for 20 minutes. Cell pellets were washed with PBS once, then flash frozen in liquid nitrogen and stored at -80°C until use.

- Lysis Buffer: 50 mM Tris pH 8.0, 200 mM NaCl, 10% (v/v) glycerol, 10 mM Imidazole pH 8.0, 1 mM PMSF and 1 pill protease inhibitor (Roche) with a total volume of 50 mL for 2L culture.
- Washing Buffer: 50 mM Tris pH 8.0, 10% (v/v) glycerol, 10 mM Imidazole pH 8.0.

- Elute Buffer: 25 mM Tris pH 8.0, 100 mM NaCl, 10% (v/v) glycerol, 250 mM Imidazole pH 8.0.
- Dialysis Buffer: 50 mM Tris pH 8.0, 100 mM NaCl, 10% (v/v) glycerol, 1 mM DTT.
- MonoQ Buffer A: 50 mM Tris pH 8.0, 5% (v/v) glycerol, 1 mM DTT.
- MonoQ Buffer B: 50 mM Tris pH 8.0, 5% (v/v) glycerol, 1 mM DTT, 1M NaCl.
- Gel Filtration Buffer: 25 mM Tris pH 8.0, 200 mM NaCl, 10% (v/v) glycerol, 0.5 mM DTT.

To purify His_6-UBA1 protein, the pellet was thawed in lysis buffer at 4°C, and then the resuspended cells were lysed by sonication on ice (10 seconds pulses at power 6.5 for 2 minutes). The lysate was centrifuged at 14,000 rpm for 30 minutes to precipitate insoluble fractions. The clarified lysate was added to approximately 2 mL of Ni-NTA agarose resin (Qiagen) that had been washed once with 1 × TBS. The lysate and beads slurry was incubated at 4°C for 1 hour with gentle mixing in order to allow binding of His_6-UBA1 protein to the resin. The protein bound bead slurry was washed with 1L washing buffer with salt gradient from 300 mM to 100 mM. Retained protein was then eluted with 4 mL elution buffer. The eluted protein was dialysed overnight at 4°C to remove excess imidazole. The protein was loaded onto a MonoQ 5/50 GL ion exchange FPLC column (GE Healthcare) with a linear gradient of 0-60% MonoQ buffer B over 40 column volumes. The desired protein was pooled and concentrated to 1 mL using a centrifugal concentrator with 30K MWCO (Pall Corporation). The concentrated protein was then loaded onto a Superdex 200 gel filtration column (GE Healthcare) for buffer exchange and further purification. The purity of resulting pooled fractions 21 – 24 was confirmed > 95% by SDS-PAGE. The

purified His_6-UBA1 was quantified by 280 nm absorbance, aliquot 100 µL in each PCR tube, and stored at -80°C until use.

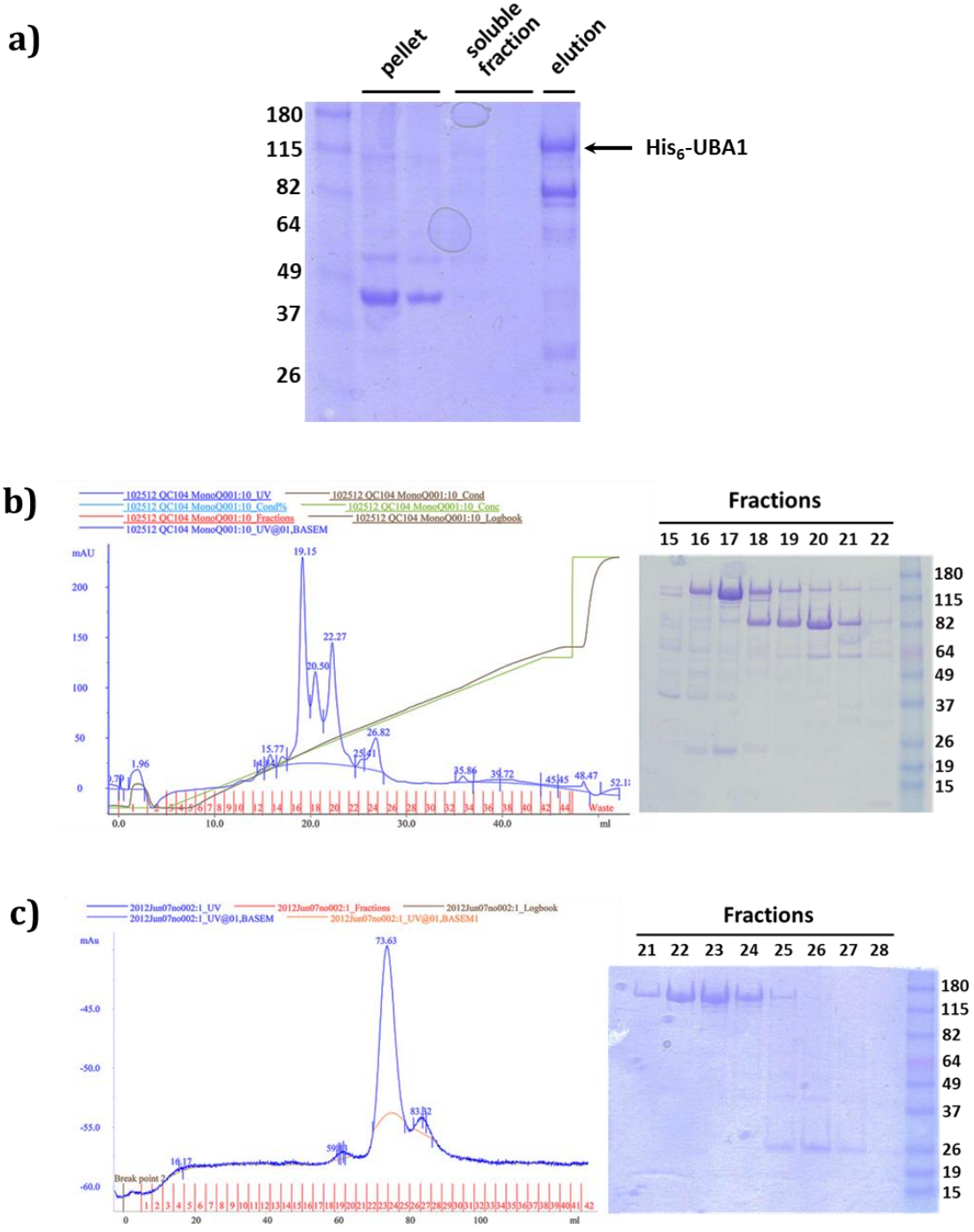

Figure 2.20 His_6-UBA1 purification. a) Coomassie staining of different fractions. b) MonoQ ion exchange column trace and coomassie stain of each fraction. c) Gel filtration column trace and coomassie stain of each fraction.

2. His_6-UbcH5c. Human UbcH5c protein was expressed as an N-terminal His_6-tagged fusion protein in *Escherichia coli* strain BL21(DE3) pLysS (Stratagene) using construct pMCSG7-TEV-UBE2D3. Transformed bacteria was grown at 37℃ until an OD600 = 0.8 was reached, at which point the culture was added with isopropyl β-D-1-thiogalactopyranoside (IPTG) to a final concentration of 0.4 mM. Induced cells were grown at 18℃ for 16 hours, before harvest by centrifugation at 3500 rpm/4℃ for 20 minutes. Cell pellets were washed with PBS once, then flash frozen in liquid nitrogen and stored at -80℃ until use.

- Lysis Buffer: 20 mM Tris pH 8.0, 300 mM NaCl, 2% (v/v) glycerol, 10 mM Imidazole pH 8.0, 1 mM PMSF and 1 pill protease inhibitor with a total volume of 50 mL for 2L culture.
- Washing Buffer: 25 mM Tris pH 8.0, 2% (v/v) glycerol, 10 mM Imidazole pH 8.0.
- Elute Buffer: 25 mM Tris pH 8.0, 100 mM NaCl, 10% (v/v) glycerol, 250 mM Imidazole pH 8.0.
- Gel Filtration Buffer: 50 mM Tris pH 8.0, 100 mM NaCl, 10% (v/v) glycerol, 0.5 mM DTT.

To purify His_6-UbcH5c protein, 2 L of pellet was thawed in 50 mL lysis buffer at 4℃, and then the resuspended cells were lysed by sonication on ice (10 seconds pulses at power 6.5 for 2 minutes). The crude lysate was centrifuged at 14,000 rpm for 30 minutes to precipitate insoluble fractions. The clarified lysate was added to approximately 2 mL of Ni-NTA agarose resin (Qiagen) that had been washed once with 1 × TBS. The lysate and beads slurry was incubated at 4℃ for 1 hour with gentle mixing in order to allow binding of His_6-UbcH5c protein to the resin. The protein bound bead slurry was washed with 1L washing buffer with salt gradient from 500 mM to 100 mM. Retained protein was then eluted with 4

× 2 mL elution buffer. The eluted protein was combined and concentrated to 2 mL by a centrifugal concentrator with 3K MWCO (Pall Corporation). The concentrated protein was then loaded onto a Superdex 75 gel filtration column (GE Healthcare) for buffer exchange and further purification. The purity of pooled fractions 24 – 27 was confirmed > 95% by SDS-PAGE. The purified His_6-UbcH5c was quantified by 280 nm absorbance, aliquot 100 µL in each PCR tube, and stored at -80°C until use.

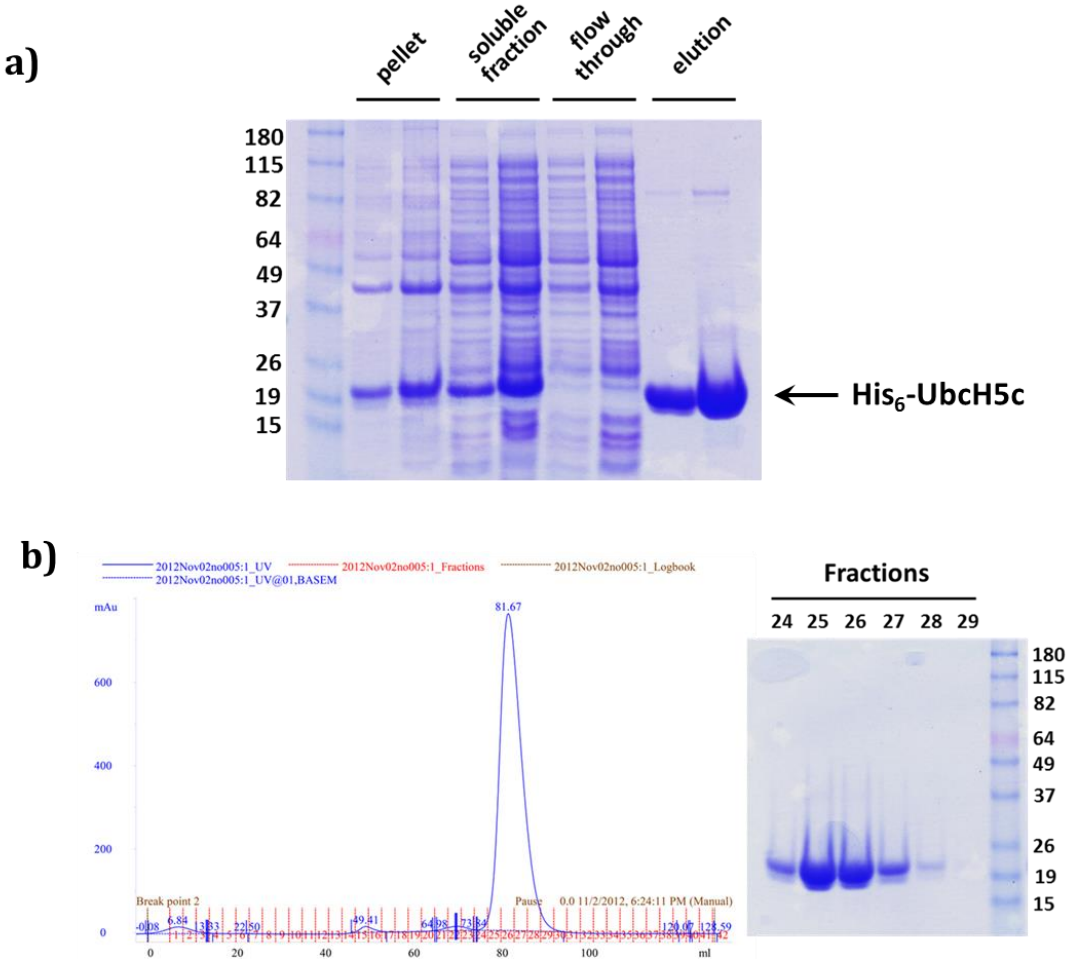

Figure 2.21 His_6-UbcH5c purification. a) Coomassie staining of different fractions. b) Gel filtration column trace and coomassie stain of each fraction.

3. β-catenin. β-catenin full length protein was expressed with an N-terminal MBP fusion protein separated by a TEV cleavage sequence in *Escherichia coli* strain BL21(DE3) pLysS (Stratagene) using construct pMAL-TEV-bCat. Transformed bacteria was grown at 37°C until an OD600 = 0.6 was reached, at which point the culture was induced with 0.4 mM isopropyl β-D-1-thiogalactopyranoside (IPTG). Induced cells were grown at 18°C for 16 hours, and then cells were harvested by centrifugation at 3500 rpm/4°C for 20 minutes. Cell pellets were washed with PBS once, then flash frozen in liquid nitrogen and stored at -80°C until use.

- Lysis Buffer: 25 mM Tris pH 8.8, 300 mM NaCl, 2% (v/v) glycerol, 2 mM DTT, 1 mM PMSF and 1 pill protease inhibitor with a total volume of 50 mL for 2L culture.
- Washing Buffer: 25 mM Tris pH 8.8, 2% (v/v) glycerol, 2 mM DTT.
- Elute Buffer: 25 mM Tris pH 8.0, 100 mM NaCl, 10% (v/v) glycerol, 2 mM DTT, 10 mM Maltose.
- MonoQ Buffer A: 25 mM Tris pH 8.8, 2% (v/v) glycerol, 2 mM DTT.
- MonoQ Buffer B: 25 mM Tris pH 8.8, 2% (v/v) glycerol, 2 mM DTT, 1M NaCl.
- Gel Filtration Buffer: 25 mM Tris pH 8.8, 150 mM NaCl, 10% (v/v) glycerol, 2 mM DTT.

To purify β-catenin protein, 2 L of bacteria pellet was thawed in 50 mL lysis buffer at 4°C, and then the resuspended cells were lysed by sonication on ice (10 seconds pulses at power 6.5 for 2 minutes). The lysate was centrifuged at 14,000 rpm for 30 minutes to precipitate insoluble fractions. The clarified lysate was loaded onto approximately 2 mL of amylose resin (New England Biochem) by gently rotating at 4°C for 3 hours to ensure the binding of desired protein to the resin.

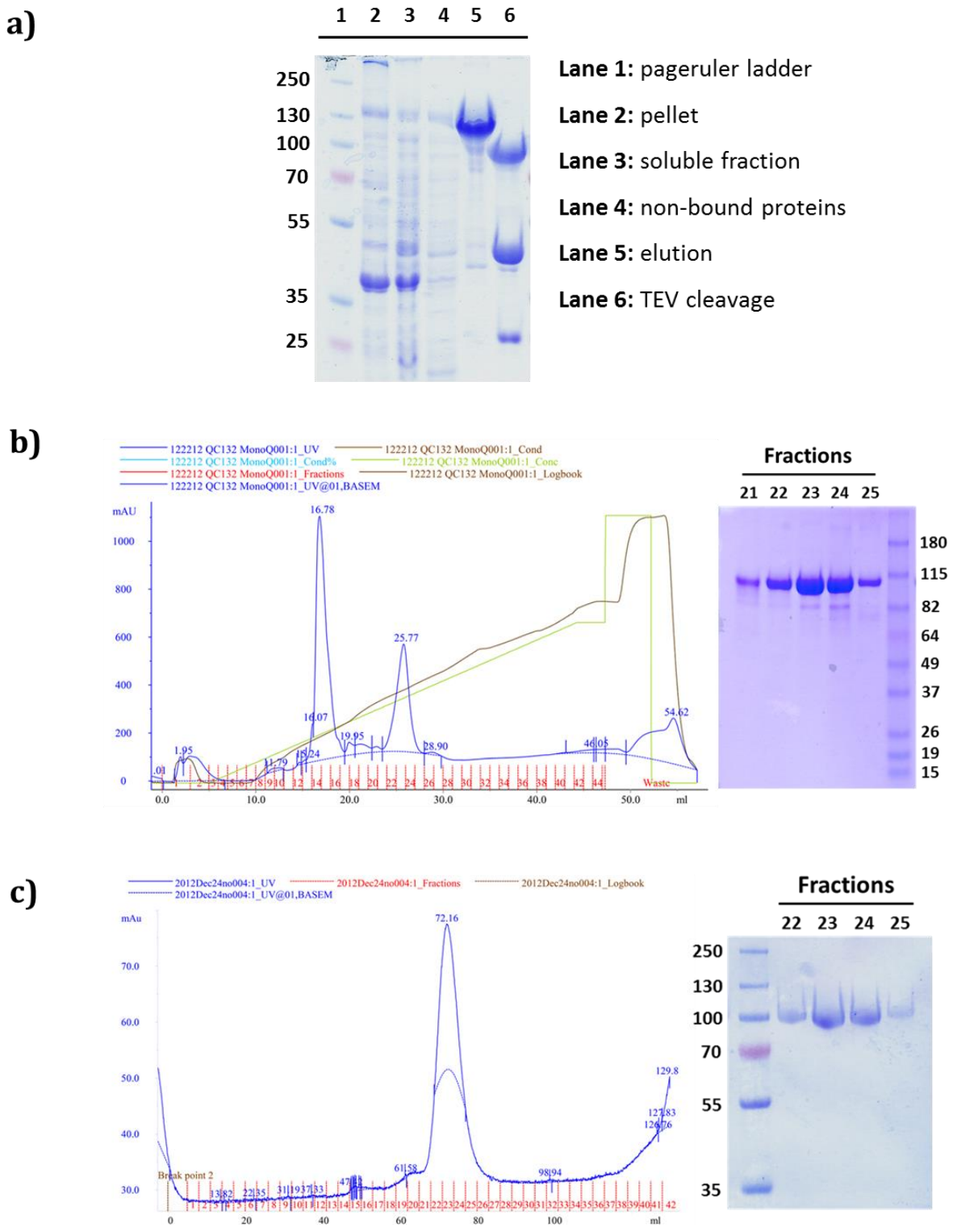

Figure 2.22 β-catenin purification. a) Coomassie staining of different fractions. b) MonoQ ion exchange column trace and coomassie stain of each fraction. c) Gel filtration column trace and coomassie stain of each fraction.

The protein bound bead slurry was washed with 1L washing buffer with salt gradient from 500 mM to 100 mM. Retained protein was then eluted with 4 mL elution buffer. The eluent was then incubated with 200 µL 1 mg/mL TEV protease at 4°C for 12 hours. The cleaved protein mixture was loaded directly onto a MonoQ 5/50 GL ion exchange FPLC column (GE Healthcare). The proteins were eluted with a linear gradient of 0-60% MonoQ buffer B over 40 column volumes. The desired protein was pooled and concentrated to 1 mL using a centrifugal concentrator with 30K MWCO (Pall Corporation). The concentrated protein was then loaded onto a Superdex 200 gel filtration column (GE Healthcare) for buffer exchange and further purification. The purity of resulting pooled fractions 22 – 25 was confirmed > 95% by SDS-PAGE. The purified His_6-UBA1 was quantified by 280 nm absorbance, aliquot 100 µL in each PCR tube, and stored at -80°C until use.

4. Biotin-β-catenin. Biotin-β-catenin was expressed similar as β-catenin protein described above. The differences were: 1) BL21(DE3) pLysS bacteria cells harboring two constructs, namely pMAL-TEV-bCat-AVI and pET28a-BirA, were grown in ampicillin and kanamycin double selection LB medium; 2) a final concentration of 50 µM Biotin (Sigma-Aldrich) was also added to the cells during IPTG induction. The purification was the same as β-catenin protein.

5. GST-β-catenin. GST-β-catenin was expressed and purified similar as β-catenin protein described above. The differences were: 1) pGEX-5x-β-catenin construct was transformed into bacteria cells; 2) Glutathione Sepharose resin (GE Healthcare) was used to bind GST

fusion β-catenin protein instead of amylose resin; 3) 10 mM maltose in elution buffer was replaced by 10 mM reduced glutathione; 4) no TEV cleavage was performed.

6. Myc-MDM2. N-terminal myc-tagged human MDM2 full length protein was expressed in *Escherichia coli* strain BL21(DE3) pLysS (Stratagene) using construct pMAL-TEV-myc-MDM2. Transformed bacteria was grown at 37°C until an OD600 = 0.6 was reached, at which point the culture was induced with a final concentration of 0.4 mM isopropyl β-D-1-thiogalactopyranoside (IPTG). Induced cells were grown at 16°C for 16 hours, before harvest by centrifugation at 3500 rpm/4°C for 20 minutes. Cell pellets were washed with PBS once, then flash frozen in liquid nitrogen and stored at -80°C until use.

- Lysis Buffer: 25 mM Tris pH 8.0, 300 mM NaCl, 2% (v/v) glycerol, 2 mM DTT, 1 mM PMSF and 1 pill protease inhibitor with a total volume of 50 mL for 2L culture.
- Washing Buffer: 25 mM Tris pH 8.0, 2% (v/v) glycerol, 2 mM DTT.
- Elute Buffer: 25 mM Tris pH 8.0, 100 mM NaCl, 10% (v/v) glycerol, 2 mM DTT, 10 mM Maltose.
- MonoQ Buffer A: 25 mM Tris pH 8.0, 2% (v/v) glycerol, 2 mM DTT.
- MonoQ Buffer B: 25 mM Tris pH 8.0, 2% (v/v) glycerol, 2 mM DTT, 1M NaCl.
- Dialysis Buffer: 25 mM Tris pH 8.0, 150 mM NaCl, 10% (v/v) glycerol, 2 mM DTT.

To purify myc-MDM2 protein, the pellet was thawed in lysis buffer at 4°C, and then the resuspended cells were lysed by sonication on ice (10 seconds pulses at power 6.5 for 2 minutes). The lysate was centrifuged at 14,000 rpm for 30 minutes to precipitate insoluble inclusion bodies. The clarified lysate was added to approximately 2 mL of amylose resin (New England Biochem) that had been washed once with 1 × TBS. The lysate and beads

slurry was incubated at 4°C for 3hour with gentle mixing in order to allow binding of desired protein to the resin.

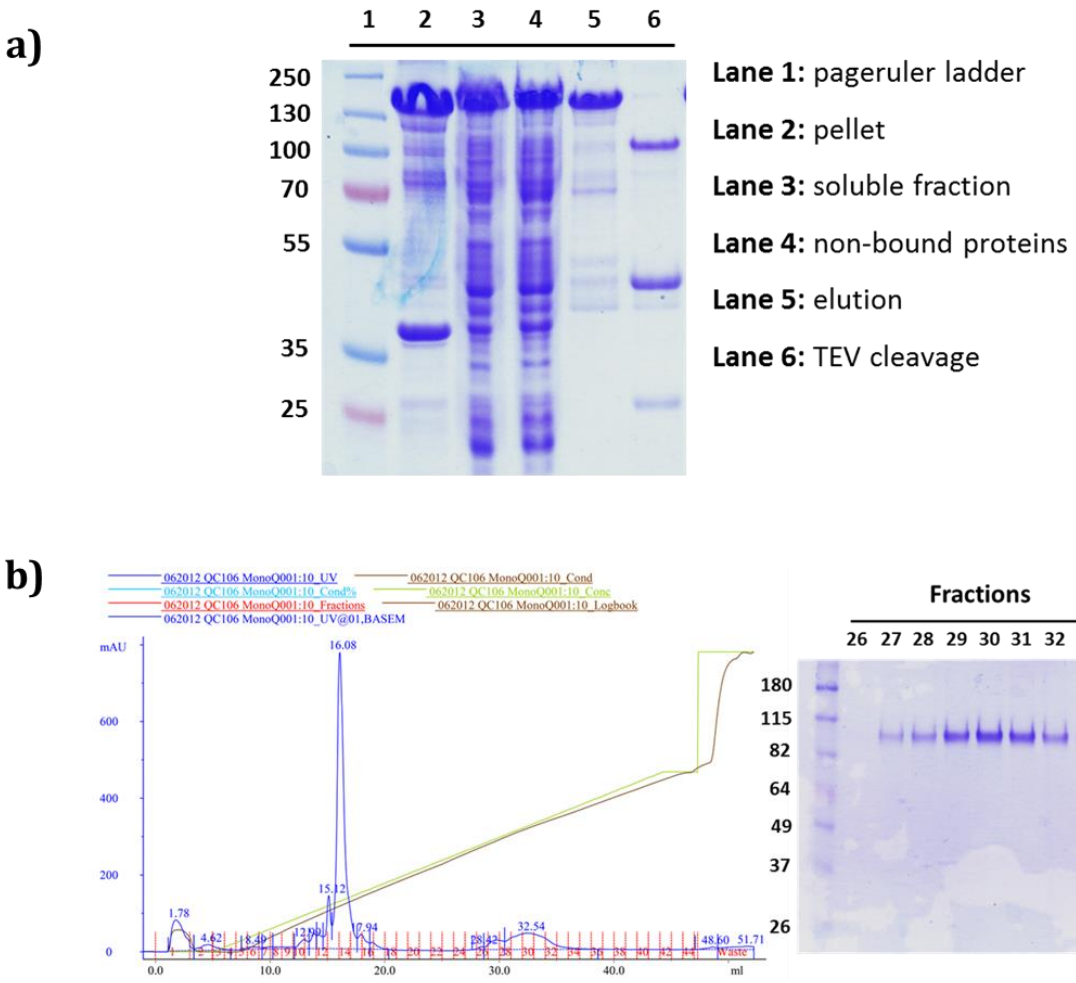

Figure 2.23 Myc-MDM2 purification. a) Coomassie staining of different fractions. b) MonoQ ion exchange column trace and coomassie stain of each fraction.

The protein bound bead slurry was washed with 1L washing buffer with salt gradient from 300 mM to 100 mM. Retained protein was then eluted with 4 mL elution buffer. The eluent was then incubated with 200 µL 1 mg/mL TEV protease at 4°C for 12 hours. The eluent was loaded onto a MonoQ 5/50 GL ion exchange FPLC column (GE Healthcare). The proteins were eluted with a linear gradient of 0-60% MonoQ buffer B over 40 column volumes. The desired protein was pooled and dialysed overnight at 4°C for

buffer exchange. The dialysed MDM2 protein was then concentrated, quantified by 280 nm absorbance, aliquot 100 µL in each PCR tube, and stored at -80°C until use.

7. Myc-MDM2 C464A. This MDM2 mutant protein was expressed and purified using the same protocol as myc-MDM2 except that pMAL-TEV-myc-MDM2 C464A construct was transformed into bacteria cells.

Fluorescence Polarization Assays. Peptide biding assays were performed in triplicates by incubating 10 nM fluorescein-labeled peptides with two-fold serial dilution of β-catenin full length protein or human MDM2 full length protein in FP binding buffer (25 mM Tris pH 8.0, 300 mM NaCl, 2 mM DTT and 2% (v/v) Glycerol). Incubations were carried out in 384-well, black flat-bottom plates (Corning) with a total volume of 80 µL and equilibrated at 4°C for 3 hours. Polarization was measured on a Spectramax-M5 plate reader with λ_{ex} = 485 nm and λ_{em} = 525 nm. Dissociation constants (K_d) were determined by nonlinear regression analysis of dose-response curves using Prism software (GraphPad).

Competition Fluorescence Polarization Assays. Competitive fluorescence polarization assays were performed by incubation of varied concentrations of non-fluorescein labeled bisax peptides with a pre-equilibrated (30 minutes at 4°C) mixture of 90 nM β-catenin full length protein with 10 nM fluorescein labeled StAx-35 or 90 nM human MDM2 full length protein with 10 nM fluorescein labeled SAH-p53-8. Polarization measurements and calculations were performed as above for fluorescence polarization assays.

Establish Stable HEK293T cells constitutively expressing myc$_3$-MDM2. HEK293T cells were grown in 6-cm plate in complete growth medium (DMEM, 10% FBS and 1% penicillin/streptomycin) and allowed to grow to ~80% confluency at the time of transfection. Transfection was performed using 3 μg of pCMV-myc$_3$-MDM2 plasmid with JetPRIME transfection reagent (Polyplus Transfection). A fresh medium was changed approximately 5 hours after transfection. 24 hours post transfection, cell culture medium was exchanged to medium supplemented with 0.6 mg/mL of G418 (EMD Millipore). The medium was kept changing every other day for about 2 weeks. Once all cells were dead in the nontransfected control plate, the remaining cells in the transfected plate were trypsinized and diluted to 150 cells/mL. Meanwhile, five 96-well clear bottom plates (Corning) were filled with 80 μL of complete growth medium containing 0.6 mg/mL G418. Then 20 μL of diluted cells were added into each well and the plates were incubated in 37°C incubator for about two weeks to allow colonies to form. Re-seeded the monoclonal cells in 24-well clear bottom plates (Corning) and waited until reaching ~80% confluency, at which point, half of the cells were passaged to new 24-well plates, and the other half were lysed and accessed for myc$_3$-MDM2 expression. The best expression monoclone (Figure 2.24 Lane 5) was selected as stable HEK293T cells for use.

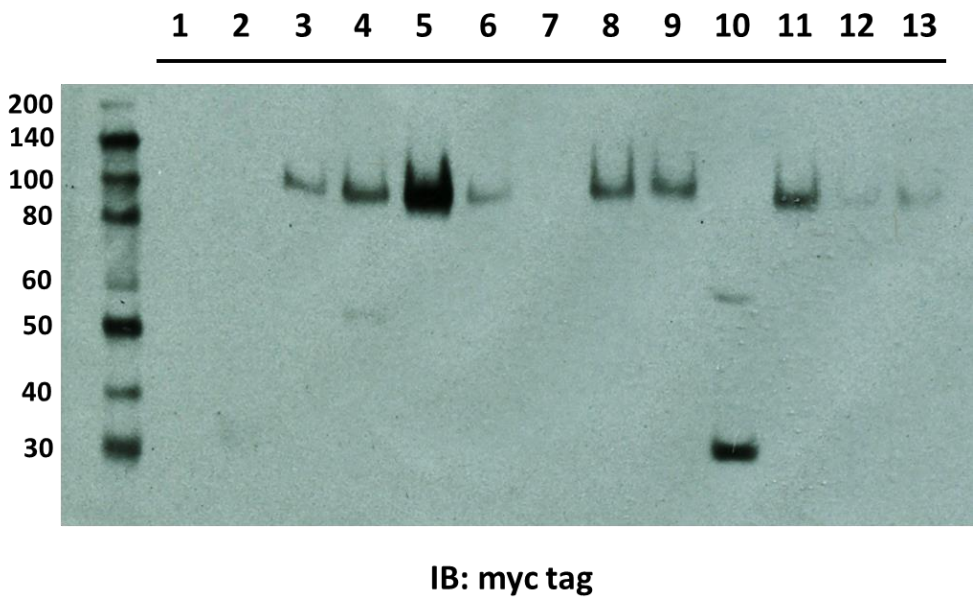

Figure 2.24 Myc_3-MDM2 expression in different monoclonal cells as visualized by western blotting.

Pull-down Assays. Glutathione functionalized agarose beads (Thermo) were washed once with pull-down buffer (25 mM Tris pH 8.0, 300 mM NaCl, 2 mM DTT, 2% (v/v) Glycerol and 0.1% Tween-20), followed by incubation with 1 μM GST-β-catenin in 1 mL pull-down buffer for 3 hours at 4°C. Excess protein was washed away from the beads three times with pull-down buffer. In the meantime, HEK293T cells which constitutively express myc-MDM2 were lysed in lysis buffer (50 mM Tris pH 7.4, 150 mM NaCl, 1 mM PMSF, 1% Triton X-100) followed by removal of insoluble debris by centrifugation at 13, 000 × g. Then GST- β-catenin immobilized beads were incubated with indicated concentration of bisax peptides, 200 μL HEK293T cell lysates and pull-down buffer to make a total volume of 500 μL. Incubation was performed at 4°C for 5 hours. The beads were washed repeatedly with pull-down buffer before elution of bound proteins by heating in SDS gel loading buffer at 95°C for 10 minutes. Bound MDM2 protein and β-catenin loadings were visualized by western

blotting following standard methods and using antibodies specific for myc-tag (2272S, Cell Signaling) and β-catenin (9581S Cell Signaling).

Competition Pull-down Assays. Streptavidin coated M-280 Dynabeads (Invitrogen) was washed with pull-down buffer once before incubation with 1 μM biotin-β-catenin in 500 μL pull-down buffer for 30 minutes at 4°C. Excess protein was washed from the beads three times with pull-down buffer. The biotin-β-catenin immobilized beads were incubated with 200 μL stable HEK293T cell lysates, 100 nM Bisax-8 and indicated concentration of StAx-35 or SAH-p53-8. Pull-down buffer was added to a final volume of 500 μL. The mixture was gently rotated at 4°C for 5 hours. The beads were washed repeated with pull-down buffer before elution of bound proteins by heating in SDS gel loading buffer at 95°C for 10 minutes. Bound MDM2 protein and β-catenin loadings were visualized by western blotting following standard methods and using antibodies specific for myc-tag (2272S, Cell Signaling) and β-catenin (9581S Cell Signaling).

***In Vitro* Ubiquitination Assays for β-catenin.** Streptavidin coated M-280 Dynabeads (Invitrogen) was washed with pull-down buffer once before incubation with 1 μM biotin-β-catenin in 500 μL pull-down buffer for 1 hour at 4°C. Excess protein was washed from the beads three times with pull-down buffer. The biotin-β-catenin immobilized beads were incubated with 200 nM Uba1, 2 μM UbcH5c, 1 mg/mL ubiquitin (Boston Biochem), 1.4 μM MDM2, 1 μM indicated bisax peptide, 5 mM ATP, 250 mM NaCl, 50 μM $ZnCl_2$ and 500 μM DTT in a total volume of 20 μL reaction buffer (50 mM Tris pH 8.0, 50 mM KCl, 5 mM $MgCl_2$) at 37°C for 2 hours. Then the beads were washed with pull-down buffer three times at

room temperature, followed by elution of bound proteins by heating in SDS gel loading buffer at 95℃ for 10 minutes. Ubiquitinated β-catenin bands were visualized by western blotting following standard methods and using antibodies specific for β-catenin (9581S Cell Signaling) and ubiquitin (3936S, Cell Signaling).

***In vitro* Ubiquitination Assay for KRas and c-myc.** *In vitro* ubiqutination assay for KRas and c-myc protein was performed following previous protocol[50]. Briefly, a mixture of 600 nM substrate protein (KRas or c-myc), 200 nM Uba1, 2 μM UbcH5c, 1 mg/mL ubiquitin (Boston Biochem), increasing amount of MDM2 (1.4, 2.8 and 4.2 μM), 1 μM bisax-8 peptide, 5 mM ATP, 250 mM NaCl, 50 μM $ZnCl_2$ and 500 μM DTT in a total volume of 20 μL reaction buffer (50 mM Tris pH 8.0, 50 mM KCl, 5 mM $MgCl_2$) was incubated at 37℃ for 2 hours. The resulting solution was added 10 μL 3 × SDS gel loading buffer and boiled at 95℃ for 10 minutes. KRas or c-myc protein was visualized by western blotting following standard methods and using antibodies specific for KRas (3339S Cell Signaling) and c-myc (5605S, Cell Signaling). Meanwhile, control experiments without either bisax-8 or MDM2 were performed in parallel following the same protocol. The KRas and c-myc proteins were generously provided by John McGee in Verdine Lab.

Cell Penetration Assays. HeLa cells grown in complete growth medium (DMEM, 10% FBS and 1% penicillin/streptomycin) were harvested, counted using a hemocytometer, and seeded in a black, clear bottom 384-well plate (Corning) with 2,000 cells per well. The plate was incubated overnight at cell incubator to allow attachment of the cells to the bottom of the well. The next morning, the cells were washed with PBS once, before incubated with

indicated concentrations of fluorescein-labeled peptides in fresh complete growth medium for 4 hours at 37℃. Cells were washed with PBS three times, fixed with 4% (w/v) paraformaldehyde and stained with Hoechst dye (Invitrogen). Then 100 μL PBS was added into each well and the plate was sealed with tape to avoid dryness. High content imaging measurements were performed to determine intracellular access on an IX5000 epifluorescence microscope (Molecular Devices Corporation). Epifluorescent images were taken at 20 × magnification in triplicate, imported into MetaXpress software. A relative fluorescence intensity was calculated for positive cells which were identified based on cell size and signal/noise ratio.

- General parameters for image acquisition:

  Wavelength One: DAPI, excitation for 20ms, laser-based and image-based autofocus,

  Wavelength Two: FITC, excitation for 5ms, offset from wavelength one = + 5 μm.

- General parameters for image analysis in MetaXpress:

  Wavelength One: DAPI, minimum cell diameter = 6 μm, maximum cell diameter = 20 μm, minimum intensity above local background = 1,000,

  Wavelength Two: FITC, minimum cell diameter = 6 μm, maximum cell diameter = 30 μm, minimum intensity above local background = 500.

β-catenin Degradation Assays. SW480 cells grown in complete growth medium (L-15, 10% FBS and 1% penicillin/streptomycin) were harvested, counted using a hemocytometer, and seeded in a clear bottom 96-well plate (Corning) with 10,000 cells per well. The plate was incubated overnight at cell incubator to allow attachment of the cells to the surface of the well. The next morning, the cells were washed with PBS once, before incubated with

indicated concentrations of bisax peptides in fresh complete growth medium for 7 hours at 37°C. The cells were then washed with PBS three times followed by lysis in SDS gel loading buffer. The lysate were heated at 95°C for 10 minutes, and β-catenin protein and β-actin loading control were visu**a**lized by western blotting following standard methods and using antibodies specific for β-catenin (9581S Cell Signaling) and β-actin (A5316, Sigma-Aldrich).

Luciferase Reporter Gene Assay. Luciferase reporter gene assay using a plasmid containing tandem wild-type TCF-4 consensus binding sites at the promoter region of firefly luciferase gene were performed to evaluate intracellular β-catenin activity. SW480 cells were plated in 6-cm plate and allowed to grow to ~80% confluency at the time of transfection. 3 μg of TOPflash plasmid and 2 μg pGLTK-renilla luciferase control plasmid were cotransfected into SW480 cells using JetPRIME transfection reagent (Polyplus Transfection) following manufacturer's protocol. A fresh medium was changed 5 hours after transfection. Cells were trypsinized approximately 24 hours after transfection and were re-seeded in 96-well clear bottom plate (Corning) with 10,000 cells per well. Cells were incubated at 37°C/5% CO_2 for 24 hours to ensure that all the cells were fully settled down. Then medium was aspirated and bisax peptides and DMSO vehicle were added at indicated concentrations with a total volume of 40 μL. Compounds were incubated for another 24 hours before measurement of luciferase activities. Cells were washed gently with 100 μL PBS once and lysed using lysis buffer supplied in dual-luciferase assay kit (Promega). After lysis, firefly and renilla luciferase activities were measured according to manufacturer's protocol. Firefly luciferase value was then normalized to renilla control

values in order to determine intracellular β-catenin activity in suppressing luciferase expression.

Reference

1. Nusse, R.; Varmus, H. E., Many Tumors Induced by the Mouse Mammary-Tumor Virus Contain a Provirus Integrated in the Same Region of the Host Genome. *Cell* **1982,** *31* (1), 99-109.

2. Rijsewijk, F.; Schuermann, M.; Wagenaar, E.; Parren, P.; Weigel, D.; Nusse, R., The Drosophila Homolog of the Mouse Mammary Oncogene Int-1 Is Identical to the Segment Polarity Gene Wingless. *Cell* **1987,** *50* (4), 649-657.

3. Nussleinvolhard, C.; Wieschaus, E., Mutations Affecting Segment Number and Polarity in Drosophila. *Nature* **1980,** *287* (5785), 795-801.

4. Huang, H.; He, X., Wnt/beta-catenin signaling: new (and old) players and new insights. *Curr Opin Cell Biol* **2008,** *20* (2), 119-125.

5. Clevers, H., Wnt/beta-catenin signaling in development and disease. *Cell* **2006,** *127* (3), 469-480.

6. Gordon, M. D.; Nusse, R., Wnt signaling: Multiple pathways, multiple receptors, and multiple transcription factors. *J Biol Chem* **2006,** *281* (32), 22429-22433.

7. Clevers, H.; Nusse, R., Wnt/beta-Catenin Signaling and Disease. *Cell* **2012,** *149* (6), 1192-1205.

8. Valenta, T.; Hausmann, G.; Basler, K., The many faces and functions of beta-catenin. *Embo J* **2012,** *31* (12), 2714-2736.

9. Cadigan, K. M.; Waterman, M. L., TCF/LEFs and Wnt Signaling in the Nucleus. *Csh Perspect Biol* **2012,** *4* (11).

10. Kimelman, D.; Xu, W., beta-Catenin destruction complex: insights and questions from a structural perspective. *Oncogene* **2006,** *25* (57), 7482-7491.

11. Ha, N. C.; Tonozuka, T.; Stamos, J. L.; Choi, H. J.; Weis, W. I., Mechanism of phosphorylation-dependent binding of APC to beta-catenin and its role in beta-catenin degradation. *Mol Cell* **2004,** *15* (4), 511-521.

12. Cadigan, K. M.; Liu, Y. I., Wnt signaling: complexity at the surface. *J Cell Sci* **2006,** *119* (3), 395-402.

13. Willert, K.; Jones, K. A., Wnt signaling: is the party in the nucleus? *Gene Dev* **2006,** *20* (11), 1394-1404.

14. Wodarz, A.; Nusse, R., Mechanisms of Wnt signaling in development. *Annu Rev Cell Dev Bi* **1998,** *14*, 59-88.

15. Reya, T.; Clevers, H., Wnt signalling in stem cells and cancer. *Nature* **2005,** *434* (7035), 843-850.

16. Nusse, R., Wnt signaling in disease and in development. *Cell Res* **2005,** *15* (1), 28-32.

17. Bienz, M.; Clevers, H., Linking colorectal cancer to Wnt signaling. *Cell* **2000,** *103* (2), 311-320.

18. Westendorf, J. J.; Kahler, R. A.; Schroeder, T. M., Wnt signaling in osteoblasts and bone diseases. *Gene* **2004,** *341*, 19-39.

19. MacDonald, B. T.; Tamai, K.; He, X., Wnt/beta-Catenin Signaling: Components, Mechanisms, and Diseases. *Dev Cell* **2009,** *17* (1), 9-26.

20. Huang, S. M. A.; Mishina, Y. M.; Liu, S. M.; Cheung, A.; Stegmeier, F.*, et al.*, Tankyrase inhibition stabilizes axin and antagonizes Wnt signalling. *Nature* **2009,** *461* (7264), 614-620.

21. Chen, B. Z.; Dodge, M. E.; Tang, W.; Lu, J. M.; Ma, Z. Q.*, et al.*, Small molecule-mediated disruption of Wnt-dependent signaling in tissue regeneration and cancer. *Nat Chem Biol* **2009,** *5* (2), 100-107.

22. Lu, J. M.; Ma, Z. Q.; Hsieh, J. C.; Fan, C. W.; Chen, B. Z.*, et al.*, Structure-activity relationship studies of small-molecule inhibitors of Wnt response. *Bioorg Med Chem Lett* **2009,** *19* (14), 3825-3827.

23. Thorne, C. A.; Hanson, A. J.; Schneider, J.; Tahinci, E.; Orton, D.*, et al.*, Small-molecule inhibition of Wnt signaling through activation of casein kinase 1alpha. *Nat Chem Biol* **2010,** *6* (11), 829-36.

24. Lepourcelet, M.; Chen, Y. N. P.; France, D. S.; Wang, H. S.; Crews, P.; Petersen, F.; Bruseo, C.; Wood, A. W.; Shivdasani, R. A., Small-molecule antagonists of the oncogenic Tcf/beta-catenin protein complex. *Cancer Cell* **2004,** *5* (1), 91-102.

25. Emami, K. H.; Nguyen, C.; Ma, H.; Kim, D. H.; Jeong, K. W.*, et al.*, A small molecule inhibitor of beta-catenin/CREB-binding protein transcription [corrected]. *Proc Natl Acad Sci U S A* **2004,** *101* (34), 12682-7.

26. Fearnhead, N. S.; Wilding, J. L.; Bodmer, W. F., Genetics of colorectal cancer: hereditary aspects and overview of colorectal tumorigenesis. *Brit Med Bull* **2002,** *64*, 27-43.

27. Kemler, R., From Cadherins to Catenins - Cytoplasmic Protein Interactions and Regulation of Cell-Adhesion. *Trends Genet* **1993,** *9* (9), 317-321.

28. Xing, Y.; Takemaru, K. I.; Liu, J.; Berndt, J. D.; Zheng, J. J.; Moon, R. T.; Xu, W. Q., Crystal structure of a full-length beta-catenin. *Structure* **2008,** *16* (3), 478-487.

29. Sampietro, J.; Dahlberg, C. L.; Cho, U. S.; Hinds, T. R.; Kimelman, D.; Xu, W. Q., Crystal structure of a beta-catenin/BCL9/Tcf4 complex. *Mol Cell* **2006,** *24* (2), 293-300.

30. Walensky, L. D.; Kung, A. L.; Escher, I.; Malia, T. J.; Barbuto, S.; Wright, R. D.; Wagner, G.; Verdine, G. L.; Korsmeyer, S. J., Activation of apoptosis in vivo by a hydrocarbon-stapled BH3 helix. *Science* **2004,** *305* (5689), 1466-1470.

31. Moellering, R. E.; Cornejo, M.; Davis, T. N.; Del Bianco, C.; Aster, J. C.*, et al.*, Direct inhibition of the NOTCH transcription factor complex. *Nature* **2009,** *462* (7270), 182-U57.

32. Xing, Y.; Clements, W. K.; Kimelman, D.; Xu, W. Q., Crystal structure of a beta-catenin/axin complex suggests a mechanism for the beta-catenin destruction complex. *Gene Dev* **2003,** *17* (22), 2753-2764.

33. Grossmann, T. N.; Yeh, J. T. H.; Bowman, B. R.; Chu, Q.; Moellering, R. E.; Verdine, G. L., Inhibition of oncogenic Wnt signaling through direct targeting of beta-catenin. *P Natl Acad Sci USA* **2012,** *109* (44), 17942-17947.

34. Hershko, A.; Ciechanover, A., The ubiquitin system. *Annu Rev Biochem* **1998,** *67*, 425-479.

35. Liu, J.; Farmer, J. D.; Lane, W. S.; Friedman, J.; Weissman, I.; Schreiber, S. L., Calcineurin Is a Common Target of Cyclophilin-Cyclosporine-a and Fkbp-Fk506 Complexes. *Cell* **1991,** *66* (4), 807-815.

36. Brown, E. J.; Albers, M. W.; Shin, T. B.; Ichikawa, K.; Keith, C. T.; Lane, W. S.; Schreiber, S. L., A Mammalian Protein Targeted by G1-Arresting Rapamycin-Receptor Complex. *Nature* **1994,** *369* (6483), 756-758.

37. Pollock, R.; Clackson, T., Dimerizer-regulated gene expression. *Curr Opin Biotech* **2002,** *13* (5), 459-467.

38. Corson, T. W.; Aberle, N.; Crews, C. M., Design and Applications of Bifunctional Small Molecules: Why Two Heads Are Better Than One. *Acs Chem Biol* **2008,** *3* (11), 677-692.

39. Sakamoto, K. M.; Kim, K. B.; Kumagai, A.; Mercurio, F.; Crews, C. M.; Deshaies, R. J., Protacs: Chimeric molecules that target proteins to the Skp1-Cullin-F box complex for ubiquitination and degradation. *P Natl Acad Sci USA* **2001,** *98* (15), 8554-8559.

40. Hines, J.; Gough, J. D.; Corson, T. W.; Crews, C. M., Posttranslational protein knockdown coupled to receptor tyrosine kinase activation with phosphoPROTACs. *P Natl Acad Sci USA* **2013,** *110* (22), 8942-8947.

41. Cyrus, K.; Wehenkel, M.; Choi, E. Y.; Swanson, H.; Kim, K. B., Two-Headed PROTAC: An Effective New Tool for Targeted Protein Degradation. *Chembiochem* **2010,** *11* (11), 1531-1534.

42. Bernal, F.; Tyler, A. F.; Korsmeyer, S. J.; Walensky, L. D.; Verdine, G. L., Reactivation of the p53 tumor suppressor pathway by a stapled p53 peptide. *J Am Chem Soc* **2007,** *129* (16), 5298-5298.

43. Prescher, J. A.; Bertozzi, C. R., Chemistry in living systems. *Nat Chem Biol* **2005,** *1* (1), 13-21.

44. Lundblad, J. R.; Laurance, M.; Goodman, R. H., Fluorescence polarization analysis of protein-DNA and protein-protein interactions. *Mol Endocrinol* **1996,** *10* (6), 607-612.

45. Li, M. Y.; Brooks, C. L.; Wu-Baer, F.; Chen, D. L.; Baer, R.; Gu, W., Mono-versus polyubiquitination: Differential control of p53 fate by Mdm2. *Science* **2003,** *302* (5652), 1972-1975.

46. Detection of protein-protein interactions using the GST fusion protein pull-down technique. *Nat Methods* **2004,** *1* (3), 275-276.

47. Fang, S. Y.; Jensen, J. P.; Ludwig, R. L.; Vousden, K. H.; Weissman, A. M., Mdm2 is a RING finger-dependent ubiquitin protein ligase for itself and p53. *J Biol Chem* **2000,** *275* (12), 8945-8951.

48. Skowyra, D.; Craig, K. L.; Tyers, M.; Elledge, S. J.; Harper, J. W., F-box proteins are receptors that recruit phosphorylated substrates to the SCF ubiquitin-ligase complex. *Cell* **1997,** *91* (2), 209-219.

49. Sadowski, M.; Sarcevic, B., Mechanisms of mono- and poly-ubiquitination: Ubiquitination specificity depends on compatibility between the E2 catalytic core and amino acid residues proximal to the lysine. *Cell Div* **2010,** *5*.

50. Lorick, K. L.; Yang, Y.; Jensen, J. P.; Iwai, K.; Weissman, A. M., Studies of the ubiquitin proteasome system. *Current protocols in cell biology* **2006,** *Chapter 15*, Unit 15 9.

51. Hershko, A.; Ganoth, D.; Pehrson, J.; Palazzo, R. E.; Cohen, L. H., Methylated Ubiquitin Inhibits Cyclin Degradation in Clam Embryo Extracts. *J Biol Chem* **1991,** *266* (25), 16376-16379.

52. Pylayeva-Gupta, Y.; Grabocka, E.; Bar-Sagi, D., RAS oncogenes: weaving a tumorigenic web. *Nat Rev Cancer* **2011,** *11* (11), 761-774.

53. Nair, S. K.; Burley, S. K., X-ray structures of Myc-Max and Mad-Max recognizing DNA: Molecular bases of regulation by proto-oncogenic transcription factors. *Cell* **2003,** *112* (2), 193-205.

54. Morin, P. J.; Sparks, A. B.; Korinek, V.; Barker, N.; Clevers, H.; Vogelstein, B.; Kinzler, K. W., Activation of beta-catenin-Tcf signaling in colon cancer by mutations in beta-catenin or APC. *Science* **1997,** *275* (5307), 1787-1790.

55. Kim, Y. W.; Grossmann, T. N.; Verdine, G. L., Synthesis of all-hydrocarbon stapled alpha-helical peptides by ring-closing olefin metathesis. *Nature protocols* **2011,** *6* (6), 761-71.

Chapter III Studies on Cell Penetration by Stapled Peptides

Stapled Peptides as a New Class of Cell Penetrating Peptides

Hydrocarbon-stapled α-helical peptides represent a new class of synthetic peptidomimetics capable of inhibiting protein-protein interactions[1]. Incorporation of α-methyl, α-alkenyl amino acids at defined positions in a synthetic peptide permits side-chain crosslinking on-resin via ring-closing olefin metathesis[2]. Our group has shown that hydrocarbon "staples" spanning one or two helical turns increase α-helical content and protease resistance, enhance target binding affinity, and promote cell membrane penetration[3-4]. This technology has been successfully utilized to address many challenging problems in biological systems, including targeting multi-component transcription factor complexes and disrupting cryptic protein-protein interactions[5-8]. One important feature enabling stapled peptides to have such promising therapeutic potential involves their exceptional cell penetration properties. Indeed, several studies have demonstrated that stapled peptides show improved cell peremeability from their parent unmodified peptides.

The cell permeability of stapled peptides has been previously studied on fluorophore-labeled peptides using flow cytometry and confocal microscopy[9]. One advantage of flow cytometry is that for each condition, one can analyze a large number of cells, typically more than 1×10^4, which provides a statistically reliable evaluation of cell penetration over a large sample size. However, this method can only generate a distribution of fluorophore intensity without visible cell images showing subcellular

localization. Confocal microscopy, on the other hand, can provide a wealth of high-resolution of cell images showing the localization of fluorophore-labeled peptides in great detail, which might provide clues as to the mechanism of cellular uptake and intracellular trafficking. However, one notable drawback for confocal microscopy is that it generally does not provide a quantitative analysis of cell penetration. In other words, one can only compare intracellular accumulations for different peptides by judging the fluorescence signal empirically. We therefore needed to develop a new image-based platform that can be used to evaluate the cell penetration property for stapled peptides quantitatively.

The improved cell permeability of stapled peptides enables them to exert potent and specific inhibition of protein-protein interactions *in vivo*, however, there is still much to learn regarding the mechanisms of cellular uptake itself. An energy-dependent endocytosis model for cell penetration by stapled peptides was establised based on preliminary results which showed impaired cell entry at 4°C as well as the colocalization of fluorescein-labeled stapled peptides and the endosomal marker TRITC (tetramethylrhodamine isothiocyanate)-dextran[9]. Given the diversity in structure and chemical properties of stapled peptides, however, this mechanism required further validation in a larger samples. The gain of cell penetration is proposed to result from the unique features of stapled peptides. For example, the introduction of an all-hydrocarbon crosslink results in the constrained α-helix conformation, which embeds the hydrophilic amide backbone in the core of the folded structure. Furthermore, the hydrocarbon brace itself introduces a significantly hydrophobic patch to one face of the peptide. The exposure of the hydrophobic moiety as well as the mask of the hydrophilic peptide backbone may facilitate the interaction of stapled peptides with the hydrophobic interior of the cell membrane and

thereby enhance the cellular uptake.

Based on this hypothesis as well as the commonly-used strategy adding cationic residues into peptide squences to improve cell entry, extensive efforts have been made to optimize cell penetration for stapled peptides[1, 4, 7]. We tried all possible stapling positions and different stpaling types (stapled or stitched) in order to identify an optimized peptide conformation for cell penetration. In some cases, the glutamic acid and aspartic acid that were putatively uninvolved in binding to the target were replaced with glutamine and asparagine respectively to increase the net charge of the stapled peptides. In addition, an arginine residue, which is believed to facilitate cell entry via its terminal guanidinium group[10], was also appended at end of stapled peptides in an attempt to increase their cell permeability. These strategies successfully increased the cell penetration for several stapled peptides, but not all sequences benefited from these strategies. Therefore, systematic studies of mechanisms of cell penetration by stapled peptides will need to be performed in order to design the next generation stapled peptides with enhanced cell permeability.

Application of Stapled Peptides in Drug Delivery

Cell internalization of large hydrophilic therapeutic molecules such as nucleic acids and proteins is a challenging task because of the poor efficiency with which they translocate across cell membranes[11-12]. In order to address this problem, significant efforts have been made to develop carrier-mediated delivery systems which can assist entry of

macromolecules with potential therapeutic applications into cellular compartments. Among them, cell penetrating peptide-based delivery has aroused extensive interest[12-14]. In recent years, a large number of successful cases using cell penetrating peptides for drug delivery have been reported. For example, the TAT peptide, derived from cell penetrating HIV TAT protein, has been demonstrated to deliver large, active proteins into the cells of live mice[15]. The TAT peptide has also been used to carry phage-encapsulated DNA into cells, as well as liposome-encapsulated DNA for gene expression in mice[16-17]. In addition, several TAT fusion proteins and peptides have been used to treat mouse models of cancer, inflammation and other diseases[18]. Given the enormous therapeutic and diagnostic potential of cell penetrating peptides and the improved cellular uptake of stapled peptides, it is promising to develop a stapled peptide based drug delivery system to facilitate a variety of macromolecular cargoes across the cell membrane.

This chapter will describe our efforts to develop a high-throughput image-based assay to quantitatively measure the cell permeability of stapled peptides. By applying this assay to the stapled peptide library generated by our group, we are aiming to correlate intracellular accumulation with intrinsic physicochemical properties, and to explore potential mechanisms of cell penetration. In addition, the differences in cell penetration by stapled peptide and unmodified cell penetrating peptides will be discussed side-by-side. Lastly, a proof-of-principle experiment will be described in which stapled peptides are applied as cargo carriers to deliver a biologically active morpholino molecule into cells.

Development of an Image-Based High-Throughput Assay to Quantitatively Measure Cell Penetration of Stapled Peptides

Understanding the internalization process of cell penetrating peptides (CPPs), especially stapled peptides, has been a subject of great interest during the last decade. The majority of previous studies have been performed by either using high-resolution microscopy to show the existence of fluorophore-labeled CPPs inside cells, or by quantitatively measuring the fluorescence distributions by fluorescence-activated cell sorting (FACS). Although these methods provided qualitative cell penetration information, a new assay combining high-resolution imaging as well as quantitative measurement needs to be developed in order to better understand the cellular uptake properties for stapled peptides. In recent years, high-throughput cell-based imaging platforms have become increasingly popular to screen for small molecule modulators in various biological processes[19-21]. Taking advantage of one of these platforms, the Molecular Devices Image Express Micro high-throughput epifluorescent microscope, we sought to develop a high-throughput quantitative assay to measure stapled peptide intracellular access.

Human U2OS osterosarcoma cells were used in this assay because they have good adherence properties as well as suitable cellular morphology, making them suitable features for imaging experiments. Cells were seeded in black, clear-bottom 384-well plates overnight, and incubated with fluorescein-labeled peptides or DMSO vehicle for 12 hours. After the treatment, cells were washed thoroughly with PBS to remove excess peptides, fixed with 4% formaldehyde, and stained with Hoechst dye to visualize nuclei. Once prepared, the plates were imaged by epifluorescence microscopy according to developed

protocols. Briefly, the microscope camera takes cell images separately on both the Hoechst channel (blue) and the FITC channel (green), which can be merged later during the analysis. It first performs a Z-scan on the Hoechst channel to locate cells, and the parameters were adjusted to optimize the cell size and fluorescence intensity. Then the parameters from this acquisition were transferred to the FITC channel to locate and take images of FITC-labeled peptides in all samples. This assay can be done in a high-throughput manner, resulting in a panel of Hoechst/FITC images from individual wells (Figure 3.1).

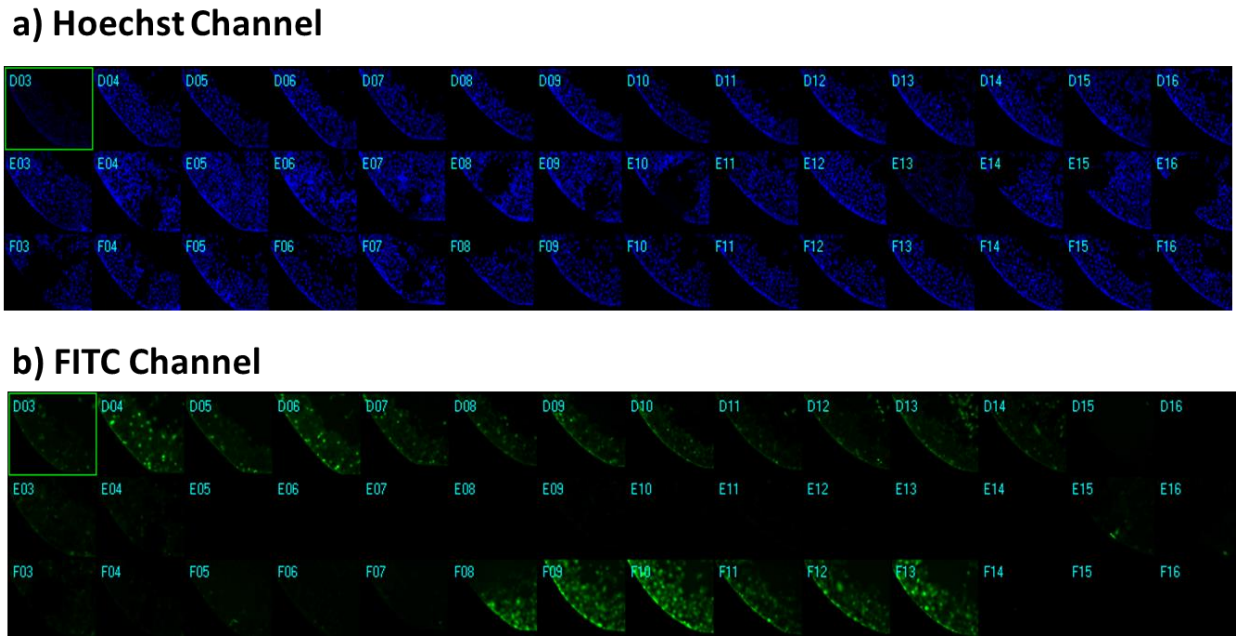

Figure 3.1 High-throughput epifluorescence microscopy images of stapled peptide intracellular access. a) Hoechst channel of a portion of a 384-well plate indicates the location and number of nuclei. b) The same portion of the 384-well plate shown in a) imaged in the FITC channel reveals different intracellular fluorescence accumulations.

The cell images were then imported to an associated software program, MetaXpress, for fluorescence quantification and analysis. Cells were identified based on the Hoechst stain of nuclei. Nuclei that were of correct size and Hoechst intensity were considered "positive" cells. The cytoplasm was designated according to the location of FITC signals as

well as empiric parameters (Details in Material and Methods). The FITC intensities in the cytoplasm and nuclei were quantified separately and the sum of these two values yielded the FITC signal for the whole cell, which can be considered the relative intracellular peptide intensity. In addition, FITC negative cells were also identified for those can be visualized by Hoechst stain but were invisible in FITC channel (Figure 3.2).

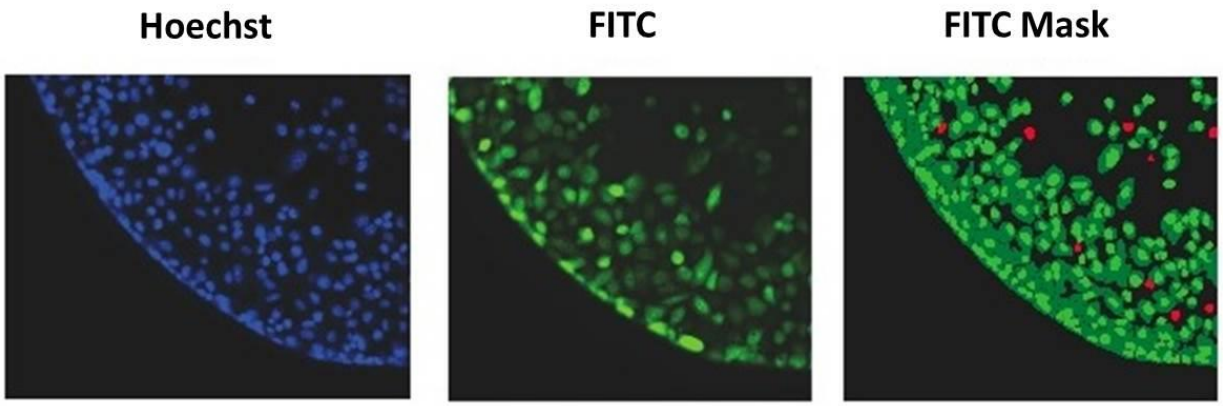

Figure 3.2 Quantitative measurement of cellular peptide intensity. a) Hoechst channel showing the location and size of nuclei. b) FITC channel showing the fluorescence intensity of the same cells. c) Information about cell size and fluorescence intensity were integrated to identify the FITC positive (Green mask) and negative (Red mask) cell. For positive cells, additional parameters allowed determination of the fluorescence intensity in nucleus (inner intense green) and cytoplasm (outer dimmer green).

With this experimental and analysis setup, we found that the system generated highly reproducible and reliable results from assay-to-assay and with different stocks of the same stapled peptides. As shown in Figure 3.3a, there were negligible fluorescence differences among experiments for cells treated with DMSO vehicle, which could be used as a fluorescence background for all following experiments. In addition, the same stapled peptides from different batches of synthesis featured almost identical intracellular fluorescence signals in different tests (Figure 3.3b), which indicated that the assay

developed in this study produces repeatable and reliable results that can be directly combined and compared from a large set of experiments.

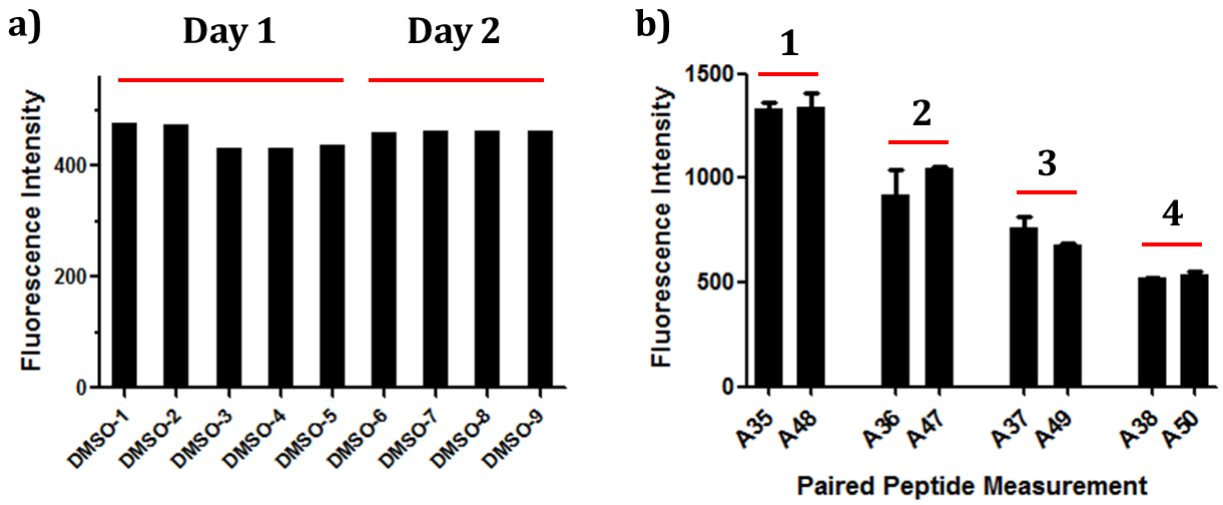

Figure 3.3 The image-based high-throughput assay yielded reproducible and reliable results. a) the background fluorescence for DMSO vehicle were almost identical among different experiments. b) Four stapled peptides from different batches of synthesis generated similar intracellular fluorescence intensity in different tests.

Analysis of Cell Penetration by Stapled Peptides

This quantitative high-throughput assay provides a reliable platform to perform a broad screen measuring cell penetration of stapled peptides and thereby investigating the mechanism beyond intracellular access. We collected and measured more than 200 distinct N-terminal FITC-labeled peptides belonging to three different classes, namely wild-type (unmodified), stapled and stitched peptides. We were aiming to compare the cell penetration capabilities for these peptides, and correlate the peptide intracellular access with their intrinsic chemical properties, which might inform future design of peptides with enhanced cell penetration.

The cell penetration assay was carried out using the same protocol as discussed above by treating cells with 1 μM FITC-labeled peptides for 12 hours in duplicate. Mean cellular fluorescence intensity was measured and the highly consistent DMSO background value was subtracted to yield a fluorescence signal for each peptide which was subject to comparison. Meanwhile, all peptides were converted to two-dimensional structures which were then imported to MarvinView software package (ChemAxon) for analysis of distinct theoretical physicochemical properties, such as molecular weight, formal charge at physiological pH, log *P* value, and 2D polar surface area (PSA), which are important parameters to evaluate "druglikeness" of small molecules according to Lipinski's rule[22]. The results are listed in Appendix Table 1.

In general, the unmodified, stapled and stitched peptide libraries present in this study had relatively similar physicochemical characteristics as shown in Figure 3.4. The mean molecular weight and calculated PSA values were nearly identical among the three peptide classes. A notable difference was observed among theoretical log *P* values, which were significantly higher for the stapled and stitched peptides relative to the unmodified peptides. This is not surprising as these modified peptides contain a solvent-exposed all hydrocarbon crosslink. Additionally, the stapled peptide class had a mean formal charge of approximately zero while the stitched and unmodified peptide classes exhibited a positive mean charge. Overall, the calculated physicochemical properties indicated that the peptide classes were quite similar in terms of their mean properties, which assures that the peptides chosen in this study were statistically significant and can be used to evaluate the penetration behavior for a broader collection of peptides.

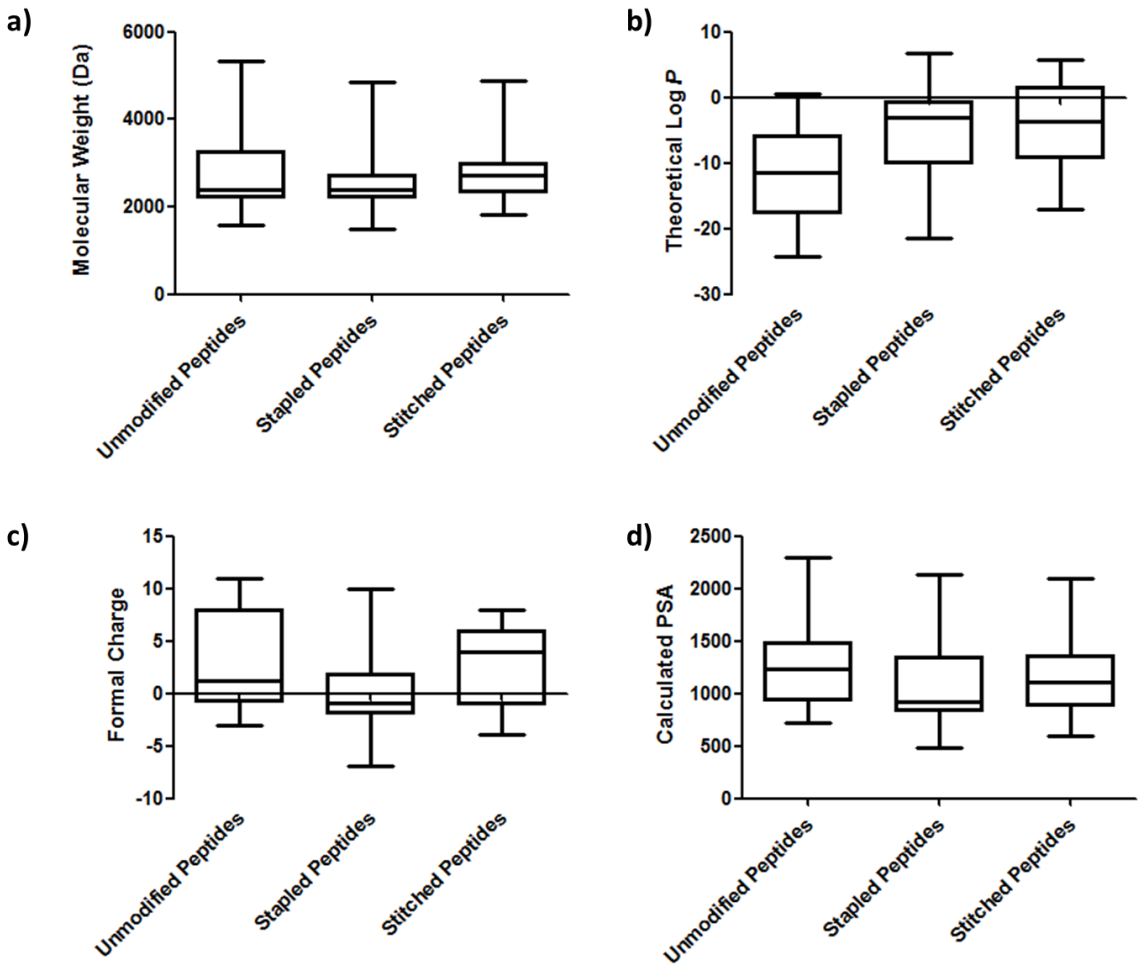

Figure 3.4 Physicochemical parameters a) molecular weight, b) theoretical Log *P*, c) formal charge at pH 7.5, d) calculated PSA of wild-type, stapled and stitched peptides. The data are plotted in whiskers format.

With these physicochemical parameters in hand, we next analyzed the mean cellular fluorescence intensity obtained from epifluorescence imaging. Interestingly, stapled and stitched peptides exhibited a significant increase in cell penetration compared with wild-type unmodified peptides (Figure 3.5a). Given that all three peptide classes have similar physicochemical properties in general, the benefit in cell penetration should be largely attributed to the synthetic stabilization of α-helical peptides, namely stapled peptide technology. Furthermore, we correlated the intracellular access with physical properties of

these peptides to figure out whether there exists any connection between cell penetration and intrinsic peptide properties. As a result, peptide charge appears to be the parameter correlated to intracellular access, which could be fitted into a Gaussian distribution with a population centroid at approximately +4 charged (Figure 3.5b). Specifically, peptides exhibiting a net negative charge (-7 to -1) showed little or no cellular uptake. Peptides of approximately neutral charge (-1 to +1) showed moderate cell penetration above background. Interestingly, peptides with a net positive charge (+1 to +7) showed significantly higher cell penetration as a group. Surprisingly, cellular uptake did not appear to increase linearly with charge, as the cell penetration decreases dramatically for peptides with charge greater than +7. This observation was not consistent with the previously reported models, which indicate that peptides with more positive charges have better penetration property due to the tighter electrostatic interaction with the negatively charged phospholipid membrane[23-24]. Although additional tests with a larger number of peptides could further confirm the results observed from this study, the unexpected relationship for highly charged peptides could result from the disruption of peptide packing during internalization or difficulty in dissociation from cell membrane. In addition, there was no discernible correlation between the penetration ability and peptide molecule weight, log *P* or PSA (Figure 3.5 c-e). The intracellular peptide levels were almost the same spanning a wide range in each class. Taken together, the stapling type and peptide charge are the key physical properties in determining peptide cell penetration ability, whereas the other parameters do not appear to have a significant effect.

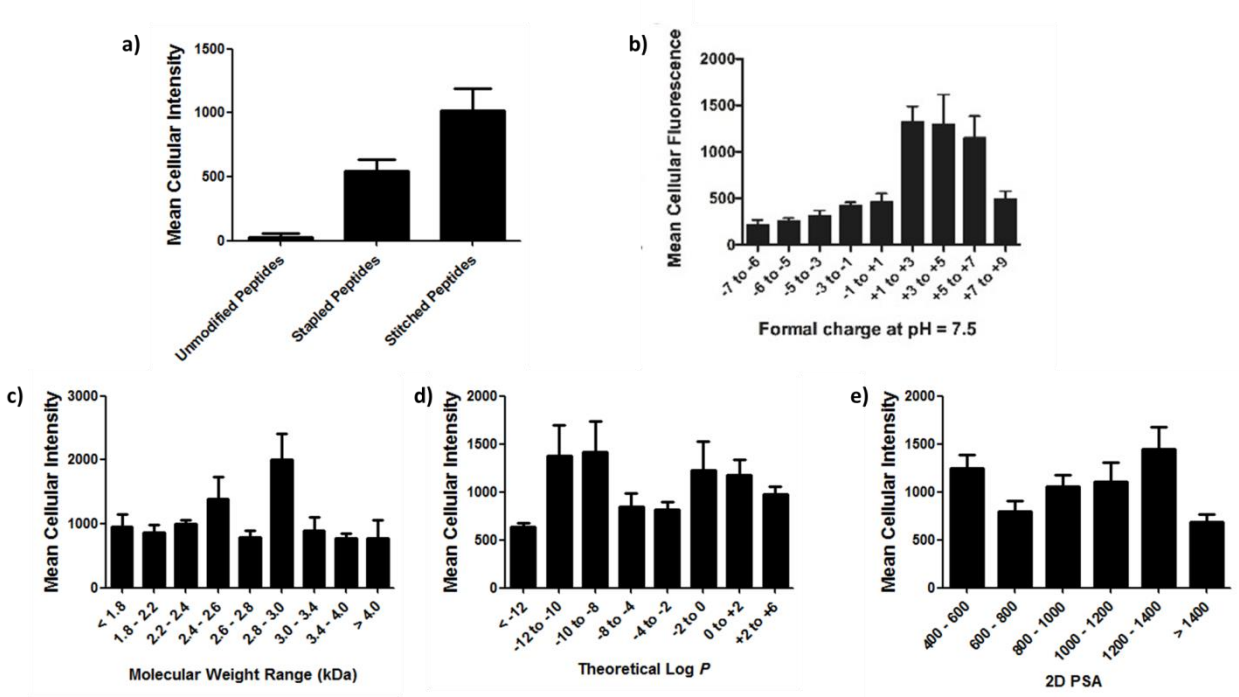

Figure 3.5 Relationship between mean cellular fluorescence intensity and physicochemical properties of peptides. a) stapling pattern, b) formal charge at pH 7.5, c) molecular weight, d) theoretical log *P*, and e) 2D PSA.

In order to further investigate the cell penetration properties for stapled peptides and systematically analyze the similarities and differences in cellular uptake between stapled peptides and other wild-type cell penetrating peptides (CPPs), several stapled peptides and CPPs were picked out from our peptide library to study their penetration behaviors side-by-side in dose-dependent manner. TAT (48 – 60), Antennapedia (Antp) and Poly-Arg_8 were used as wild-type (unstapled) peptides in this experiment since they are frequently used as model cell penetrating peptides in mechanism investigation and cargo delivery studies[25-27]. For stapled peptides, SAHM1, SAH-p53-8, SAHBa, TNG90 and TNG147 were chosen because they have different stapled patterns and exhibit distinct cellular uptake according the aforementioned broad screen. The experiments were carried out as described previously except that cells were incubated with a series of concentrations of peptides for 12 hours.

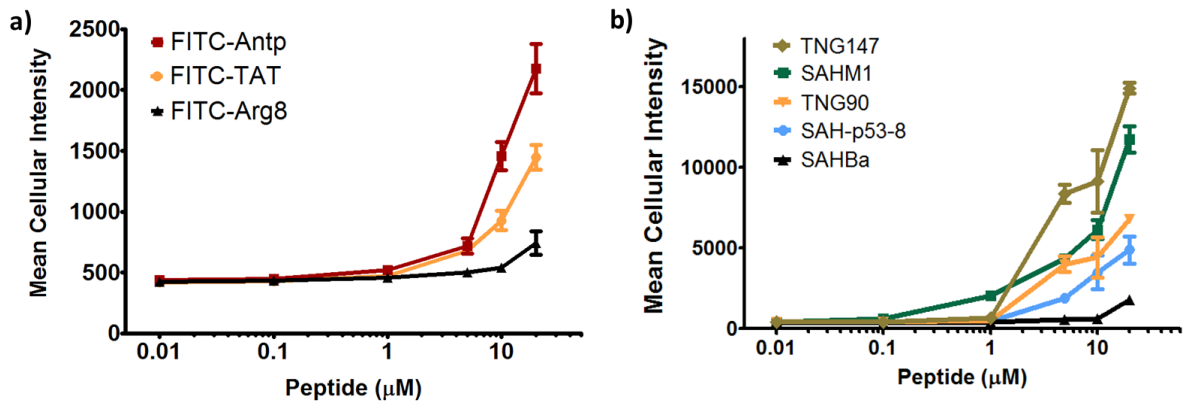

Figure 3.6 Dose-dependent cell penetration of a) wild-type and b) stapled peptides.

The results are shown in Figure 3.6. Generally, both wild-type and stapled peptides did not appear to have any cellular uptake below 1 μM except for the SAHM1 peptide which showed modest penetration at 1 μM. Starting at 1 μM, they showed enhanced intracellular access with increased peptide concentrations. Although the increases were different for distinct peptides, stapled peptides featured much faster growth rate in general. It is interesting to point out that TNG147 were poorly permeable at 1 μM but showed dramatic increase at 5 μM, which might suggest that a concentration-dependent peptide packing or a receptor-mediated mechanism facilitating the cell penetrating process. Furthermore, it is worth noting that stapled peptides are more cell permeable than wild-type peptides at all concentrations, especially at higher doses.

In addition, a time-course penetration assay was also performed to better understand peptide internalization kinetics. Antp and SAHM1 peptides were used as wild-type and stapled examples in this assay since they showed better cellular uptake in each class in the concentration-dependent assay discussed above. Cells were treated with Antp or SAHM1 peptide at two concentrations (5 and 10 μM, respectively), harvested at different

incubation time points and were subjected to imaging and analysis. As shown in Figure 3.7, wild-type and stapled peptides showed completely different penetration properties for different incubation durations. 5 μM and 10 μM Antp peptides had nearly identical cellular uptake for 2 hours incubation. After 2 hours, the intracellular fluorescence for both 5 μM and 10 μM treatments started to decrease until reaching a stable stage around 8 hours, and the signal remained unchanged up to 24 hours. This pattern could be attributed to the balance between cell penetration and fast proteolysis of wild-type Antp peptide. For the first 2 hours, cellular uptake predominated the process, while simultaneously the peptide underwent degradation through proteolysis as they accumulated inside cells. Equilibrium was achieved at approximately 8 hours incubation where the rate of penetration was almost the same as proteolysis. Notably, fluorescence intensity for 5 μM treatment dropped faster and was lower at the stable stage compared with 10 μM incubation. This might result from the slower peptide uptake at a lower concentration after 2 hours due to the decreased concentration potential across cell membrane. However, SAHM1 peptide showed increased cellular uptake for the first 8 hours at both concentrations, although the intracellular fluorescein intensity accumulated faster for 10 μM incubation. Fluorescence signal values were much higher than those observed in Antp treatment. After 8 hours, the fluorescence signal remained unchanged for 5 μM treatment and was slightly decreased after 16 hours incubation. However, treatment of 10 μM SAHM1 still showed slightly increasing cellular uptake up to 24 hours. Although stapled SAHM1 peptides exhibited distinctly improved penetration properties over time, it can be explained by the same model for Antp peptides which refers that the observed cellular uptake process is actually the consequence of cell penetration and intracellular proteolysis. Stapled SAHM1 has an all hydrocarbon crosslink

in peptide sequence, resulting in better cellular uptake yet much slower proteolysis, which makes it continuously accumulated in cells at 10 μM. The slight decrease in fluorescence intensity after 16 hours for 5 μM incubation could be attributed to attenuated penetration resulted from the less concentration potential across cell membranes.

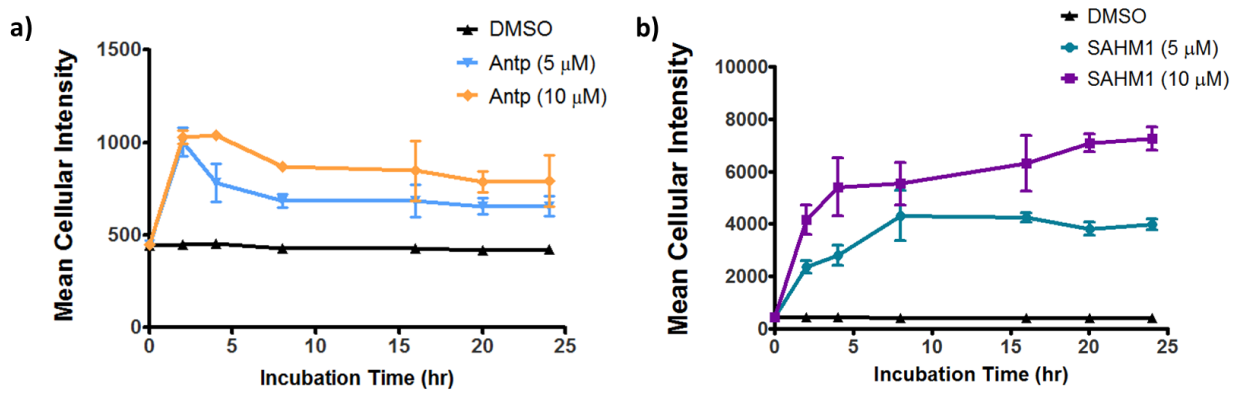

Figure 3.7 Cell penetration for a) Antp and b) SAHM1 peptides over time at concentrations of 5 and 10 μM. DMSO was also included in this assay as background reference.

Given the good cell penetration of SAHM1 peptide, a pulse-chase assay was performed to understand what the cellular uptake behaves if the peptide is removed from cell culture medium. The experiment was carried out using a similar protocol as before. 1 μM SAHM1 peptide was used in this assay because it would not saturate the intracellular fluorescence at early stage of the incubation. 12 hours after initial incubation, the cell culture medium was aspirated and cells were extensively washed with PBS to completely remove excess SAHM1 peptide. Then fresh medium containing either a new batch of 1 μM peptide or DMSO vehicle were added to incubate with cells for additional time periods as indicated. Cells were imaged and mean cellular fluorescence intensity was quantified and plotted at different time spots.

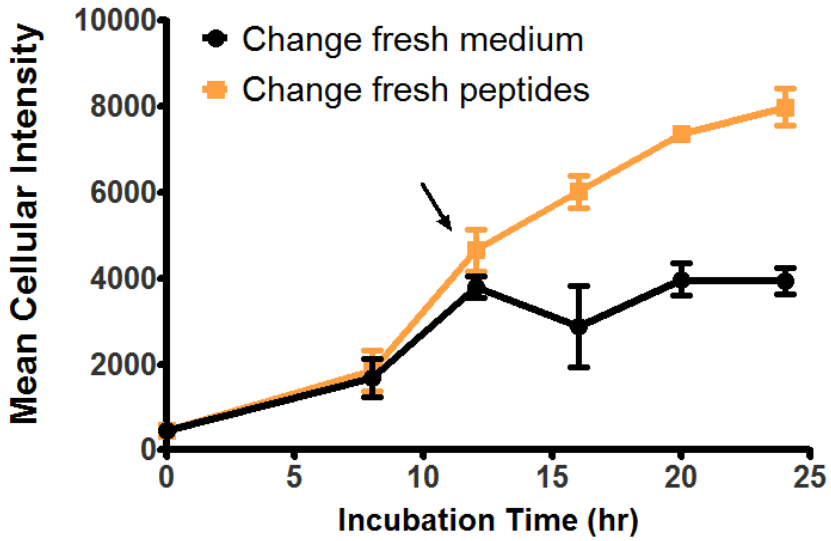

Figure 3.8 A pulse-chase penetration assay for SAHM1 peptide in which fresh medium containing either a new batch of peptide or DMSO vehicle were exchanged at 12 hours after initial treatment.

As expected, the cellular uptake kept growing for the first 12 hours incubation. After medium exchange, cells incubated with fresh medium containing DMSO vehicle retained the intracellular fluorescence intensity. Interestingly the signal for cells treated with the new batch of SAHM1 peptide continued to increase (Figure 3.8). It can be explained by the same notion that the observed intracellular fluorescence is actually the equilibrium between cell penetration and proteolysis. Upon exchanging to peptide-free medium, there should be no new peptide penetration, but the fluorescence signal remained almost unchanged due to the slow proteolysis degradation for stapled peptides. However, when a new batch of peptide was added into cell culture medium, the cell penetration process became more robust, resulting in a continued increase in fluorescence intensity inside cells.

Mechanism study of Cell penetration of stapled peptides

According to the experiments shown above, we figured out that a) stapled peptides exhibit better cell penetration properties than wild-type peptides, b) the cell penetration depends largely on stapled pattern and peptide charge, c) the observed intracellular fluorescence is actually a result of equilibrium between cell penetration and cellular proteolysis which confers peptide cellular uptake in dose- and time-dependent manner. However, the mechanisms utilized by peptides to translocate across the cell membrane are still unclear. Herein, efforts were made to unveil the uptake mechanisms for cell penetrating peptides, especially for stapled peptides.

Wild-type CPPs, TAT, Antp and poly-Arginine for example, have been used as model peptides to study their uptake mechanism by several research groups. Some evidence indicated that they enter cells via an energy-dependent endocytosis, which is an active transport process. However, we cannot neglect the data supporting the passive diffusion mechanism. So far, no clear conclusion has been achieved based on previous research[23, 28]. Therefore, the first experiment in this study was designed to figure out whether the cell penetration process is an ATP-dependent endocytosis. Cells were pre-treated with NaN_3 together with 2-Deoxyglucose (2-DG) to reduce cellular ATP levels, and then incubated with FITC-labeled peptides for 4 hours. The intracellular fluorescence intensity was quantified and compared with that observed from normal cells without NaN_3 and 2-DG treatment to clarify whether ATP depletion affected cell penetration. Similar as the aforementioned dose-dependent assay, TAT, Antp and poly-Arg_8 peptides were used as wild-type CPPs in this experiment, and SAHM1, PEN2, SAHBa and SAH-p53-8 were chosen

as stapled peptide candidates due to their distinct cell penetration properties. As a result, cellular ATP levels were confirmed to be dramatically decreased by approximately 90% after NaN_3 and 2-DG treatment as shown in Figure 3.9a. TAT and poly-Arg_8 exhibited almost identical cellular uptake in ATP-depleted and normal cells, which supported the model that they utilized passive diffusion pathway to penetrate cells. However, Antp and all the stapled peptides showed less permeable in ATP-depleted cells with a decrease by a range of 20 – 50%, indicating an active trans-membrane process which required cellular ATP. Therefore, the evidence shown in this study reveals that stapled peptides penetrate cells via an ATP-dependent endocytosis, whereas the internalization of wild-type CPPs needs to be analyzed case-by case.

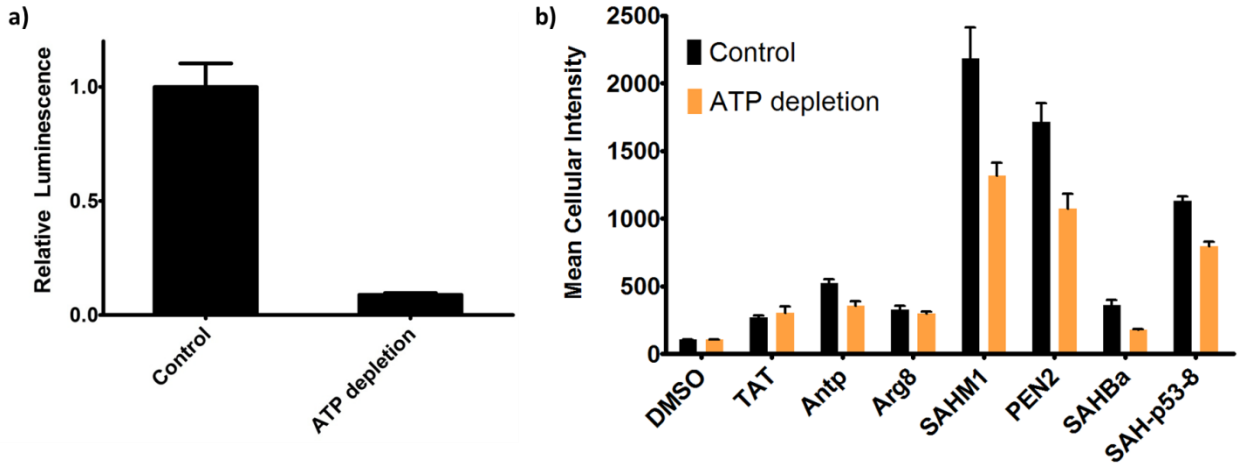

Figure 3.9 Stapled peptides penetrate cells via an ATP-dependent endocytosis. a) Cellular ATP decreased by approximately 90% upon NaN_3 and 2-Deoxyglucose (2-DG) treatment. b) Cellular uptake of CPPs in ATP-depleted and normal cells.

Energy-dependent endocytosis can be accomplished by several different pathways, for example, caveolin- and clathrin-mediated endocytosis. Further studies were performed to identify which specific pathway peptides utilize to penetrate cell membrane. A useful

tool to interrogate the endocytosis system is to take advantage of the small molecules that have been discovered to inhibit each possible pathway[29-33] (Table 3.1).

Table 3.1 Small molecule inhibitors in modulating energy-dependent endocytosis.

Modulator	Target	Mechanism
NaN_3	ATP production	Affect mitochondrial oxidative phosphorylation
2-Deoxyglucose	ATP production	Inhibit glycolysis
Filipin	Caveolin-mediated endocytosis	Bind to lipid bilayer to prevent assembly of Caveolin-coated invaginations
Nystatin	Caveolin-mediated endocytosis	Bind to lipid bilayer to prevent assembly of Caveolin-coated invaginations
Chlorpromazine	Clathrin-mediated endocytosis	Prevent clathrin-coated pit formation
Cytochalasin D	Actin polymerization	Bind to actin and prevent polymerization
$NaClO_3$	Proteoglycan synthesis	Inhibit ATP Sulfurylase

Using these small molecules, I repeated the cell penetration experiments under a variety of conditions that each blocked a different endocytosis pathway. If the pathway by which CPPs enter cells was inhibited, a decrease in intracellular fluorescence would be observed. Otherwise, the intracellular access should keep the same. As a result, I found the internalization process for both wild-type and stapled peptides required sulfated proteoglycans on cell surface (Figure 3.10a). It is reasonable to connect this result with the previous conclusion that peptide charge is a key factor determining cell penetration. Proteoglycans are usually negatively charged under physiological conditions due to the occurrence of sulfate groups, which might form electrostatic pairs with positively charged peptides to facilitate them anchoring on the cell membrane. However, blocking the other possible pathways did not appear to have any effect on peptide cell penetration (Figure 3.10 b-d).

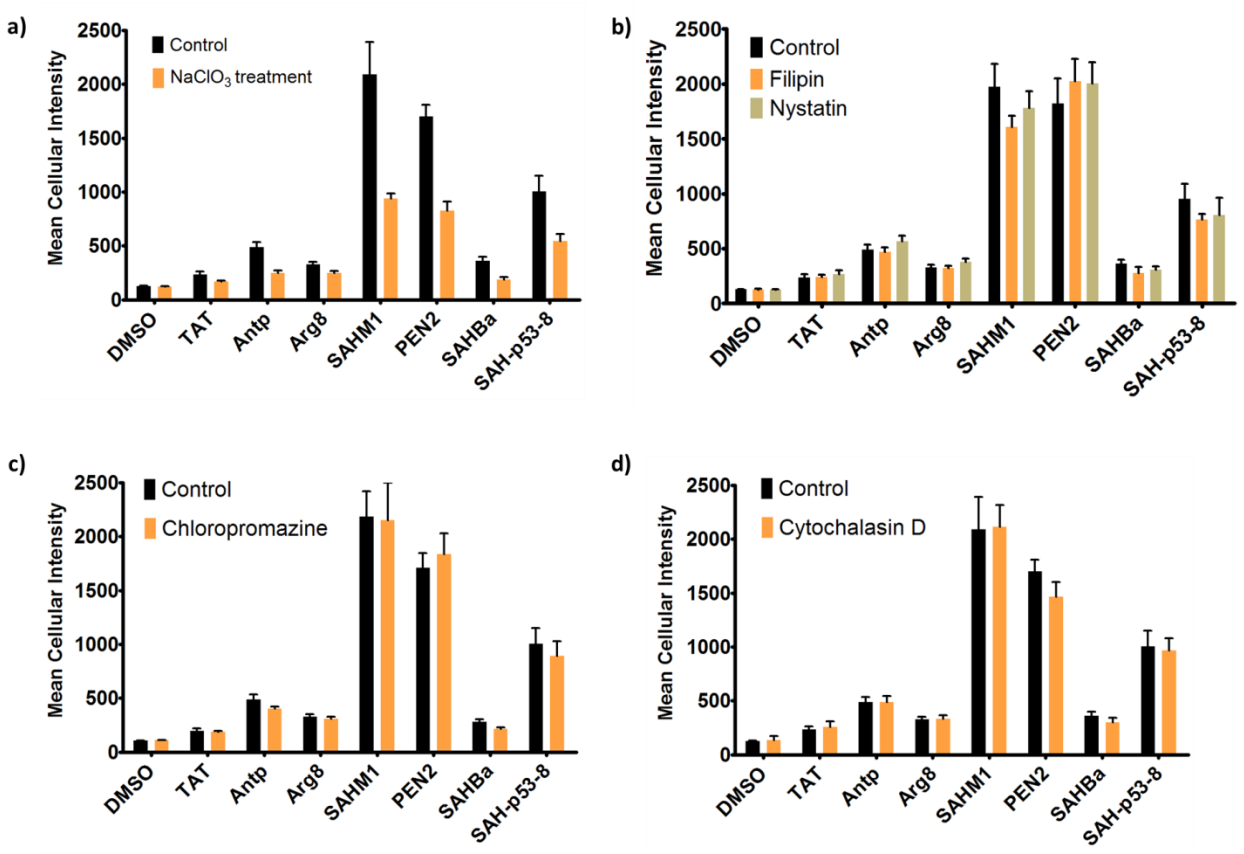

Figure 3.10 Quantitative illustration showing cellular uptake for cell penetration peptides under various conditions that each blocked an endocytosis pathway. a) $NaClO_3$ inhibits proteoglycan biosynthesis, b) Filipin and Nystatin prevent assembly of caveolin-coated invaginations, c) Chloropromazine prevents clathrin-coated pit formation, and d) Cytochalasin D blocks actin polymerization.

In order to further confirm that sulfated proteoglycan is important to mediate cellular uptake for peptides, a secondary assay was performed by using wild-type CHO cells (CHO-K1) and proteoglycan-deficient CHO cells (pgsA-745) which have a defect in xylosyltransferase and thereby prevent glycosaminoglycan biosynthesis[34]. As a result, all peptides showed similar penetration properties in wild-type CHO cells as previous experiments in U2OS cells, but the uptake decreased by approximately 50% in proteoglycan-deficient CHO cells, which was consistent with the experiment by using small molecule inhibitor (Figure 3.11). Taken together, CPPs penetrate cells through a clathrin-

and caveolin-independent endocytosis pathway that requires anionic cell surface proteoglycans which might associate with peptides via electrostatic interactions and thereby facilitates the internalization. This result is very similar as cellular uptake for supercharged GFP (scGFP), which does not utilize clathrin- or caveolin-mediated endocytosis either. But scGFP internalization needs actin polymerization, which is not required for peptide penetration[35].

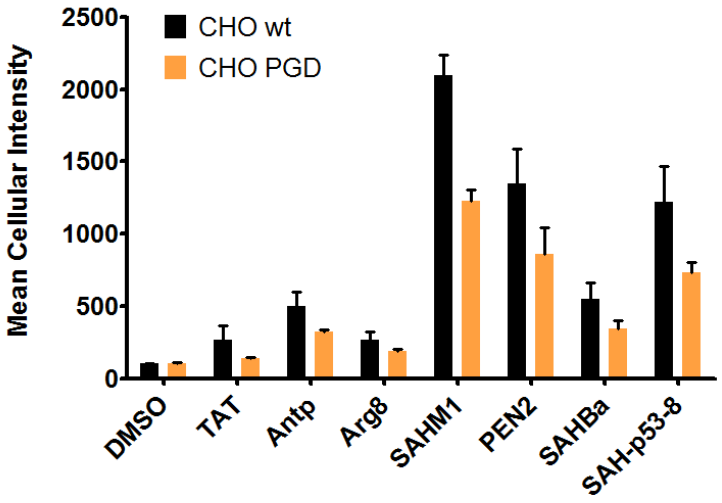

Figure 3.11 Cell penetration of wild-type and stapled peptides in wild-type CHO and proteoglycan-deficient CHO cells.

Peptide Stapling Improves Cell Penetration

Stapled peptides exhibit better cell penetration properties in general than wild-type peptides, we wonder whether peptide stapling strategy can be applied to any wild-type peptide to improve cellular uptake. To test this hypothesis, I designed a list of stapled peptides based on TAT, Antp and poly-Arg_8 peptide sequence (Figure 3.12a). The stapled peptides and their parent unmodified peptides were incubated in U2OS cells for 12 hours

with a concentration range from 10 nM to 20 μM. The intracellular fluorescence intensity was then measured and plotted as dose-dependent curve for each peptide class.

a)

Peptide	Sequence[#]
FITC-TAT	FITC-bA-GRKKRRQRRRPPQ
SAH-TAT-1	FITC-bA-GRKK*RQR*RPPQ
SAH-TAT-2	FITC-bA-GRK*RRQ*RRPPQ
FITC-Antp	FITC-bA-RQIKIWFQNRRMKWKK
SAH-Antp-1	FITC-bA-RQI*IWF*NRRMKWKK
SAH-Antp-2	FITC-bA-RQIKIWFQ*RRM*WKK
FITC-Arg_8	FITC-bA-RRRRRRRR
SAH-Arg_8	FITC-bA-R*RRR*RR

[#] bA = β-alanine, * = S5

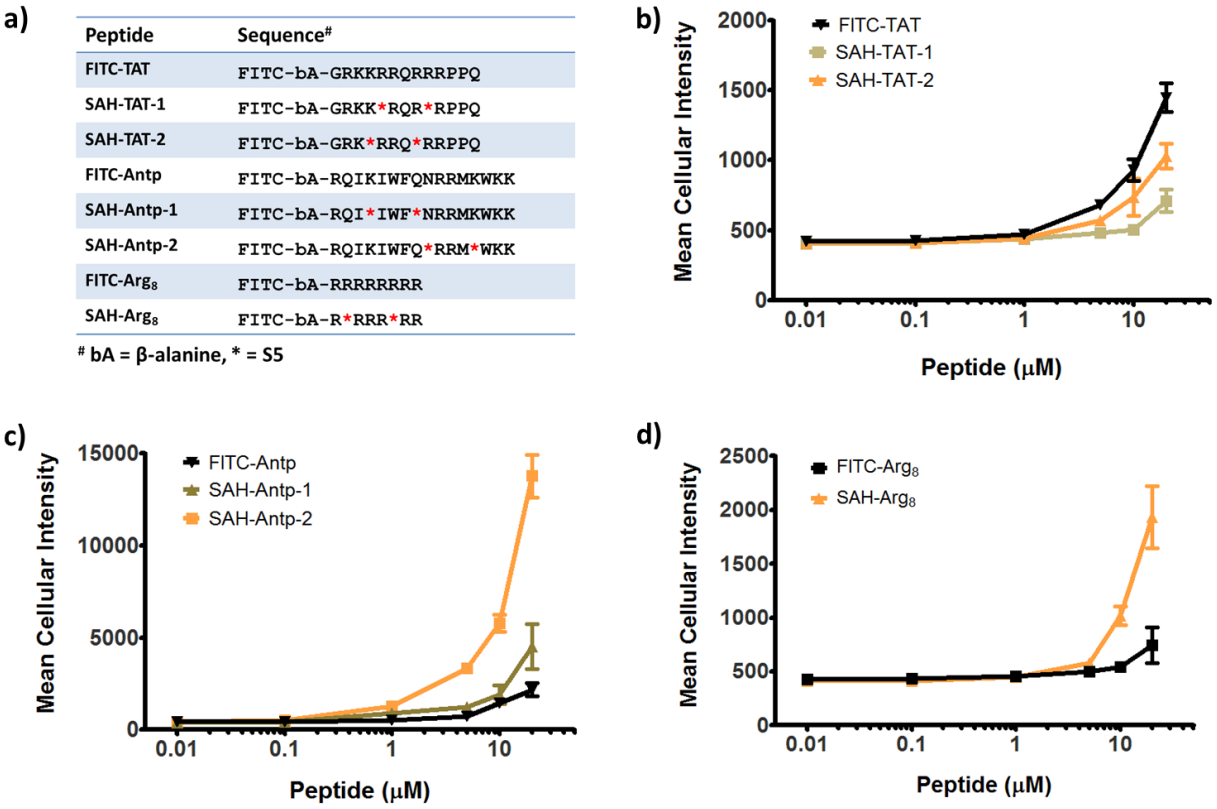

Figure 3.12 Improvement of cell penetration for wild-type peptide by stapling strategy is a case-by-case scenario. a) Peptides investigated in this assay with sequence illustration. b) – d) dose-dependent cell penetration assays for TAT, Antp and poly-Arg_8 peptides and their stapled derivatives.

As a result, all peptides showed a dose-dependent increase of cell penetration, which is as expected according to previous experiments (Figure 3.12 b-d). Interestingly, stapled peptides derived from Antp and poly-Arg_8 peptide class showed improved cell permeability at concentration starting from 1 μM for Antp and 5 μM for poly-Arg_8. Below 1 μM, both wild-type peptides and stapled version did not appear to penetrate cells. It is noteworthy that the stapling position also affected the cellular uptake as the two stapled Antp peptides with different staple positions exhibited varied cell penetration, albeit both

of them were better than wild-type Antp. However, reduced cellular uptake was observed for stapled peptides derived from TAT sequence. This could be explained by many possible reasons, including that the residues replaced by S5 unnatural amino acids were actually essential in TAT internalization, and stapling at these positions disrupted peptide secondary structure or packing which was favored by the penetration process. Taken together, peptide stapling strategy indeed improves cellular uptake for some peptide sequences but it cannot be applied to every case since the cellular internalization is a complicated process regulated by many factors.

Application of Stapled Peptides in Oligonucleotide Delivery

Cell penetrating peptides (CPPs) have become extremely popular in recent years due to their potential therapeutic application in drug delivery. Indeed, CPPs have been demonstrated to assisst to internalize many non-cell-permeable cargoes, including DNA, RNA and even proteins, resulting in profound biological activities inside cells. Although these CPPs show promising activities in several cases, there is still great room to advance this technology by improving the cell penetration. Given that stapled peptides exhibit much better cellular uptake than these widely used CPPs in general, a reasonable strategy is to apply stapled peptides as a new class of cargo carrier.

In this study, we aimed to set up a proof-of-principle experiment to demonstrate that stapled peptides can efficiently deliver a biologically meaningful oligonucleotide into cells, and show better cellular activity than oligonucleotide alone. Based on this pilot experiment, we will expand the cargo category to many other biologics with diverse

applications in the future. The oligonucleotide used in this study is a phosphorodiamidate morpholino oligomer (PMO) which induces dystrophin exon 23 skipping during processing of the primary transcript, and hence can treat a type of degenerative muscle diseases named as Duchenne Muscular Dystrophy (DMD)[36]. The genetic causes of this disease typically involve nonsense or frame-shift mutations within the *Dystrophin* gene, causing premature termination of translation and synthesis of a non-functional dystrophin protein. In particular, there is a spontaneous cytosine to thymidine mutation at position 3185 of Exon 23, which results in failure of full-length protein production[37-39]. One unique feature making the dystrophin protein unusual is that the internally deleted protein that maintains the reading frame is still functional[40-41]. Therefore, one solution to treat this disease is using antisense oligonucleotides to redirect gene transcript processing by blocking mutated exons in pre-mRNA splicing, which will result in a shortened version of dystrophin protein[42-43]. The morpholino chemistry produces a neutral oligonucleotide that has exceptional biological stability and has been applied to treat Duchenne Muscular Dystrophy in clinical trials[44-45]. However, the poor cellular delivery limits their further therapeutic applications. Therefore, we collaborated with Professor Keith Foster at University of Reading to conjugate one of our best cell penetrating stapled peptide (SAH-ARA) with the PMO molecule targeting exon 23 of dystrophin, and further investigate the biological activity of the conjugate *in vivo*.

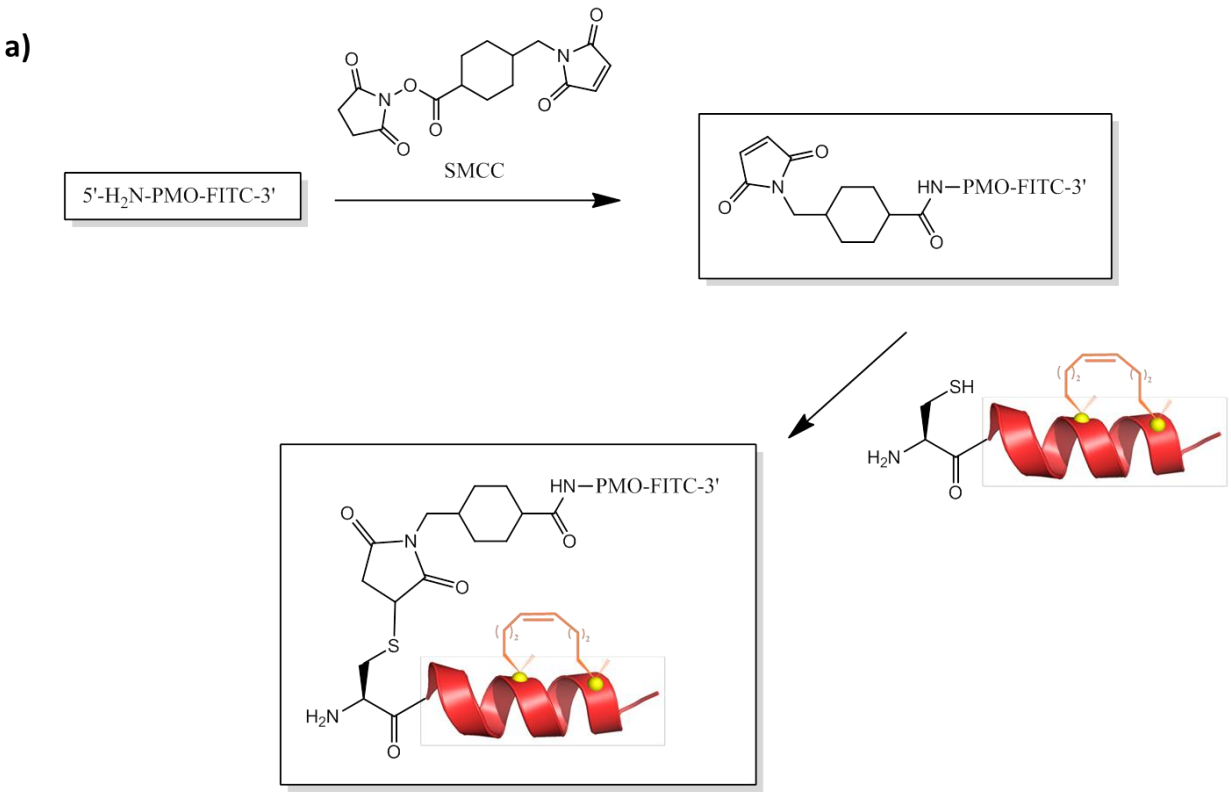

b) **SAH-ARA:**

Sequence	Cys-PEG_2-RKF*RLF*
Chemical Formula	$C_{73}H_{121}N_{19}O_{15}S$
Molecular Weight	1536.93

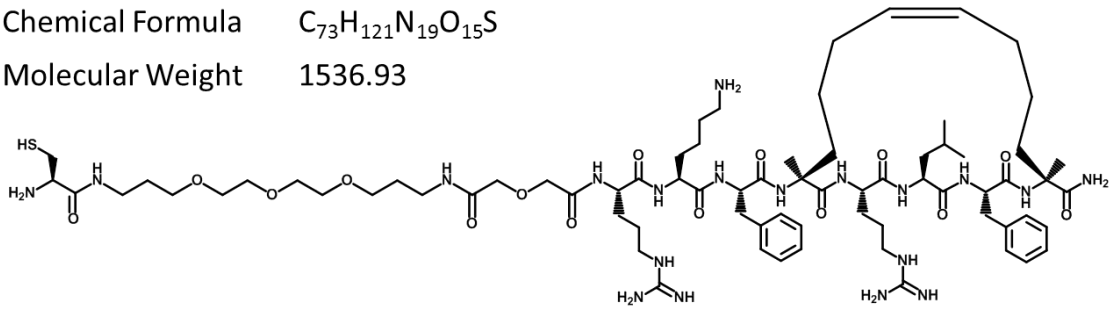

Figure 3.13 Schematic illustration of the synthesis of SAH-ARA-PMO conjugate. a) Synthesis route for SAH-ARA-PMO conjugate. b) SAH-ARA peptide information.

The SAH-ARA peptide, derived from Androgen Receptor (AR) targeting peptides, was used in this study for several reasons[46-47]. First, it shows great cellular uptake in previous high-throughput cell penetration assay. Second, it is not functional in cells, with limited toxicity and no activity. Lastly, it is a peptide with only eight amino acids, which

would not interfere with any biological activity of the PMO. In addition, we used a non-cleavable covalent linkage to conjugate SAH-ARA and the PMO together rather than formulation or cleavable linkage like disulfide bonds. This non-cleavable linkage is proposed to efficiently facilitate PMO molecule in the entire delivery process, including cell membrane internalization, release from endosomes, and translocation into nucleus. The SAH-ARA peptide was synthesized with an N-terminal cysteine for conjugation purpose, and a 20-atom-long PEG_2 linker was added between the cysteine residue and core peptide sequence to avoid unnecessary interaction with the PMO molecule. Meanwhile, exon 23 targeting PMO molecule was ordered from Gene Tools (Philomath, OR) with 5'- primary amine for conjugation and 3'- FITC for imaging purpose. PMO was first reacted with succinimidyl-4-(N-maleimidomethyl)Cyclohexane-1-carboxylate (SMCC) to generate a maleimide functional group at 5'- end, which allowed the reaction with the cysteine containing SAH-ARA peptide to form the final conjugate (Figure 3.13).

Once the SAH-ARA-PMO conjugate was prepared, the cell penetration assay was performed to verify whether SAH-ARA can effectively deliver the PMO molecule into cells and to figure out the subcellular distribution of the conjugate. The experiment was carried out by treating U2OS cells with compound concentrations ranging from 500 nM to 10 μM for 12 hours. As a result, the PMO itself didn't appear to penetrate cells even at a concentration as high as 10 μM. As expected, SAH-ARA showed robust cellular uptake starting from 500 nM. Promisingly, there was a fair amount of SAH-ARA-PMO conjugate accumulating inside cells at 5 and 10 μM although the uptake efficiency was about 10 times less than the SAH-ARA peptide. In addition, it is noteworthy that the conjugate was observed to spread over the entire cell, indicating that SAH-ARA not only facilitates PMO

molecule to translocate across the plasma membrane, but also contributes in endosomal release and nucleus transport as well (Figure 3.14).

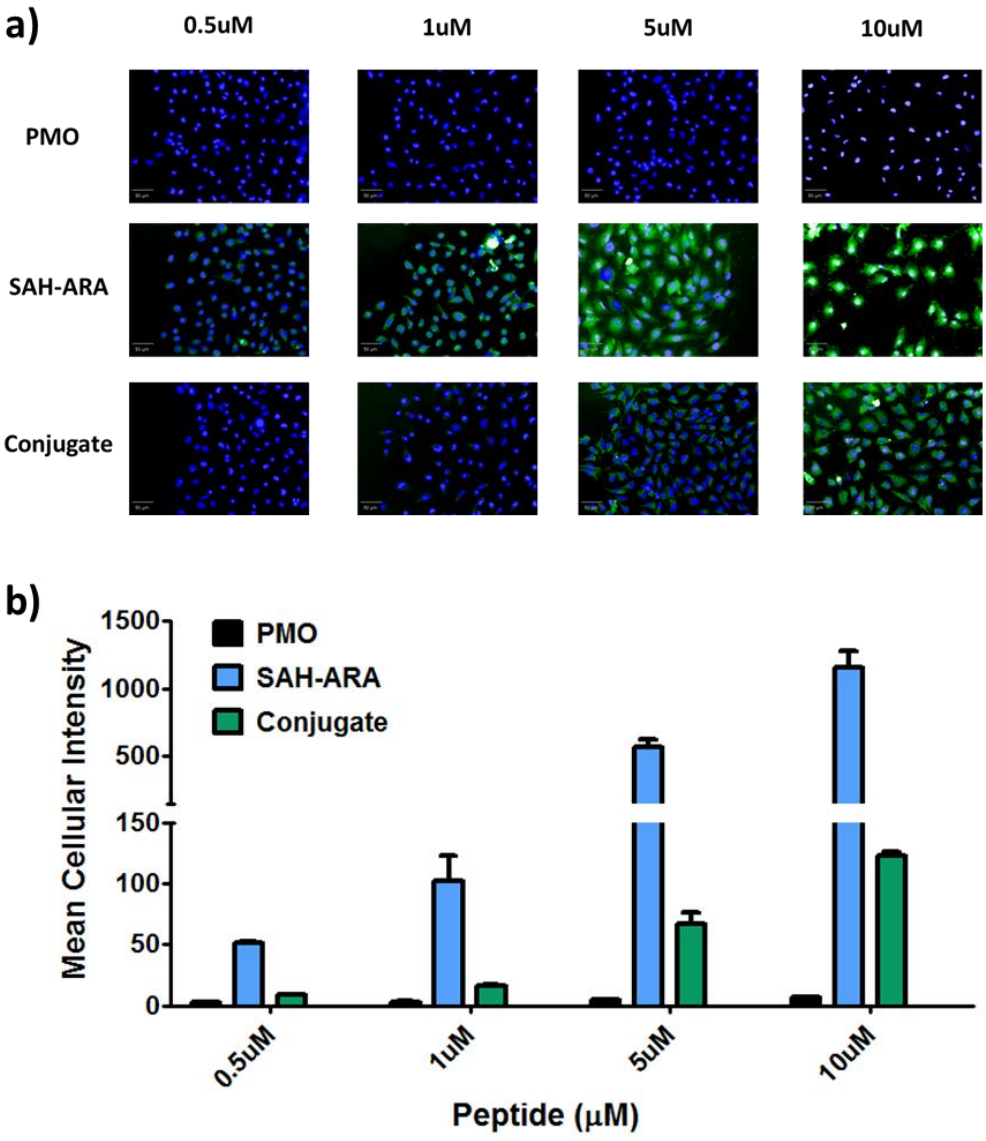

Figure 3.14 Cell penentration of SAH-ARA-PMO conjugate and its individual components. a) Image view of cellular fluorescein intensity for all compounds at various concentrations. b)Quantitative illustration showing relative cell penetration of each compound at different concentrations.

Given the effective cell penetration of SAH-ARA-PMO conjugate, *in vivo* assays were carried out at Professor Keith Foster's lab to evaluate the biological activity of the

conjugate. One common assay to analyze the exon skipping activity is to use RT-PCR to visualize the production of the transcript. In particular, H2K cells from mdx mice harboring the non-sense mutation in exon 23 were incubated with 5 μM SAH-ARA-PMO conjugate or PMO alone at 37 ℃ for 4 hours, followed by culturing at differentiation medium for another 48 hours. Then RT-PCR was performed to amplify and visualize the transcription product of *dystrophin* gene.

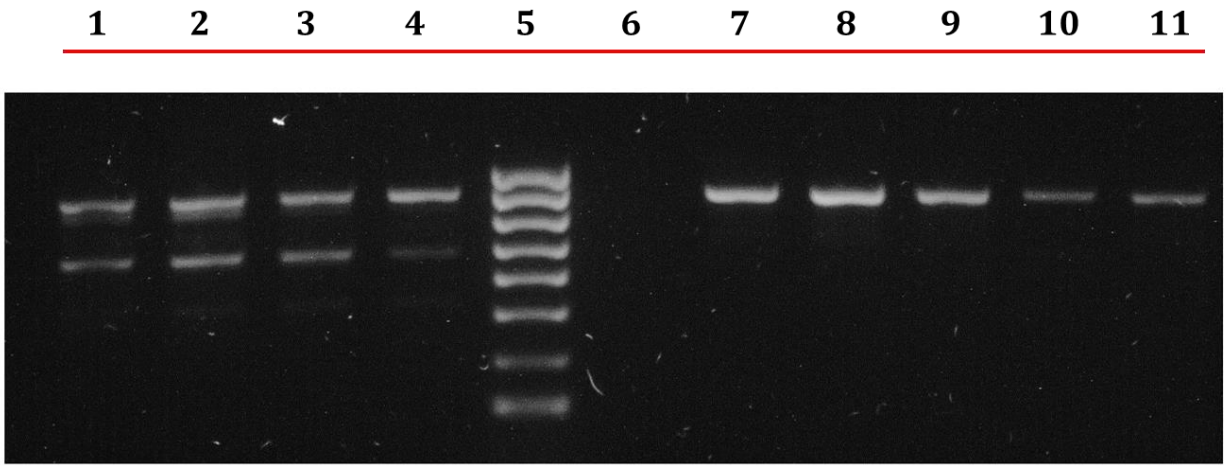

Lane 1 - 4	Conjugate treatment replicates
Lane 5	100bp DNA ladder
Lane 6	blank
Lane 7	DMSO vehicle
Lane 8 - 11	PMO treatment replicates

Figure 3.15 Reverse-transcription-polymerase chain reaction (RT-PCR) analysis of H2K cells from an mdx mouse with treatment of SAH-ARA-PMO conjugate or PMO alone. The 901 bp product represents the full-length transcript, and the product of 688 bp indicates transcript that excludes exon 23.

As shown in Figure 3.15, a band with 901 bp product was observed in all samples, indicating that the full-length transcript with exon 23 mutation was produced in both conjugate and PMO treated cells. However, a 688 bp product, representing the exon 23

skipping product, was only observed in cells treated with SAH-ARA-PMO conjugate. It is worth to mention that this exon skipping transcript was observed in all four replicates, meaning the results shown here was reproducible and reliable. According to this result, we concluded that the stapled peptide conjugated PMO can efficiently mask exon 23 during pre-mRNA splicing whereas the PMO molecule alone couldn't, which can be attributed to the benefit of better cell penetration of the SAH-ARA-PMO conjugate.

The exon skipping assay shown above indicates that the PMO conjugate is active in cells with a peptide leash. An *in vivo* assay was then performed to evaluate the biological activity of the PMO conjugate in mdx mouse model by intramuscular injection. The purpose of this assay was to figure out whether the PMO conjugate is functional in animal models, so both the conjugate and PMO control were forced into tissues by intramuscular injection, which means the cell penetration was not a hurdle here for exhibiting any *in vivo* activity. Female mdx mice were intramuscular injected a single dose of 20 μg either SAH-ARA-PMO conjugate or PMO molecule alone with a total volume of 50 μL at 16 weeks old. The mice were excised 4 weeks post-injection, and the muscle tissues were analyzed for dystrophin expression by immunohistochemistry staining with anti-dystrophin monoclonal antibody recognizing the C-terminus of the protein. Since the non-sense mutation in exon 23 causes an early termination of dystrophin protein translation and hence resulting in the failure to produce full length protein, the observed dystrophin protein in this assay should be the slightly truncated version translated from exon 23 skipped transcripts. As a result, the treatment by the unconjugated PMO yielded an efficient formation of dystrophin positive fibres, which was consistent with previous studies. Promisingly, SAH-ARA-PMO also successfully induced the expression of shortened dystrophin proteins, and the efficiency

was as good as the unconjugated PMO, indicating that SAH-ARA peptide facilitates PMO cellular trafficking but not interfering with its biological activity (Figure 3.16).

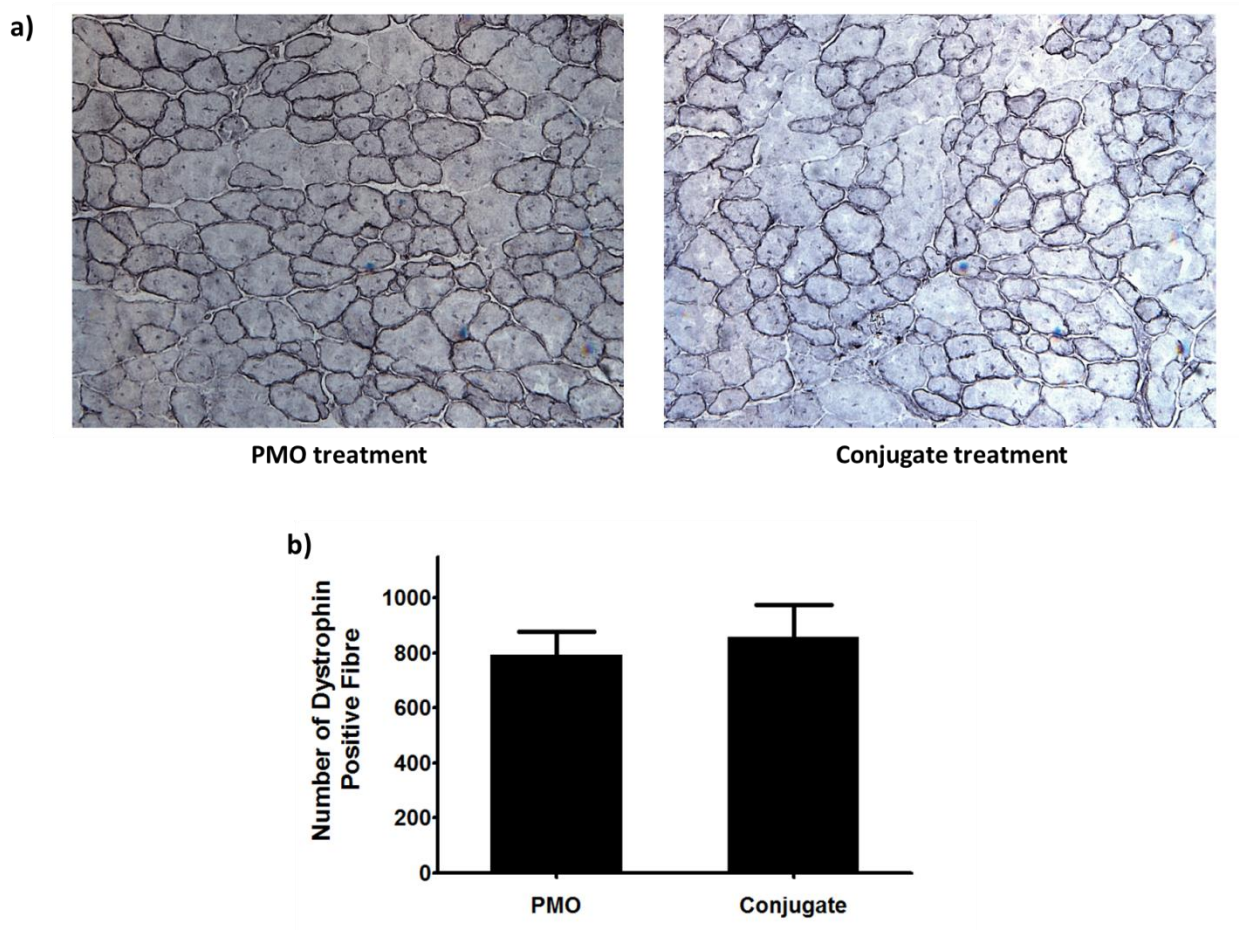

Figure 3.16 Intramuscular injection of mdx mice with PMO and SAR-ARA-PMO conjugate. a) Expression of dystrophin in muscle fibres after treatment. b) Quantitative illustration showing the number of dystrophin positive fibres upon PMO and conjugate treatment.

Taken together, we demonstrated that a stapled peptide (SAH-ARA) with good cell permeability can efficiently deliver a poor penetrating PMO molecule into cells by covalent conjugation of the two components. Furthermore, the conjugate exhibited improved exon skipping activity in cell-based assay and induced expression of shortened dystrophin protein in mdx mice. An ongoing effort is made by intravenous injection of SAH-ARA-PMO

conjugate in order to demonstrate an improved *in vivo* efficacy as a result of better cellular uptake.

Conclusion

In this study, we investigated the cell penetration for stapled peptides, which is one of the most significant and poorly understood aspects of peptide stapling technology. In order to address this problem, we developed a high-throughput microscopy assay to quantitatively measure stapled peptide intracellular accumulation. We demonstrated that this assay yielded highly reproducible results when testing peptide intracellular access. Using this assay, we analyzed more than 200 discrete peptides with various sequences, stapling positions and patterns, and distinct physicochemical properties. As a result, we found that stapled peptides penetrate cells much better than wild-type ones, and the cell penetration ability is strongly related to stapling patterns and formal charge, whereas the other physical parameters do not appear to have a significant effect. We further studied the relation between cellular uptake and peptide concentration and incubation time, and figured that the intracellular accumulation is actually the consequence of equilibrium of peptide penetration and cellular proteolysis. In addition, a chemical genetic screen was performed to illustrate that stapled peptides penetrate cells through clathrin- and caveolin-independent endocytosis pathway that requires sulfated proteoglycans on cell surface. Furthermore, we demonstrated that peptide stapling strategy improves cellular uptake for some wild-type peptide sequences by simply grafting the all hydrocarbon crosslink to the wild-type peptides. Finally, one stapled peptide, SAH-ARA derived from AR targeting

peptides, was demonstrated to deliver a non-penetrating morpholino molecule into mammalian cells without affecting its biological activity.

Future Directions

The work in this study shows a systematic study on cell penetration by stapled peptides, which enriches our understanding of stapled peptides as chemical probes and potential targeted therapeutics. In order to further explore the penetration properties for stapled peptides and apply the information learned in the design of next-generation stapled peptides with improved biological activities, future studies should be focused on the following aspects.

1) Analysis of cell penetration for a larger set of peptides. In current study, we tested more than 200 distinct peptides with different stapling patterns and physicochemical properties, which indicated that stapled peptides are better cell penetrators than wild-type ones and the permeability is largely related to the formal charge at physiological pH. However, this peptide pool was not completely unbiased although the overall physicochemical properties for these peptides were quite similar in terms of the mean values. For example, some peptides were designed to gain extra cellular uptake by coupling additional arginine residues into peptide sequences. Furthermore, the distribution of peptides in each physical parameter range was not quite even. For example, the number of peptides with positive net charge was much larger than those negatively charged peptides. Therefore, a larger set of peptides with diverse intrinsic properties need to be analysed to generate more statistically meaningful results.

2) Identification of the mechanism of cell penetration by stapled peptides using unbiased methods. The mechanism of cell penetration by stapled peptides is one of the most important aspects in peptide stapling technology, however it is still not very clear so far. We were making efforts to address this question by biasedly using small molecule inhibitors to block each possible trafficking pathway and as a result, we got several pieces of information regarding this complicated penetration process. In order to elucidate the uptake process systematically, following studies should be performed by employing an unbiased screen method, like genome-wide RNAi screen, to identify all proteins affecting the intracellular accumulation of stapled peptides. The results of this unbiased screen will generate a global map of the genes facilitating the uptake and intracellular retention of stapled peptides, and thereby dramatically advance our ability to design next-generation compounds with enhanced potency.

3) Application of stapled peptides in the delivery of diverse non-penetrating biologics. In this study, we showed an 8-mer stapled peptide derived from AR targeting peptides can efficiently facilitate the cellular trafficking of a non-penetrating PMO molecule without interfering with its intracellular exon skipping activity. This study opened a promising avenue to further the application of stapled peptides in the delivery of a larger collection of biologics, for example, siRNAs for targeted gene knockdown, and proteins with diverse biological activities. Furthermore, given the exceptional penetration of stapled peptides, it is entirely possible and promising to utilize stapled peptides in *in vivo* delivery, such as targeted tissue delivery, and translocation through brain-blood-barrier. In addition, with ongoing efforts to unveil the mechanism of cell penetration by stapled peptides, we

can also design novel stapled peptides suitable for different delivery applications in the future.

Materials and Methods:

Peptides. Wild-type CPPs and stapled peptides were synthesized manually by standard solid phase peptide synthesis using Fmoc-chemistry. They were HPLC purified and verified >95% purity as indicated by LC/MS. The peptide sequences are listed in Table 3.2.

Table 3.2 Peptides used in this study and their sequences.

Peptide	Sequence[#]
SAHM1	FITC-bA-ERLRRRI*LCR*HHST
SAHBa	FITC-bA-EDIIRNIARHLA*VGD*N_LDRSIW
SAH-p53-8	FITC-bA-QSQQTF^NLWRLL*QN
TNG-90	FITC-bA-RWPQ*ILD*HVRRVWR
TNG-147	FITC-bA-RRWPQ*ILD*HVRRVWR
PEN2	FITC-bA-RQIKIWFQ*RRM*WKK
FITC-TAT	FITC-bA-GRKKRRQRRRPPQ
SAH-TAT-1	FITC-bA-GRKK*RQR*RPPQ
SAH-TAT-2	FITC-bA-GRK*RRQ*RRPPQ
FITC-Antp	FITC-bA-RQIKIWFQNRRMKWKK
SAH-Antp-1	FITC-bA-RQI*IWF*NRRMKWKK
SAH-Antp-2	FITC-bA-RQIKIWFQ*RRM*WKK
FITC-Arg_8	FITC-bA-RRRRRRRR
SAH-Arg_8	FITC-bA-R*RRR*RR
SAH-ARA	FITC-bA-RKF*RLF*

[#] bA = β-alanine, N_L = Norleucine, ^ = R8, * = S5

PMO MDEX23. The PMO molecule targeting exon 23 of dystrophin gene was ordered from Gene Tools (Philomath, OR). The sequence is GGCCAAACCTCGGCTTACCTGAAAT with 5'-primary amine and 3'-fluorescein modification for conjugation and imaging purposes. The chemical structure of this PMO molecule is shown in Figure 3.17.

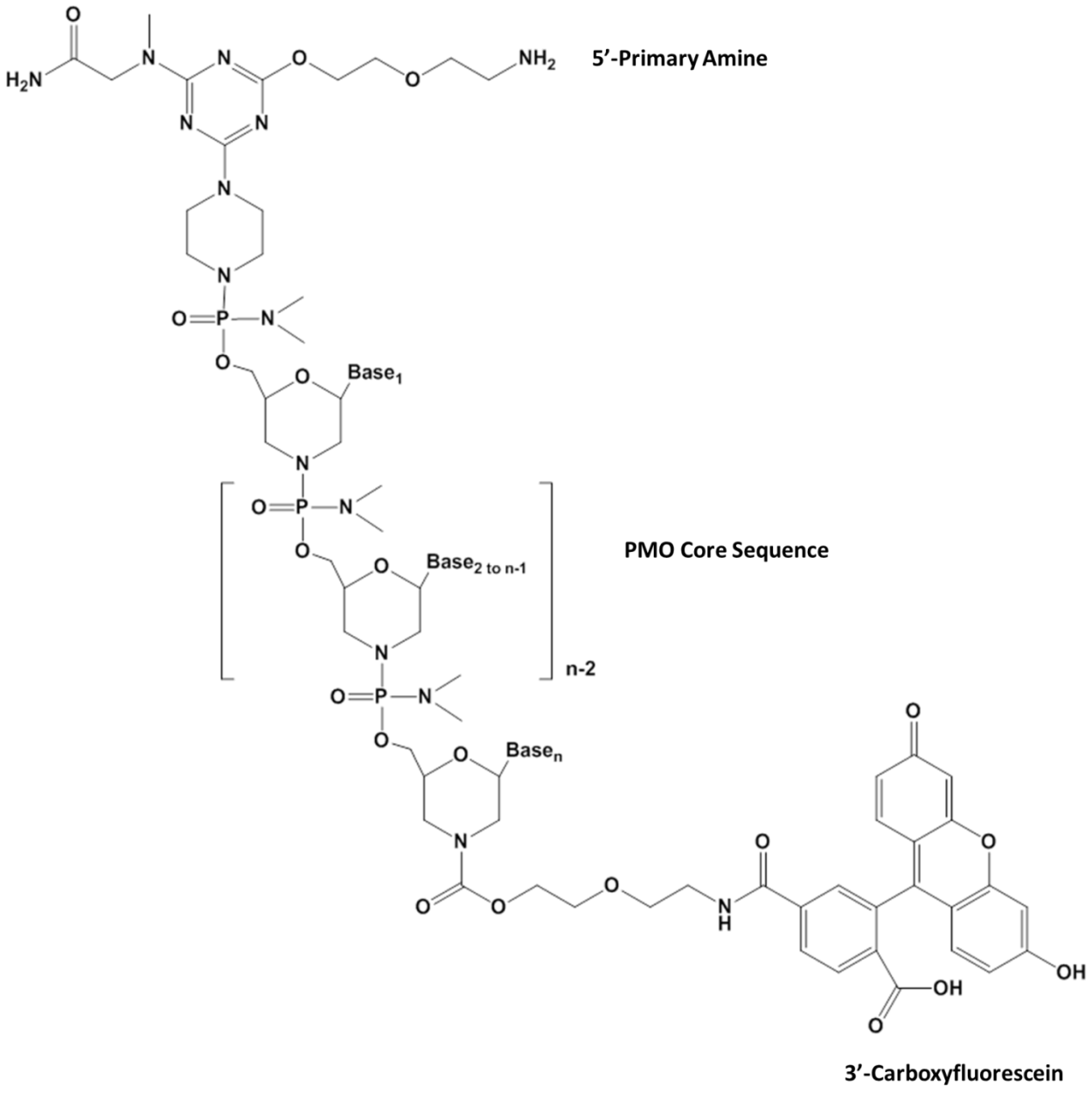

Figure 3.17 Chemical structure of PMO molecule used in this study.

Cell Penetration Assays. The cell penetration assay was performed following the same protocol as that in Chapter two except U2OS cells were used. For dose-dependent assay, peptides were treated at 10 nM, 100 nM, 1 μM, 5 μM, 10 μM and 20 μM for 12 hours before analysis. For time-course assay, peptide was added at final concentration of 5 μM or 10 μM, and cells were harvested for analysis 2, 4, 8, 16, 20 and 24 hours post-treatment. The pulse-chase experiment was performed similar as normal penetration assay. 12 hours after initial treatment, cell culture medium was aspirated and cells were washed extensively to remove excess FITC-labeled peptides. A fresh medium containing either a new batch of peptide or DMSO vehicle was added to incubate for longer time as indicated. Cells were imaged and analyzed 8, 12, 16, 20 and 24 hours after the initial treatment. For cell penetration assay with small molecule inhibitors, cells seeded in 384-well clear bottom plates (Corning) were pre-incubated with indicated small molecules for 1 hour (10 mM NaN_3 and 30 mM 2-DG for ATP depletion, 5 μg/mL filipin or 25 μg/mL nystatin for blocking caveolin-mediated endocytosis, 5 μg/mL chlorpromazine for blocking clathrin-dependent endocytosis, 10 μg/mL cytochalasin D for inhibiting actin polymerization, and 80 mM $NaClO_3$ for disrupting proteoglycan synthesis). Then a final concentration of 10 μM FITC-labeled peptide was added to the cell culture medium containing the small molecule inhibitor and incubated for additional 4 hours. Cells were then washed, stained and analyzed by the same protocol as before. All cell penetration assays were performed in duplicate or triplicate, and the data were plotted in GraphPad Prism 5 (GraphPad software).

ATP Depletion Assay. U2OS cells were seeded in a 96-well white opaque plate (Corning) with 10,000 cells per well. The plate was incubated overnight at cell incubator to allow attachment of the cells to the bottom of the well. The next morning, the cells were washed

with PBS once, followed by incubation with a fresh medium containing 10 mM NaN_3 and 30 mM 2-Deoxyglucose (2-DG) for 1 hour. The cellular ATP level was then measured using CellTiter-Glo Luminescent Kit (Promega) following the manufacturer's protocol.

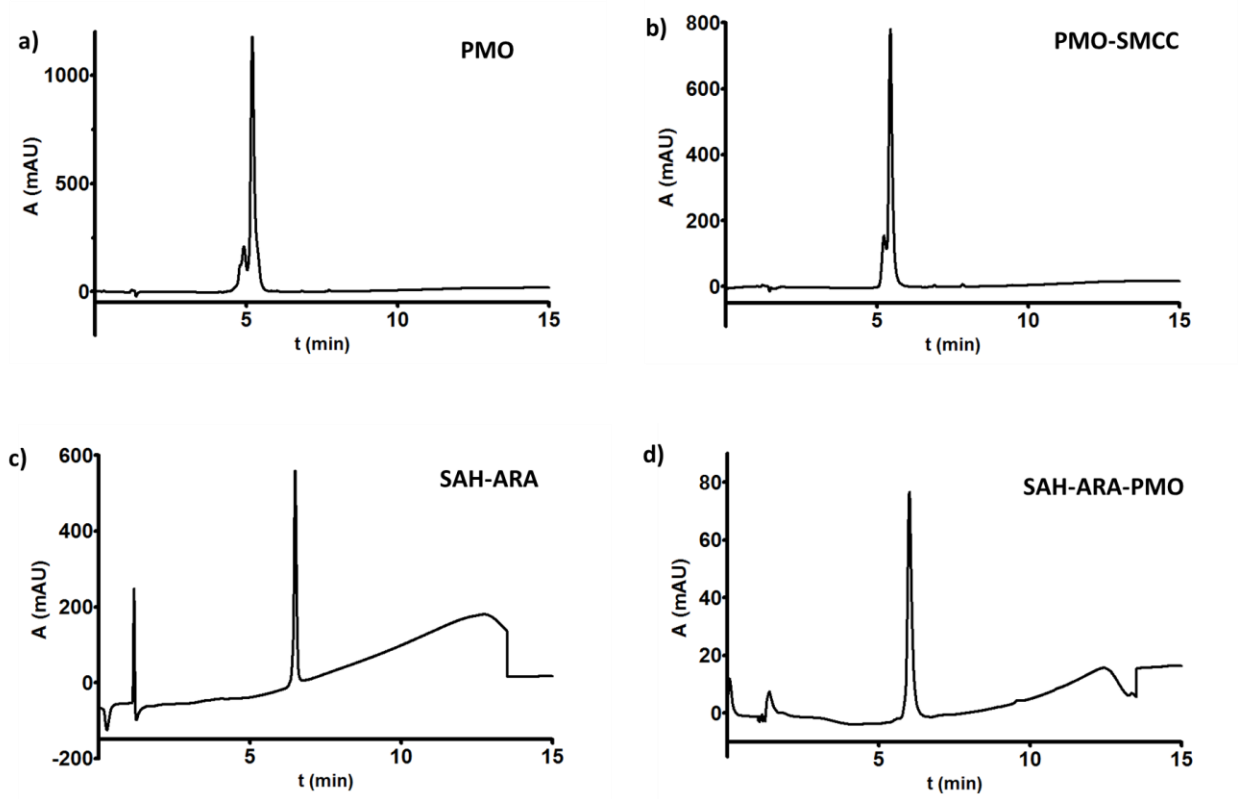

Figure 3.18 HPLC trace showing the purity of components in SAH-ARA-PMO conjugation, a) PMO, b) PMO-SMCC, c) SAH-ARA, and d) SAH-ARA-PMO.

Conjugation of SAH-ARA-PMO. A 8 mL 50% acetonitrile/PBS (v/v) solution containing 0.5 mL 1 mM PMO with 5'-primary amine and 2 mL 5 mg/mL succinimidyl-4-(N-maleimidomethyl) Cyclohexane-1-carboxylate (SMCC) was allowed to gently mix at room temperature for 1 hour to generate PMO-SMCC. The PMO-SMCC product was then purified with a 2% - 70% linear acetonitrile gradient in 0.1 M triethylammonium acetate (TEAA) buffer pH 7.0 over 20 minutes by reverse phase HPLC using a C-18 column (Agilent, Palo Alto, CA). The pooled fractions were concentrated and lyophilized to dryness. The

lyophilized powder was resuspended in H_2O to a final concentration approximately 500 μM. Then a 1:1 mixture of PMO-SMCC and N-terminal Cysteine SAH-ARA in 50% acetonitrile/PBS (v/v) was incubated at room temperature overnight to yield final product SAH-ARA-PMO conjugate. The conjugate was purified by HPLC again following the same protocol. The purity of conjugate product was confirmed using LC/MS results (Figure 3.18). The purified conjugate product were lyophilized, re-dissolved in DMSO, quantified by 254 nm and 494 nm absorbance and stored at -20°C until use.

Exon Skipping Assay. H2K cells from mdx mice harboring the non-sense mutation in exon 23 were harvested and seeded in 48-well clear bottom plate (Corning). The cells were incubated at 37°C/5% CO_2 overnight to allow attachment of cells to the bottom of the well. The next morning, cells were treated with a fresh medium containing 5 μM SAH-ARA-PMO or 5 μM PMO alone. Cell culture medium containing DMSO vehicle was also included as control. After 4 hours incubation, cells were transferred to differentiation medium for 48 hours. Then total RNA was extracted from the cells and approximately 200 ng RNA subjected to RT-PCR using dystrophin exon-specific primers following manufacturer's protocol. An aliquot of the resulting cDNA was used as a template for a second round of PCR amplification. Full length dystrophin gene transcript and the exon 23 skipping gene product were analyzed on 1% agarose gels in Tris-borate/EDTA buffer. The experiments were performed with four replicates for both SAH-ARA-PMO conjugate and PMO molecule alone.

Intramuscular Injection Assay. Female mdx mice (16 weeks) were injected with 20 μg of SAH-ARA-PMO (or PMO) suspended in PBS with a total volume of 50 μL (n = 4). Four weeks

after injection, muscles were harvested and processed for cryosectioning. Expressed dystrophin protein was visualized by immunohistochemistry staining with a mouse antidystrophin monoclonal 10-11c antibody at 1:100 dilutions. The dystrophin positive fibers were counted as reported.

Reference

1. Verdine, G. L.; Hilinski, G. J., Stapled Peptides for Intracellular Drug Targets. *Method Enzymol* **2012,** *503*, 3-33.

2. Schafmeister, C. E.; Po, J.; Verdine, G. L., An all-hydrocarbon cross-linking system for enhancing the helicity and metabolic stability of peptides. *J Am Chem Soc* **2000,** *122* (24), 5891-5892.

3. Kim, Y. W.; Verdine, G. L., Stereochemical effects of all-hydrocarbon tethers in i,i+4 stapled peptides. *Bioorg Med Chem Lett* **2009,** *19* (9), 2533-2536.

4. Bernal, F.; Tyler, A. F.; Korsmeyer, S. J.; Walensky, L. D.; Verdine, G. L., Reactivation of the p53 tumor suppressor pathway by a stapled p53 peptide. *J Am Chem Soc* **2007,** *129* (9), 2456-+.

5. Walensky, L. D.; Pitter, K.; Morash, J.; Oh, K. J.; Barbuto, S.; Fisher, J.; Smith, E.; Verdine, G. L.; Korsmeyer, S. J., A stapled BID BH3 helix directly binds and activates BAX. *Mol Cell* **2006,** *24* (2), 199-210.

6. Moellering, R. E.; Cornejo, M.; Davis, T. N.; Del Bianco, C.; Aster, J. C.*, et al.*, Direct inhibition of the NOTCH transcription factor complex. *Nature* **2009,** *462* (7270), 182-U57.

7. Grossmann, T. N.; Yeh, J. T. H.; Bowman, B. R.; Chu, Q.; Moellering, R. E.; Verdine, G. L., Inhibition of oncogenic Wnt signaling through direct targeting of beta-catenin. *P Natl Acad Sci USA* **2012,** *109* (44), 17942-17947.

8. Chang, Y. S.; Graves, B.; Guerlavais, V.; Tovar, C.; Packman, K.*, et al.*, Stapled alpha-helical peptide drug development: A potent dual inhibitor of MDM2 and MDMX for p53-dependent cancer therapy. *P Natl Acad Sci USA* **2013,** *110* (36), E3445-E3454.

9. Walensky, L. D.; Kung, A. L.; Escher, I.; Malia, T. J.; Barbuto, S.; Wright, R. D.; Wagner, G.; Verdine, G. L.; Korsmeyer, S. J., Activation of apoptosis in vivo by a hydrocarbon-stapled BH3 helix. *Science* **2004,** *305* (5689), 1466-1470.

10. Stanzl, E. G.; Trantow, B. M.; Vargas, J. R.; Wender, P. A., Fifteen Years of Cell-Penetrating, Guanidinium-Rich Molecular Transporters: Basic Science, Research Tools, and Clinical Applications. *Accounts of chemical research* **2013**.

11. Hassane, F. S.; Saleh, A. F.; Abes, R.; Gait, M. J.; Lebleu, B., Cell penetrating peptides: overview and applications to the delivery of oligonucleotides. *Cell Mol Life Sci* **2010,** *67* (5), 715-726.

12. Deshayes, S.; Morris, M. C.; Divita, G.; Heitz, F., Cell-penetrating peptides: tools for intracellular delivery of therapeutics. *Cell Mol Life Sci* **2005,** *62* (16), 1839-1849.

13. Gupta, B.; Levchenko, T. S.; Torchilin, V. P., Intracellular delivery of large molecules and small particles by cell-penetrating proteins and peptides. *Advanced drug delivery reviews* **2005,** *57* (4), 637-651.

14. Snyder, E. L.; Dowdy, S. F., Cell penetrating peptides in drug delivery. *Pharm Res* **2004,** *21* (3), 389-393.

15. Snyder, E. L.; Dowdy, S. F., Recent advances in the use of protein transduction domains for the delivery of peptides, proteins and nucleic acids in vivo. *Expert opinion on drug delivery* **2005,** *2* (1), 43-51.

16. Eguchi, A.; Akuta, T.; Okuyama, H.; Senda, T.; Yokoi, H.*, et al.*, Protein transduction domain of HIV-1 Tat protein promotes efficient delivery of DNA into mammalian cells. *J Biol Chem* **2001,** *276* (28), 26204-26210.

17. Glover, D. J.; Lipps, H. J.; Jans, D. A., Towards safe, non-viral therapeutic gene expression in humans. *Nat Rev Genet* **2005,** *6* (4), 299-U29.

18. Wadia, J. S.; Dowdy, S. F., Transmembrane delivery of protein and peptide drugs by TAT-mediated transduction in the treatment of cancer. *Advanced drug delivery reviews* **2005,** *57* (4), 579-96.

19. Zhang, L. H.; Yu, J.; Pan, H. L.; Hu, P.; Hao, Y.*, et al.*, Small molecule regulators of autophagy identified by an image-based high-throughput screen. *P Natl Acad Sci USA* **2007,** *104* (48), 19023-19028.

20. Carpenter, A. E., Image-based chemical screening. *Nat Chem Biol* **2007,** *3* (8), 461-465.

21. Xia, X. F.; Wong, S. T., Concise Review: A High-Content Screening Approach to Stem Cell Research and Drug Discovery. *Stem Cells* **2012,** *30* (9), 1800-1807.

22. Lipinski, C. A.; Lombardo, F.; Dominy, B. W.; Feeney, P. J., Experimental and computational approaches to estimate solubility and permeability in drug discovery and development settings. *Advanced drug delivery reviews* **2001,** *46* (1-3), 3-26.

23. Madani, F.; Lindberg, S.; Langel, U.; Futaki, S.; Graslund, A., Mechanisms of cellular uptake of cell-penetrating peptides. *J Biophys* **2011,** *2011*, 414729.

24. Vives, E., Cellular uptake of the Tat peptide: an endocytosis mechanism following ionic interactions. *J Mol Recognit* **2003,** *16* (5), 265-271.

25. Futaki, S., Membrane-permeable arginine-rich peptides and the translocation mechanisms. *Advanced drug delivery reviews* **2005,** *57* (4), 547-558.

26. Vives, E.; Schmidt, J.; Pelegrin, A., Cell-penetrating and cell-targeting peptides in drug delivery. *Bba-Rev Cancer* **2008,** *1786* (2), 126-138.

27. Lindgren, M.; Hallbrink, M.; Prochiantz, A.; Langel, U., Cell-penetrating peptides. *Trends Pharmacol Sci* **2000,** *21* (3), 99-103.

28. Heitz, F.; Morris, M. C.; Divita, G., Twenty years of cell-penetrating peptides: from molecular mechanisms to therapeutics. *Brit J Pharmacol* **2009,** *157* (2), 195-206.

29. Kondo, T.; Beutler, E., Depletion of Red-Cell Atp by Incubation with 2-Deoxyglucose. *J Lab Clin Med* **1979,** *94* (4), 617-623.

30. Kang, J.; Heart, E.; Sung, C. K., Effects of cellular ATP depletion on glucose transport and insulin signaling in 3T3-L1 adipocytes. *Am J Physiol-Endoc M* **2001,** *280* (3), E428-E435.

31. Schnitzer, J. E.; Oh, P.; Pinney, E.; Allard, J., Filipin-Sensitive Caveolae-Mediated Transport in Endothelium - Reduced Transcytosis, Scavenger Endocytosis, and Capillary-Permeability of Select Macromolecules. *J Cell Biol* **1994,** *127* (5), 1217-1232.

32. Vercauteren, D.; Vandenbroucke, R. E.; Jones, A. T.; Rejman, J.; Demeester, J.; De Smedt, S. C.; Sanders, N. N.; Braeckmans, K., The Use of Inhibitors to Study Endocytic Pathways of Gene Carriers: Optimization and Pitfalls. *Mol Ther* **2010,** *18* (3), 561-569.

33. Lamaze, C.; Fujimoto, L. M.; Yin, H. L.; Schmid, S. L., The actin cytoskeleton is required for receptor-mediated endocytosis in mammalian cells. *J Biol Chem* **1997,** *272* (33), 20332-20335.

34. Cuellar, K.; Chuong, H.; Hubbell, S. M.; Hinsdale, M. E., Biosynthesis of chondroitin and heparan sulfate in chinese hamster ovary cells depends on xylosyltransferase II. *J Biol Chem* **2007,** *282* (8), 5195-200.

35. McNaughton, B. R.; Cronican, J. J.; Thompson, D. B.; Liu, D. R., Mammalian cell penetration, siRNA transfection, and DNA transfection by supercharged proteins. *P Natl Acad Sci USA* **2009,** *106* (15), 6111-6116.

36. Gebski, B. L.; Mann, C. J.; Fletcher, S.; Wilton, S. D., Morpholino antisense oligonucleotide induced dystrophin exon 23 skipping in mdx mouse muscle. *Hum Mol Genet* **2003,** *12* (15), 1801-1811.

37. Hoffman, E. P.; Brown, R. H.; Kunkel, L. M., Dystrophin - the Protein Product of the Duchenne Muscular-Dystrophy Locus. *Cell* **1987,** *51* (6), 919-928.

38. Sicinski, P.; Geng, Y.; Rydercook, A. S.; Barnard, E. A.; Darlison, M. G.; Barnard, P. J., The Molecular-Basis of Muscular-Dystrophy in the Mdx Mouse - a Point Mutation. *Science* **1989,** *244* (4912), 1578-1580.

39. Heemskerk, H. A.; de Winter, C. L.; de Kimpe, S. J.; van Kuik-Romeijn, P.; Heuvelmans, N.; Platenburg, G. J.; van Ommen, G. J.; van Deutekom, J. C.; Aartsma-Rus, A., In vivo comparison of 2'-O-methyl phosphorothioate and morpholino antisense oligonucleotides for Duchenne muscular dystrophy exon skipping. *The journal of gene medicine* **2009,** *11* (3), 257-66.

40. Nowak, K. J.; Davies, K. E., Duchenne muscular dystrophy and dystrophin: pathogenesis and opportunities for treatment - Third in Molecular Medicine Review Series. *Embo Rep* **2004,** *5* (9), 872-876.

41. Heemskerk, H.; de Winter, C. L.; van Ommen, G. J. B.; van Deutekom, J. C. T.; Aartsma-Rus, A., Development of Antisense-Mediated Exon Skipping as a Treatment for Duchenne Muscular Dystrophy. *Ann Ny Acad Sci* **2009,** *1175*, 71-79.

42. Lu, Q. L.; Mann, C. J.; Lou, F.; Bou-Gharios, G.; Morris, G. E.; Xue, S. A.; Fletcher, S.; Partridge, T. A.; Wilton, S. D., Functional amounts of dystrophin produced by skipping the mutated exon in the mdx dystrophic mouse. *Nat Med* **2003,** *9* (8), 1009-1014.

43. Mann, C. J.; Honeyman, K.; Cheng, A. J.; Ly, T.; Lloyd, F.; Fletcher, S.; Morgan, J. E.; Partridge, T. A.; Wilton, S. D., Antisense-induced exon skipping and synthesis of dystrophin in the mdx mouse. *P Natl Acad Sci USA* **2001,** *98* (1), 42-47.

44. Summerton, J.; Weller, D., Morpholino antisense oligomers: design, preparation, and properties. *Antisense & nucleic acid drug development* **1997,** *7* (3), 187-95.

45. Cirak, S.; Arechavala-Gomeza, V.; Guglieri, M.; Feng, L.; Torelli, S.*, et al.*, Exon skipping and dystrophin restoration in patients with Duchenne muscular dystrophy after systemic phosphorodiamidate morpholino oligomer treatment: an open-label, phase 2, dose-escalation study. *Lancet* **2011,** *378* (9791), 595-605.

46. He, B.; Minges, J. T.; Lee, L. W.; Wilson, E. M., The FXXLF motif mediates androgen receptor-specific interactions with coregulators. *J Biol Chem* **2002,** *277* (12), 10226-35.

47. Estebanez-Perpina, E.; Moore, J. M.; Mar, E.; Delgado-Rodrigues, E.; Nguyen, P.*, et al.*, The molecular mechanisms of coactivator utilization in ligand-dependent transactivation by the androgen receptor. *J Biol Chem* **2005,** *280* (9), 8060-8.

Appendix Table 1. The physiochemical properties and intracellular access of peptides in cell penetration assays.

Peptide Entry	Molecular Weight	Log *P*	Theoretical pI	Formal Charge	PSA	Peptide Type*	Fluorescence Intensity		Mean Fluorescence Intensity
A1	2987.498	-8.45	11.88	5.9	1355.33	4	3043.84	5604.59	4324.215
A2	3001.524	-8.17	11.71	5.9	1355.33	4	3817.07	4041.81	3929.44
A3	2971.412	-11.14	11.93	5.9	1375.56	4	3009.63	4414.14	3711.885
A4	2985.439	-10.85	11.89	5.9	1375.56	4	3069.98	4593.74	3831.86
A5	2928.387	-9.69	11.75	5.9	1332.47	4	2989.85	3872.72	3431.285
A6	2975.444	-10.42	11.93	5.9	1375.56	4	4484.2	5423.02	4953.61
A7	2768.095	-17.7	12.22	7.9	1386.17	1	756.557	648.657	702.607
A8	2391.725	-13.23	12.19	6.9	1192.08	2	524.128	653.377	588.7525
A9	2433.805	-11.9	12.21	6.9	1192.08	3	613.807	911.278	762.5425
A10	2616.077	-12.55	12.59	9.9	1314.46	3	1200.32	911.4	1055.86
A11	2217.576	-12.58	12.44	5.9	1084.54	2	545.937	506.065	526.001
A12	2561.88	-14.72	12.44	5.9	1200.94	2	562.223	583.499	572.861
A13	2546.919	-13.23	12.35	6.9	1204.64	3	566.461	631.856	599.1585
A14	2632.027	-14.14	12.33	7.9	1266.54	3	626.639	578.61	602.6245
A15	2689.075	-14.3	12.35	6.9	1262.84	3	661.275	573.647	617.461
A16	2661.028	-15.31	12.21	7.9	1362.05	2	751.496	726.077	738.7865
A17	2661.028	-15.31	12.23	7.9	1362.05	2	655.747	1015.37	835.5585
A18	2702.127	-15.58	12.49	9.9	1386.65	2	1562.8	947.344	1255.072
A19	2744.207	-14.24	12.5	9.9	1386.65	3	1508.86	1590.82	1549.84
A21	2897.213	-19.59	12.13	7.9	1499.36	1	505.075	495.357	500.216
A22	2301.678	-3.69	11.65	3.9	999.85	4	1085.04	1118.66	1101.85
A23	2934.312	-15.53	12.08	6.9	1437.46	2	575.099	577.835	576.467
A24	2877.258	-13.57	11.91	5.9	1375.56	3	569	571.396	570.198
A25	2877.258	-13.57	11.91	5.9	1375.56	3	534.381	547.054	540.7175
A26	2971.412	-11.14	11.93	5.9	1375.56	4	1743.3	1834.78	1789.04
A27	2985.439	-10.85	11.89	5.9	1375.56	4	1437.88	1495.01	1466.445
A28	2928.387	-9.69	11.75	5.9	1332.47	4	1495.81	1133.34	1314.575
A29	2975.444	-10.42	11.93	5.9	1375.56	4	1236.64	1184.89	1210.765
A30	2987.498	-8.45	11.88	5.9	1355.33	4	1137.32	1374.89	1256.105

Appendix Table 1 (Continued)

Peptide Entry	Molecular Weight	Log *P*	Theoretical pI	Formal Charge	PSA	Peptide Type*	Fluorescence Intensity		Mean Fluorescence Intensity
A31	3001.524	-8.17	11.71	5.9	1355.33	4	1257.53	1361.26	1309.395
A32	2328.75	-4.25	12.09	5.9	1024.45	4	1247.29	1492.27	1369.78
A33	2342.777	-3.96	11.85	5.9	1024.45	4	1168.67	1147.77	1158.22
A34	2285.725	-2.8	11.94	5.9	981.36	4	1238.57	1523.29	1380.93
A35	2370.833	-3.71	12.05	6.9	1043.26	4	1359.59	1300.68	1330.135
A36	2340.809	-6.06	12.25	7.9	1089.37	4	793.942	1039.95	916.946
A37	2361.787	-7.05	12.36	7.9	1105.16	3	812.375	706.958	759.6665
A38	2381.742	-13.07	12.63	9.9	1228.96	1	518.251	520.961	519.606
A39	2706.201	-5.81	11.15	5.89	1124.6	1	482.995	500.584	491.7895
A40	2665.234	-4.71	11.32	5.89	1108.81	3	570.84	531.727	551.2835
A41	2717.309	-3.62	11.32	5.89	1108.81	4	658.971	675.52	667.2455
A43	2158.611	1.62	10.37	2.89	810.08	4	961.253	959.043	960.148
A44	2116.531	0.21	10.3	2.89	810.08	4	809.83	890.876	850.353
A45	2351.717	-15.42	12.72	10.9	1275.07	1	525.115	533.447	529.281
A46	2331.762	-9.4	12.22	8.9	1151.27	3	660.104	658.93	659.517
A47	2340.809	-6.06	12.25	7.9	1089.37	4	1052.81	1035.36	1044.085
A48	2370.833	-3.71	12.05	6.9	1043.26	4	1408.85	1270.41	1339.63
A49	2361.787	-7.05	12.36	7.9	1105.16	3	670.339	684.697	677.518
A50	2381.742	-13.07	12.63	9.9	1228.96	1	552.135	522.907	537.521
A51	2116.417	-10.33	11.58	6.88	1010.24	1	477.591	473.034	475.3125
A52	2183.546	-6.27	11.6	5.88	993.01	3	562.385	537.512	549.9485
A53	2185.605	-5.19	11.93	5.9	972.78	4	970.934	1027.99	999.462
B1	3435.792	-12.24	3.26	-4.96	1488.6	2	572.779	693.676	633.2275
B2	3411.81	-10.13	2.8	-5.1	1459.92	3	673.145	786.046	729.5955
B3	3411.81	-10.13	2.8	-5.1	1459.92	3	638.178	1025.9	832.039
B4	3434.847	-9.45	3.25	-4.96	1445.51	3	751.087	696.879	723.983
B5	3450.803	-11.14	3.1	-5.96	1482.21	2	760.544	588.222	674.383
B6	3397.741	-11.19	2.68	-6.1	1476.99	2	535.12	512.897	524.0085

Appendix Table 1 (Continued)

Peptide Entry	Molecular Weight	Log *P*	Theoretical pI	Formal Charge	PSA	Peptide Type*	Fluorescence Intensity		Mean Fluorescence Intensity
B7	3408.724	-12.39	3.09	-5.96	1482.81	2	579.51	522.387	550.9485
B8	3449.858	-8.36	3.1	-5.96	1439.72	3	619.602	599.81	609.706
B9	3420.777	-10.51	3.1	-5.96	1462.58	2	850.458	647.007	748.7325
B10	3448.83	-9.47	3.11	-5.96	1462.58	3	633.623	649.646	641.6345
B11	3449.819	-11.87	3.26	-4.96	1488.6	3	815.385	657.586	736.4855
B12	3406.794	-10.5	3.28	-4.96	1445.51	2	644.214	779.029	711.6215
B13	3407.775	-8.9	2.66	-6.96	1420.91	3	781.2	523.513	652.3565
B14	3351.669	-10.52	2.67	-6.96	1420.91	2	767.472	695.511	731.4915
C1	2981.511	-2.31	4.09	-1.1	1164.93	4	686.475	697.567	692.021
C2	3065.671	0.48	4.09	-1.1	1164.93	4	932.295	942.385	937.34
C3	3008.62	1.56	4.09	-1.1	1121.84	4	785.527	896.131	840.829
C4	3049.715	2.08	6.27	-0.1	1127.63	4	790.587	781.239	785.913
C5	3008.62	1.56	4.09	-1.1	1121.84	4	972.677	1090.05	1031.3635
D1	1502.774	4.94	5.96	-0.1	477.91	2	1644.55	929.536	1287.043
D2	1596.909	6.74	5.92	-0.13	503.21	2	1942.4	1780.12	1861.26
D3	1520.813	5.08	5.92	-0.13	503.21	2	1319.53	830.63	1075.08
D4	1833.11	5.76	3.75	-1.12	593.64	4	1129.77	882.068	1005.919
D5	1833.11	5.76	3.75	-1.12	593.64	4	1384.76	1269.1	1326.93
D6	1732.008	2.08	5.97	-0.1	599.43	2	1007.14	869.611	938.3755
D7	1733.937	0.18	3.68	-1.1	636.73	2	702.898	519.423	611.1605
D8	2379.597	-5.07	3.15	-3.1	940.64	1	460.747	487.38	474.0635
D9	2487.821	-0.1	3.19	-3.1	929.02	3	575.609	595.273	585.441
D10	2524.924	3.49	3.2	-3.1	885.93	4	981.586	700.025	840.8055
D11	2448.828	1.84	3.2	-3.1	885.93	4	1271.7	778.68	1025.19
D12	2437.893	2.64	5.97	-0.1	837.35	4	800.699	676.661	738.68
E1	3065.53	0.07	3.56	-3.95	1142.16	4	1030.43	599.24	814.835

Appendix Table 1 (Continued)

Peptide Entry	Molecular Weight	Log *P*	Theoretical pI	Formal Charge	PSA	Peptide Type*	Fluorescence Intensity		Mean Fluorescence Intensity
E2	2440.81	1.19	3.39	-2.95	860.16	4	1087	747.6	917.3
E3	2440.81	1.99	3.39	-2.95	860.16	4	764	922.23	843.115
E4	2240.576	2.78	3.41	-2.95	781.73	4	948.928	853.246	901.087
E5	1942.237	4.5	3.41	-2.95	651.34	4	524.418	665.808	595.113
E6	1942.237	4.5	3.41	-2.95	651.34	4	849.054	743.958	796.506
F1	2392.882	-2.46	9.85	2.05	911.39	3	1437.47	1065.54	1251.505
F2	2392.882	-2.46	9.85	2.05	911.39	3	2046.6	1630.37	1838.485
F3	2392.882	-2.24	9.85	2.05	885.37	3	986.649	1525.75	1256.1995
F4	2326.797	-1.82	7.6	0.05	869	3	1710.44	1711.45	1710.945
J1	2188.46	-3.28	4.01	-1.1	892.65	3	624.782	630.873	627.8275
J2	2172.46	-2.24	4.01	-1.1	872.42	3	910.781	765.676	838.2285
J3	2213.512	-2.35	4	-1.1	895.28	3	651.648	814.064	732.856
J4	2220.5	-0.83	3.3	-2.1	853.61	3	1032.71	950.423	991.5665
J5	2163.448	0.33	3.31	-2.1	810.52	3	895.491	1804.1	1349.7955
J6	2374.67	-2.37	4.01	-1.1	937.54	3	624.778	772.729	698.7535
J7	2204.5	0.22	3.3	-2.1	833.38	3	798.9	731.273	765.0865
J8	2203.516	-0.59	3.67	-1.1	839.17	3	1314.17	1264.92	1289.545
J9	2467.831	-0.87	3.67	-1.1	894.55	3	916.016	1292.76	1104.388
J10	2467.831	-0.87	3.67	-1.1	894.55	3	598.879	635.706	617.2925
J11	2459.772	-6.11	8.9	0.9	982.47	1	476.233	481.78	479.0065
J12	2467.831	-0.87	3.67	-1.1	894.55	3	2040.37	2004.04	2022.205
J13	2467.831	-0.87	3.67	-1.1	894.55	3	585.671	554.415	570.043
J14	2467.831	-0.87	3.67	-1.1	894.55	3	1079.38	1195.99	1137.685
J15	2203.559	0.44	6.27	-0.1	822.1	3	1160.5	1998.67	1579.585
J16	2196.654	0.32	10.12	2.89	824.81	3	3446.2	3242.54	3344.37
J17	2204.5	0.22	3.3	-2.1	833.38	3	1114.13	981.989	1048.0595
J18	2217.585	0.73	6.26	-0.1	822.1	3	3017.35	3513.49	3265.42

Appendix Table 1 (Continued)

Peptide Entry	Molecular Weight	Log *P*	Theoretical pI	Formal Charge	PSA	Peptide Type*	Fluorescence Intensity		Mean Fluorescence Intensity
J19	2196.442	-5.02	6.33	-0.1	921.3	1	482.644	473.349	477.9965
J20	3339.771	-6.93	3.84	-2.11	1319.62	3	471.842	488.486	480.164
J21	3325.701	-8.25	3.46	-3.1	1336.69	3	647.768	631.281	639.5245
J22	3341.7	-8.9	3.57	-3.11	1356.92	2	489.011	484.439	486.725
J23	2195.457	-5.83	8.9	0.9	927.09	1	468.336	474.074	471.205
J24	2219.515	-1.25	3.97	-1.1	859.4	2	490.935	489.105	490.02
J25	2134.601	3.68	5.39	-0.96	739.73	3	827.712	928.865	878.2885
J26	2277.594	-0.92	3.67	-1.1	857.63	3	963.093	981.505	972.299
J27	2304.81	2.83	5.39	-0.96	797.93	3	725.679	665.469	695.574
J28	2447.803	-1.77	3.67	-1.1	915.83	3	8644.99	7146.64	7895.815
J29	2335.673	-0.73	3.67	-1.1	866.86	3	1195.69	1030.08	1112.885
J30	2128.616	3.96	9.2	1.86	729.22	3	1059.86	2442.36	1751.11
J31	2687.006	-11.14	9.83	2.05	1240.05	3	475.395	485.988	480.6915
J32	2558.877	-9.5	9.83	2.05	1153.87	3	469.684	463.521	466.6025
J33	2203.516	-0.59	3.67	-1.1	839.17	3	1347.67	1235.88	1291.775
J34	2203.516	-0.59	3.67	-1.1	839.17	3	1317.22	1322.91	1320.065
J35	2189.489	-1.04	3.67	-1.1	839.17	3	622.526	633.052	627.789
J36	2203.516	-0.59	3.67	-1.1	839.17	3	1287.33	1343.84	1315.585
J37	2231.569	0.52	3.67	-1.1	839.17	1	889.65	863.598	876.624
J38	2203.516	-0.59	3.67	-1.1	839.17	3	540.274	717.801	629.0375
J39	2203.516	-0.59	3.67	-1.1	839.17	3	789.287	676.368	732.8275
J40	2203.516	-0.59	3.67	-1.1	839.17	3	1063.44	1064.19	1063.815
J41	4211.896	-9.31	10.62	3.05	1757.56	4	2494.602216	3076.09955	2785.35088
J42	2443.78	-6.25	7.59	0.05	1031.04	2	432.028094	435.647261	433.837678
J43	2434.813	-5.61	8.82	0.89	1028.38	2	469.0993641	485.868766	477.484065
J44	3246.696	-11.37	9.29	1.87	1417.99	1	472.6533212	472.791893	472.722607
J45	2105.371	-3.55	4	-1.1	859.4	1	529.7367192	508.954666	519.345693
J46	3282.81	-5.88	8.64	0.87	1348.88	3	488.0584951	465.789945	476.92422
J47	2426.832	-2.04	8.69	0.88	962.43	2	785.4423016	658.812202	722.127252

Appendix Table 1 (Continued)

Peptide Entry	Molecular Weight	Log *P*	Theoretical pI	Formal Charge	PSA	Peptide Type*	Fluorescence Intensity		Mean Fluorescence Intensity
J48	2235.645	0.1	6.4	-0.1	878.21	3	1983.279974	1443.821	1713.55049
J49	2414.775	-2.79	6.36	-0.13	963.85	2	450.3951458	434.870667	442.632906
J50	2226.634	2.67	4.09	-1.1	816.31	3	1015.990077	1064.62356	1040.30682
J51	2181.596	1.92	6.25	-0.1	801.87	3	579.1616212	567.71945	573.440536
J52	2278.673	-2.06	8.9	0.9	940.11	3	1294.823057	1124.28351	1209.55328
J53	2113.433	0.9	3.39	-2.1	790.29	2	1141.238164	819.010745	980.124455
J54	2269.662	0.5	6.4	-0.1	878.21	3	1087.4175	839.551965	963.484733
J55	2163.412	-3.54	6.72	-0.77	850.81	2	547.1723022	480.83424	514.003271
J56	1579.65	-8.27	6.72	-0.77	715.15	1	435.5546332	449.736374	442.645504
J57	1564.718	-3.48	5.52	-0.95	643.38	2	473.5588541	473.33877	473.448812
J58	2113.35	-3.82	5.5	-0.95	842.36	2	456.1351274	449.155411	452.645269
J59	3385.803	-8.85	7.48	-0.01	1422.07	3	495.9630114	464.831059	480.397035
J60	5260.81	-24.26	8.53	1.18	2291.33	1	431.5049302	437.145614	434.325272
J63	5341.024	-20.04	9.45	2.84	2292.26	1	496.3883599	443.158293	469.773327
J65	2212.527	-3.16	6.28	-0.1	901.07	3	632.0604495	689.194237	660.627343
J67	3540.052	-6.09	4.47	-1.11	1405.42	3	845.1689366	1229.82032	1037.49463
J68	3425.996	-5.9	9.33	1.88	1361.96	3	1263.618484	1865.90157	1564.76003
J69	4807.281	-23.39	7.71	0.19	2167.55	1	439.364244	440.488379	439.926312
J70	4892.553	-14.58	7.7	0.19	2048.12	4	493.4865051	498.443964	495.965235
J71	4835.42	-19.92	7.74	0.21	2127.09	3	462.6465163	445.234646	453.940581
J72	4765.331	-21.53	8.67	1.21	2110.02	2	563.1502886	539.621996	551.386142
J73	4871.539	-17.14	8.67	1.21	2089.79	4	516.6628107	549.448732	533.055771
J74	3345.613	-14.46	6.71	-0.82	1488.05	1	427.2114299	428.277024	427.744227
T048	2332.651	-1.46	3.5	-3.95	918.95	3	420.5785129	428.829088	424.7038
T049	2220.478	-3.74	3.17	-3.95	883.07	2	456.2188633	439.275321	447.747092
T050	2289.587	-3.6	3.8	-2.95	924.74	2	420.5933334	426.310343	423.451838
T058	2046.37	-0.72	4.19	-1.95	786.15	2	584.1776211	597.00625	590.591936
T059	2160.473	-2.71	4.19	-1.95	858.34	2	428.4593164	443.523619	435.991468

Appendix Table 1 (Continued)

Peptide Entry	Molecular Weight	Log *P*	Theoretical pI	Formal Charge	PSA	Peptide Type*	Fluorescence Intensity		Mean Fluorescence Intensity
T060	2232.58	0.49	4.19	-1.95	831.04	2	513.2926279	490.684689	501.988658
T061	2174.542	-1.39	5.58	-0.95	841.27	2	454.7264384	461.938837	458.332638
T071	2304.691	-2.25	7.6	0.05	914.42	2	558.3565963	458.181098	508.268847
T072	2490.901	-1.03	7.6	0.05	959.31	2	560.343285	479.275864	519.809574
T073	2460.876	-3.7	8.99	1.05	1005.42	2	474.3524921	421.063143	447.707818
SAHM1	2542.944	-8.02	10.61	3.23	1132.09	2	2790.31	7653.2	5221.755
SAHM1-D1	2515.872	-7.46	8.84	1.12	1107.49	2	4598.86	2355.2	3477.03
SAHM1-D2	2488.8	-6.23	6.53	-0.88	1082.89	2	2823.97	3542.12	3183.045

* Peptide Type: 1 = WT, 2 = i, i+4 stapled, 3 = i, i+7 stapled, 4 = stitched